GEOLOGICAL SURVEY OF CANADA
OPEN FILE 7201

A Preliminary Tsunami Hazard Assessment of the Canadian Coastline

L.J. Leonard, G.C. Rogers, and S. Mazzotti

2012

Natural Resources Canada | Ressources naturelles Canada

Canada

GEOLOGICAL SURVEY OF CANADA
OPEN FILE 7201

A Preliminary Tsunami Hazard Assessment of the Canadian Coastline

L.J. Leonard, G.C. Rogers, and S. Mazzotti

2012

doi:10.4095/292067

This publication is available for free download through GEOSCAN (http://geoscan.ess.nrcan.gc.ca/).

Recommended citation
Leonard, L.J., Rogers, G.C., and Mazzotti, S., 2012. A preliminary tsunami hazard assessment of the Canadian coastline; Geological Survey of Canada, Open File 7201, 126 p. doi:10.4095/292067

Publications in this series have not been edited; they are released as submitted by the author.

TABLE OF CONTENTS

LIST OF TABLES

LIST OF FIGURES

ABSTRACT

The Canadian coastline is the longest of any country in the world, and is at risk from tsunamis generated in three oceans. The current state of knowledge precludes a complete probabilistic tsunami hazard assessment, which would require quantification of a wide range of possible scenarios for each tsunami source, coupled with modelling that incorporates fine-resolution bathymetry and onland topography to adequately assess potential runup at the coast. This preliminary assessment presents a first attempt to quantify the tsunami hazard on the Canadian Pacific, Atlantic and Arctic coastlines from local and far-field, earthquake and large landslide sources. For each source considered, we calculate the probability that tsunami runup at the coast will exceed 1.5 m (threshold for potential damage) and 3 m (significant damage potential), in a 50-year period. For each coastal region, we then combine the relative hazard from each source to calculate the overall probability that the coastline in question will experience tsunami runup exceeding 1.5 m (and 3 m) within a 50-year period, from any geological source. We also consider the maximum runup levels expected to occur within time periods of 100, 500, 1000, and 2500 years.

Our assessment indicates that the overall tsunami hazard (runup ≥ 1.5 m) of the outer Pacific coastline (~40-80% probability of exceedance in 50 y) is an order of magnitude greater than that of the outer Atlantic coastline (~1-15%), which in turn is an order of magnitude greater than the Arctic coastline (< 1%). These probabilities are equivalent to an expected recurrence of runup exceeding 1.5 m of ~30-100 years for the outer Pacific coast, ~300-1700 for the Atlantic, and ~6500-17,000 years for the Arctic. For larger runup (≥ 3 m), the estimated Pacific hazard (~10-30% probability of exceedance in 50 y) is significantly larger than both the Atlantic (~1-5%) and the Arctic (< 1%). Equivalent recurrence intervals are ~150-500 years for the Pacific, ~650-4000 years for the Atlantic, and ~7000-20,000 years for the Arctic. On the outer Pacific coastline, the 1.5 m runup hazard is dominated by far-field subduction zone sources, whereas the more severe 3 m runup hazard is almost entirely contributed by local subduction zone sources. The Cascadia subduction zone presents the highest tsunami hazard to the Pacific coast, with the most extreme potential runup; potential thrust sources along the Explorer and Queen Charlotte margins contribute a significant proportion of the estimated tsunami hazard for the northern BC coastline. For the more sheltered inner Pacific coasts of Juan de Fuca and Georgia Straits, the hazard at both levels is contributed mostly by Cascadia subduction zone events. Tsunami hazard on the Atlantic coastline is dominated by far-field subduction zone sources, but this hazard is poorly constrained. Significant tsunami hazard is also provided by near-field continental slope failures similar to the 1929 Grand Banks event. Tsunami hazard on the Arctic coastline remains poorly constrained, but these regions are assumed to be sheltered from far-field tsunamis, so the hazard is provided by local sources. A hypothetical earthquake source beneath the Mackenzie delta requires further study.

We discuss briefly but do not quantify the hazard of locally-damaging waves triggered by subaerial or submarine landslides, but we highlight susceptible areas. A probabilistic analysis of local landslide tsunamis would require (1) the identification of potential sources; (2) evidence for past tsunamigenic events to establish frequency-size relationships and/or slope stability analyses that incorporate expected earthquake shaking levels; (3) probabilistic tsunami modelling of a wide range of possible failures.

INTRODUCTION

With a longer coastline than any other country in the world, Canada is at risk from tsunamis generated in three oceans – the Pacific, Atlantic, and Arctic (Figs. 1 and 2). Many previous studies concern historical tsunamis on the Pacific and Atlantic coasts (Table 1), and the threat that future tsunamis may present to certain areas (references in Leonard et al., 2010a). This analysis presents a first attempt to quantify the tsunami hazard on each coast, from both near- and far-field sources. Earthquakes represent the greatest and most easily quantified source of tsunami threat, but we also consider hazard contributions from mass movement sources. We do not assess the threat of tsunamis on inland waterways, although several historical occurrences involving landslide mechanisms have resulted in damage and loss of life (e.g., Evans, 2001; Stephenson and Rabinovich, 2009). We do not account for the likely common regional hazard from meteorological tsunamis (tsunami-like waves, generated in the open ocean by atmospheric disturbances such as pressure jumps, frontal passages, or squalls, and amplified near the coast by resonance mechanisms; e.g., Monserrat et al., 2006; Stephenson and Rabinovich, 2009); these do not result from geological phenomena and are likely ubiquitous rather than having a distinct source area. We also omit the potentially devastating but very rare hazard presented by asteroid impact tsunamis (e.g., Ward and Asphaug, 2000; Hills and Goda, 2001; Gisler et al., 2011).

This assessment, based on the currently available constraints, is intended for use as a starting point to establish priorities for future work. Identification of poorly-constrained sources with potentially high hazard highlights the need to better quantify both the source potential and tsunami impact. Probabilities determined in this report will undoubtedly need to be updated as more data are collected regarding: evidence for the occurrence, frequency, and size of past tsunamis; better constraints on the tectonic parameters of various potential fault tsunami sources; stability assessments of potential landslide tsunami sources; tsunami modelling of a wide range of potential sources from tsunamigenesis through propagation to inundation, incorporating fine-resolution bathymetry and coastal topography.

Tsunami Wave Height Threshold for Potential Damage

In this report, as in most scientific literature, wave height or amplitude is defined as the zero-to-peak wave amplitude (equivalent to the height above the state of tide; also see Appendix A for a glossary of technical terms). Runup height (*Hr*), which determines the inland extent of inundation, is defined as approximately double the wave height, or equivalent to the peak-to-trough wave amplitude (Abe, 1995). Based on historical tsunamis in the Pacific Ocean, Whitmore et al. (2008; 2009) determined the minimum height of damaging tsunami waves to be used as response criteria for the West Coast and Alaska Tsunami Warning Center (both Pacific and Atlantic Oceans). Damage to boats, docks, and swimmers may occur due to strong currents for tsunami amplitude or runup as low as 0.5 m, whereas more severe damage and inundation is likely with a minimum amplitude or runup of 1.5-2.0 m. For the purposes of this preliminary tsunami hazard assessment, we follow Whitmore et al. (2008; 2009) and use a tsunami runup (*Hr*) threshold of 1.5 m (assumed equivalent to a peak-to-trough amplitude of 1.5 m or a wave height/amplitude of ~0.75 m) for potentially damaging coastal waves. We also assess a tsunami runup threshold of 3 m, which we define here as having significant damage potential, i.e., major damage expected that may be geographically extensive.

Tsunami Hazard Analysis

Probabilistic tsunami hazard analysis (e.g., Geist and Parsons, 2006; Burbidge et al., 2008; Thio et al., 2010; Sørensen et al., 2012) involves a number of steps with the ultimate aim of estimating the probabilities of exceeding specific tsunami wave heights (or runup) at given locations, from any possible source. The first step takes into account all potential sources, their possible variations and their likelihoods (recurrence rates). This is followed by numerical simulation of the generation, propagation and inundation of all possible tsunamis from these sources. The probabilities are then aggregated, and a logic tree approach can be used to integrate the uncertainties. Thus, ideally the following are needed: (1) the range of possible parameters (including maximum size) for all potential sources, including near- and far-field faults and mass movements; (2) the recurrence interval or probability of each event type; (3) models for tsunami generation, propagation, and inundation, incorporating detailed bathymetry and coastal topography data. An alternative to the model-driven approach outlined above involves the use of empirical data (e.g., Geist et al., 2009a). Analysis of past tsunami runup or wave amplitudes can be used to estimate return periods and probabilities of exceedance, assuming that the historical record is both complete and sufficiently long to provide meaningful statistics.

If the annual rate, λ (inverse of recurrence period), of a particular tsunami runup height Hr_0 is known, the probability of exceeding that runup at least once in a certain time period T is given by:

$$P(Hr > Hr_0, T) = 1 - e^{-\lambda T} \tag{1}$$

assuming a Poisson process (Geist and Parsons, 2009). Thus, for multiple independent sources with individual annual rates (λ_1, λ_2, λ_3 …) of runup height Hr_0, the combined probability of exceedance in a time T is given by:

$$P(Hr > Hr_0, T) = 1 - e^{-\lambda_c T} \tag{2}$$

where λ_c is the cumulative annual rate. For each tsunami source, we estimate minimum, best, and maximum annual rates of runup height. These values are not intended to represent specific probabilities (e.g., mean and standard deviations), but rather represent the combined effect of uncertainties on the source parameterization (e.g., earthquake magnitude, tsunami wave propagation, etc.). For multiple sources, we estimate the combined best annual rate (λ_{c_best}) by simply adding the best values of each source:

$$\lambda_{c\_best} = \sum_{i=1}^{N} \lambda_{i\_best} \tag{3}$$

The combined minimum and maximum annual rates are calculated by treating the individual source minimum and maximum values as relative uncertainties and adding them geometrically:

$$\lambda_{c\_\min} = \lambda_{c\_best} - \sqrt{\sum_{i=1}^{N} (\lambda_{i\_best} - \lambda_{i\_\min})^2} \tag{4}$$

$$\lambda_{c\_\max} = \lambda_{c\_best} + \sqrt{\sum_{i=1}^{N} (\lambda_{i\_best} - \lambda_{i\_\max})^2} \tag{5}$$

Assessment of subduction earthquake sources

Modelling of the many tsunami sources with the potential to impact Canadian coasts is beyond the scope of this report; more extensive analyses are needed. For many of the potential

earthquake sources, modelling has been previously done to assess the impact of various scenario tsunamis at particular locations, often with constraints from historical data (e.g., Knight, 2006; Cherniawsky et al., 2007; Roger et al., 2010a). In such cases we can augment the model output with estimates of recurrence intervals from paleoseismic and/or geodetic data to provide a preliminary probabilistic analysis. For Pacific far-field sources, a century-long tide gauge dataset allows us to carry out an empirical probabilistic analysis without the need for complex modelling; however such modelling is desirable for future studies, as the results are only strictly valid at the tide gauge locations.

For potential earthquake tsunami sources without published constraints on event size or recurrence, we estimate these quantities via the following empirical calculations. Steps 1-4 provide an estimate of the potential earthquake magnitude and recurrence, with the corresponding tsunami runup approximated for each coastal zone in Step 5. Finally, in Step 6, the probabilities of potentially damaging (≥ 1.5 m) and significant (≥ 3 m) tsunami runup resulting from the source earthquake are estimated for each zone.

Step 1: We estimate the maximum potential earthquake magnitude using an empirical relation between moment magnitude (M_w) and fault rupture area (A, km^2) as determined by Strasser et al. (2010):

$$M_w = 4.441 + 0.846(\log_{10} A) \qquad (\sigma = 0.286) \tag{6}$$

Minimum and maximum values are calculated by adding/subtracting the standard deviation, i.e. $M_w \pm \sim 0.3$. The Strasser et al. (2010) relation is based on a global dataset of 85 reverse-fault M_w 6.3-9.4 earthquakes that includes fault rupture areas estimated from earthquake source models, observed data (seismological, geodetic, geological, tsunami), and 1-day aftershock distributions. The resulting magnitude estimates are approximately consistent with previous empirical A-M_w relations arising from smaller databases. For example, the relation of Somerville et al. (2002), based on 10 subduction thrust earthquakes of M_w 7.1-8.1, provides M_w estimates within 0.1 of the Strasser et al. (2010) relation for $M_w \geq 8.3$; M_w estimates within 0.1 of the Strasser et al. relation for $M_w \leq 8.3$ result from the relation of Wells and Coppersmith (1994) based on 43 thrust fault (non-subduction) earthquakes of M_w 4.8-7.6.

Step 2: Seismic moment M_o (Nm) is calculated from M_w (Hanks and Kanamori, 1979):

$$\log_{10} M_o = 1.5(M_w + 6.03) \tag{7}$$

Step 3: The average fault slip (s) in an earthquake of magnitude M_w can be calculated from the seismic moment, coseismic rupture area (A), and the shear modulus or rigidity (μ) (Hanks and Kanamori, 1979):

$$s = M_o / (\mu A) \tag{8}$$

Step 4: The average recurrence interval (R) of events can then be calculated using the average earthquake slip s and the long-term fault slip rate c (e.g., convergence rate across a subduction zone), assuming that 100% of the convergence is released in seismic events:

$$R = s / c \tag{9}$$

The annual frequency of each event of M_w (λ, equivalent to $1/R$) of each event type can then be used to calculate the probability of exceedance in a time period T:

$$P(M_w, T) = 1 - e^{-\lambda T} \quad (10)$$

For the above calculations, necessary input parameters include fault rupture area, long-term fault slip rate, and shear modulus. In Appendix B, we use the example of the well-studied Cascadia subduction zone to illustrate and define these parameters. For example, an "effective" shear modulus of ~1 x 10^{10} N/m^2 is consistent with the estimated rupture area at Cascadia, and with the coseismic slip in the last great earthquake as indicated by modelling of far-field tsunami data.

Alternative to Steps 2 and 3: Similar results are obtained for Cascadia by using a different approach, substituting Steps 2 and 3 with an empirical relation between M_w and average fault displacement (AD), as derived by Wells and Coppersmith (1994):

$$\log_{10}(AD) = -4.80 + 0.69 M_w \quad (\sigma = 0.36) \quad (11)$$

This relation is based on a database of 56 earthquakes of M_w 5.6-8.1, incorporating a mixture of strike-slip, normal and reverse fault (non-subduction) events. For the Cascadia subduction zone, an M_w 8.8 earthquake involves an average seismogenic zone displacement of 18.7 m (8.2-42.9 m), with an average recurrence interval of 520 years (227-1190 y). Although consistent with the paleoseismic data, in further calculations we prefer the use of Steps 2 and 3 as outlined above, to avoid using an additional empirical relation that is not based on any subduction thrust events.

Step 5: Where no detailed tsunami modelling has been carried out, we use the following empirical relations between M_w and tsunami runup determined by Abe (1995) to estimate the potential runup resulting at near-field locations from earthquakes on reverse faults. For near-source coastlines up to a distance D_L from the source, where

$$\log_{10} D_L = 0.5 M_w - 2.25 , \quad (12)$$

limiting local mean runup (H_L) and limiting local maximum runup ($2H_L$) can be calculated for an earthquake of given M_w:

$$\log_{10} H_L = 0.5 M_w - 3.3 \quad (13)$$

Further from the source (at distances greater than D_L), local mean runup (Hr) and local maximum runup ($2Hr$) can be calculated, proportional to the distance D from the source as well as to M_w:

$$\log_{10} Hr = M_w - \log_{10} D - 5.55 \quad (14)$$

To illustrate these relations of Abe (1995) for values of M_w between 6.3 and 9.2, Table 2 includes the limiting near-source local mean and maximum runup possible up to a given distance from the source. Also listed are the distances at which mean runups of 3 m and 1.5 m are predicted for each M_w, as well as the furthest distance at which local maximum runup may equal 1.5 m.

At far-field distances, tsunami runup varies significantly depending on the relationship between the source and the runup site (e.g., Abe, 1979), based on the directivity of the tsunami (maximum amplitudes occur in the direction perpendicular to the fault strike, Ben-Menahem and Rosenman, 1972), as well as the vulnerability of particular coastal sites due to the influence of nearshore bathymetry, coastline shape, and local resonance. Therefore estimates of far-field tsunami runup based solely on source earthquake magnitude and propagation distance are unreliable. We examined $M > 8.0$ tsunamigenic earthquakes in the historical global tsunami runup database of the National Geophysical Data Center (NGDC, accessed 2011 for events since 1900). As expected, larger earthquakes are more likely than smaller events to produce potentially

damaging runup (≥ 1.5 m) at one or more sites at distances greater than 2000 km from the source. Few historical events of $M_w < 8.5$ have produced runup exceeding 1.5 m at such far-field distances; we use this as a guideline.

Step 6: Finally, for each source we integrate the probability of a tsunamigenic earthquake (Equation 10) with its estimated runup for each coastal region (Step 5). Where local mean runup Hr (or H_L) is calculated to exceed 1.5 or 3 m for a tsunamigenic event of given M_w, the probability of exceeding 1.5 or 3 m runup can be approximated directly as the probability of exceedance of the source earthquake M_w. However, the caveat is that not all earthquakes of a given size may be equally tsunamigenic, e.g., if an earthquake has a strike-slip component the probability of exceedance of the runup thresholds will be less than that of the source earthquake M_w. In a coastal zone where only local runup maxima ($2Hr$ or $2H_L$) exceeding 1.5 or 3 m are expected, the actual probabilities of exceedance of these runup thresholds will vary within the zone depending on various factors (e.g., source location, propagation direction, bathymetry) that require detailed tsunami modelling. We assume that in these zones the overall probability of exceeding the threshold runup is lower than in zones with local mean runup exceeding the threshold; without further constraints we approximate the probability of exceedance as half the probability of the source earthquake M_w.

Assessment of landslide sources

The tsunami hazard from landslide sources is more difficult to assess (e.g., Watts, 2003). In contrast to earthquake tsunamis, generally only mass failure sources relatively close to the coastal location need to be considered, because significant attenuation occurs at far-field distances (e.g., Geist and Parsons, 2009). However, modelling suggests that very large failures (e.g., catastrophic volcanic flank collapses) may result in potentially damaging tsunami runup at transoceanic distances. Mass movements, like many other natural systems, follow an inverse power-law frequency-size relationship (e.g., Korup and Clague, 2009). Where identification and dating of past slides is sufficiently complete, the frequency of large events may be approximated (e.g., Masson et al., 2002; Chaytor et al., 2009; Piper et al., 2011). Coupled with tsunami modelling, we can then approximate the probability of potentially damaging tsunami runup related to such failures. However, for smaller failures such empirical data are difficult to collect - estimation of tsunamigenic slide frequency requires detailed seafloor mapping, sub-seafloor sampling, and dating. Failures are often triggered by earthquakes, and the earthquake statistics of an area may be used to aid in landslide tsunami hazard analysis where slope stability data are available (e.g., Grilli et al., 2009; ten Brink et al., 2009a); such an analysis is beyond the scope of this report.

Local coastal landslide-generated waves are generally triggered by subaerial failures on steep fjord walls or submarine failures of delta fronts; these failures in turn may be triggered by strong ground shaking or other factors such as heavy rainfall or construction. Isolated cases have occurred in various locations in Canada (Table 1), but there is no long-term history of events at any one locality and thus it is currently impossible to calculate the probability of future local landslide-generated waves. Instead, we highlight coastal areas that may be at risk from such waves, aided by the national landslide susceptibility map (Bobrowsky and Dominguez, 2010), without providing a specific probabilistic hazard analysis. Bobrowsky and Dominguez (2010) assessed various factors including topography, geology, vegetation and precipitation to divide the Canadian landscape into landslide susceptibility classes ranging from 1 (lowest) to 6

(highest). We consider coastal areas with susceptibility levels of 5 to 6 to be at risk from landslide-generated waves, as well as nearby coastlines that may be affected by waves generated in these areas. Additionally, in the Arctic (particularly within fjords), local waves may be triggered by iceberg calving and jökulhlaup events at coastal glacier termini and ice shelves; these susceptible areas are also highlighted.

PACIFIC COAST

Of events that comprise the global historical tsunami record (since ~2000 BCE), ~56% were generated in the Pacific Ocean (compared to ~12% in the Atlantic, and none recorded in the Arctic; Gusiakov, 2009). In the time of written history on the British Columbia coast (about 150 years since the establishment of local newspapers), recorded tsunamis have mostly been far-field events (e.g., Stephenson et al., 2007; 2012). The two largest and most damaging were triggered by giant megathrust earthquakes in Alaska (M_w 9.2 1964) and Chile (M_w 9.5 1960) (Table 1; Fig. 2). Tsunamis from the M_w 8.8 2010 Chile and M_w 9.0 2011 Japan earthquakes were the largest recorded since 1964. The only known tsunami fatality resulted from a local tsunami triggered by the failure of a sandy spit during the M_s 7.3 crustal earthquake on central Vancouver Island in 1946 (Table 1; Fig. 1). However, a very large earthquake and tsunami that occurred in 1700 CE is documented in the oral history of First Nations peoples on the west coast of North America (e.g., Ludwin et al., 2005); the far-field tsunami was recorded in Japan, and paleoseismic data confirm a Cascadia subduction zone source (e.g., Atwater et al., 2005). The next Cascadia megathrust event presents the largest tsunami threat to the Pacific coast of North America.

Earthquake Tsunamis

Far-field tsunamis from Pacific subduction zones

The tide gauge at Tofino on the west coast of Vancouver Island (Fig. 1) provides the most complete record of tsunamis in coastal BC since operation began in 1906. Analysis of the tide gauge data (Wigen, 1983; Stephenson and Rabinovich, 2009; NOAA West Coast/Alaska Tsunami Warning Center, 2009a, b) has identified 61 tsunamis from 1906 to 2009. Over a sufficiently long period, a tide gauge should record tsunamis from all types of sources, but no local subduction or landslide tsunamis have occurred near Tofino since 1906. The tsunami record is made up mostly of far-field events (teletsunamis), but since the installation of digital high-precision instruments in 1998 it also includes a few small tsunamis generated by local/regional earthquakes and two regional meteorological tsunamis (Stephenson and Rabinovich, 2009). Thus, the Tofino tsunami record is effectively a record of far-field tsunamis, and can be used to assess their frequency. Other data are necessary to assess the tsunami hazard from landslide sources and from local submarine earthquakes on the Cascadia subduction zone and other faults.

Figure 3 shows the tsunami wave peak-to-trough amplitude data (i.e., double-amplitude or approximately equivalent to runup; Abe, 1995) for Tofino plotted as a function of frequency (i.e., power-law distribution). It is possible to predict the recurrence of rare large events from that of more frequent smaller ones with well-defined statistics. It is also assumed that the recurrence relation is a valid representation of the observed activity, and that the statistics of the area are constant over time.

When analysing frequency-amplitude data, it is necessary to define intervals of completeness (to ensure that all events of a given size are recorded for given time periods) – the completeness threshold will change over time due to equipment changes (e.g., instrument upgrades and higher sensitivity). For most of the Tofino record, tsunami events down to a peak-to-trough amplitude of 6 cm can be identified; this is reduced to 3 cm after the instrument upgrade in 1998. However, from 1975 to at least 1980 and possibly extending into the 1980s, the tide gauge response was compromised due to sediment buildup (Stephenson and Rabinovich, 2009). We assume that no tsunamis could be recorded from 1975-1980; we do not extend this into the 1980s because it appears to have been a quiescent time for Pacific tsunamis, e.g., the tide gauge at Crescent City, California, a tsunami-sensitive site, recorded no tsunamis from 1980 to 1985 (Dengler and Magoon, 2006). These completeness levels appear to be correct, with no observed flattening of the frequency-amplitude curve at low wave heights (Fig. 3).

The shape of the curve at high wave amplitudes is important for the estimation of the frequency of the larger, more damaging events, and it is largely dependent on the estimated maximum wave amplitude. The 1964 Alaska tsunami (2.4 m at Tofino) represents a near maximum possible tsunami from a far-field megathrust event, although paleoseismic data suggest that previous Alaskan events may have involved longer ruptures (Shennan et al., 2009), and Dunbar et al. (1989) suggest that a tsunami originating from the Aleutian megathrust could be larger. Thus, we assign a maximum peak-to-trough wave amplitude of 3.0 ± 0.5 m for far-field tsunamis at the Tofino tide gauge location (Fig. 3).

The resultant recurrence relation provides estimates of the rate of recurrence of tsunamis of various wave amplitudes, with uncertainties propagated from those of the recurrence parameters and the maximum wave amplitude. Estimated frequencies of tsunami wave runup of 1.5 m+ and 3 m+ are given in Table 3, along with their probabilities of exceedance in 50 years.

These results are only strictly applicable to the location of the tide gauge at Tofino; other localities on the BC coast exhibit different responses for the same event, depending mainly on near-field variations in the tsunami travel paths, e.g., Port Alberni tends to experience significantly larger wave amplitudes than Tofino (e.g., > 6 m in 1964 compared to 2.4 m at Tofino), due to resonance amplification effects in the Alberni Inlet (Henry and Murty, 1995; Fine et al., 2009). However, the available data indicate that the response ratios between specific sites tend to be similar for far-field events, e.g., the response at Victoria is typically ~0.6 times that of Tofino (Table 4). Thus the frequency-wave amplitude data from Tofino can be scaled to approximate the probabilities of exceedance at Victoria (Table 3; Fig. 3). We make the further assumptions that the probabilities calculated for Tofino can be applied to the rest of the outer BC coast and Haida Gwaii (Fig. 1), and that the lower probabilities calculated for Victoria can be applied to the rest of Juan de Fuca Strait as well as Queen Charlotte Strait where recent events recorded by the Port Hardy tide gauge show similar amplitudes to Victoria (Stephenson and Rabinovich, 2009). We assume that Georgia Strait and the adjoining Discovery Passage and Johnstone Strait (zone GS, see Appendix C) are sheltered from far-field tsunamis, with no reports of damaging waves from the 1964 tsunami.

Cascadia subduction zone

Great megathrust earthquakes on the Cascadia subduction zone, where the oceanic Juan de Fuca plate subducts eastward beneath continental North America (Fig. 1), represent the most significant and widespread tsunami threat to the Pacific coast of Canada as a whole. The recurrence of such events is fairly well constrained, and there is a significant probability (~10%)

that the next great earthquake will occur within the next 50 years, particularly given that over 300 years have passed since the previous one (Mazzotti and Adams, 2004; Goldfinger, 2009). The most recent event preceded the written history of the region, but it is documented by Native American oral records as a shaking and flooding event between 1690 and 1715 (Ludwin et al., 2005) and Japanese written records that detail a damaging tsunami in January 1700 (Satake et al., 1996). Correlative paleoseismic evidence comes from submerged trees, buried soils, and sand layers in coastal marshes along the Pacific coast from northern California to Vancouver Island, as well as turbidite deposits offshore (e.g., Goldfinger et al., 2003; Atwater et al., 2005). Modelling to match the tsunami and coastal paleoseismic data indicates a magnitude of M_w~9.0 for the 1700 CE earthquake (Satake et al., 2003; Leonard et al., 2004). Further paleoseismic data provide evidence that similar M~9 earthquakes and tsunamis have occurred throughout the Holocene, with a recurrence interval that averages ~500 years (mean 530 ± 260 y) but has been as short as ~200 years and as long as ~800 years or more (Atwater et al., 2004; Goldfinger et al., 2012).

The paleoseismic data point to the occurrence of additional megathrust earthquakes ($M_w \geq 8$) that rupture the southern part of the subduction zone; Goldfinger et al. (2012) report turbidite evidence for an additional 22 Holocene events in the south. Treating southern Cascadia as an additional tsunami source, independent of the long ruptures, implies an average recurrence of ~450 years for these smaller events. However, the frequency of southern Cascadia ruptures remains under debate, with some turbidites of questionable origin (e.g., Atwater and Griggs, 2012); we follow Frankel (2011) in assuming a longer recurrence interval of 1000 years, and assume an uncertainty of ± 250 years. We do not consider an additional northern Cascadia source suggested by Atwater and Griggs (2012); possible evidence includes a 2500-year paleotsunami record at Discovery Bay, Washington (E. Juan de Fuca Strait; Fig. 1) where an average recurrence interval of ~300 years was previously attributed to a mixture of full-rupture Cascadia events and local crustal earthquake sources (Williams et al., 2005). If 300 years is taken as the average recurrence of megathrust rupture in the north (full-length and northern events), and full-rupture events occur every ~500 years, short northern ruptures are implied to have an average recurrence of ~750 years.

Tsunami modelling of the seismic release of 500 years of accumulated strain on the full length of the Cascadia subduction zone (equivalent to an M~9.0 Cascadia megathrust earthquake) indicates that the west coast and inlets of Vancouver Island are most at risk (e.g., Ng et al., 1992; Whitmore, 1993; Cherniawsky et al., 2007), as is the case for teletsunamis. The modelling shows tsunami wave amplitudes of 5-8 m (above the state of tide, or zero-to-peak) on the southwestern coast of Vancouver Island (> 11 m at several locations, up to a maximum of 16 m at one location) and currents of up to 17 m/s in narrow channels and near headlands (Cherniawsky et al., 2007, with animations at http://www.pac.dfo-mpo.gc.ca/science/oceans/tsunamis/modele-tsunami-model-eng.htm; Fig. 4). The first positive wave crests would reach communities on the west coast of Vancouver Island 20-30 minutes after the earthquake, and Victoria, BC after ~1.3 hours. Throughout much of the area modelled, the first positive wave is not the largest; dangerously high waves and strong currents continue for at least the 12 hours of the model run. Only just over 300 years of strain has accumulated since the A.D. 1700 megathrust event, so modelling the release of 500 years of strain may overestimate the present-day tsunami hazard (Cherniawsky et al., 2007), although Cascadia paleoseismic data do not show a clear relationship between the inferred size of an event and the time since its predecessor (e.g., Leonard et al., 2010b).

In the Strait of Juan de Fuca, tsunami amplitudes are reduced by about one half compared with the outer coast, as indicated by both model results and actual tsunamis observed on tide gauges (Table 4; Fig. 3). Similarly in the Gulf Islands maximum amplitudes occurring in narrow channels and some bays are attenuated about 50% from the outer coast, although true maxima in bays and harbours are likely higher than predicted with the medium-resolution grid, as discussed later.

Once a tsunami reaches the open Strait of Georgia, wave amplitudes are attenuated even further. The largest observed tsunami, the 1964 event, had amplitudes at the Point Atkinson and Vancouver Harbour tide gauges (Burrard Inlet; Fig. 4) of about 10% of the Tofino measurement (Spaeth and Berkman, 1967). Six other tsunamis observed with amplitudes of 0.1-0.6 m at Tofino had no discernable record at Point Atkinson (D. Sinnott, Canadian Hydrographic Service, personal communication). The modelling of Cherniawsky et al. (2007) is consistent with these observations, with amplitudes in the Vancouver and southern Strait of Georgia regions respectively ~10% and less than 20% of outer coast values. Some local resonances were identified, e.g., amplitudes in Boundary Bay are at least double those in the Vancouver region (Fig. 4). The model does not extend into northernmost Georgia Strait or Johnstone Strait at the northern entrance and, without further constraints, we assume that runup is similar to that in southern Georgia Strait and that higher amplitudes are possible in inlets and narrow passes.

Cherniawsky et al. (2007) caution that the resolution used in most of their modelling is insufficient to accurately define amplitudes in bays and harbours. Tsunami runup is strongly dependent on bathymetry, and the determination of wave amplitudes depends on the resolution of the bathymetric grid used. Use of a fine-scale (~10 m) grid (modelled at two locations) shows wave amplitudes near Victoria (up to 4.2 m above the state of tide in Esquimalt Harbour; Fig. 4) that are not apparent in either the coarse (~1300 m grid size) or medium (~200 m) scale grids (Cherniawsky et al., 2007). Even where the fine grid is used, tsunami runup may be higher than the amplitudes estimated, because land topography data were not included.

Modelling of a southern Cascadia subduction zone source (Cherniawsky et al., 2007; Fig. 5) reveals that most of the tsunami energy propagates east and west of the rupture, but trapped edge waves travel up the coast to reach Juan de Fuca Strait after ~1.3 hours, with runup likely to exceed 1.5 m only on southwestern Vancouver Island. Wave amplitudes up to 1.1 m are revealed with the use of a fine-scale grid in the harbours of Victoria, suggesting that local runup maxima ≥ 1.5 m are possible. In the absence of fine-scale modelling in Georgia Strait, similar runup maxima cannot be ruled out.

Estimated probabilities of tsunami runup exceeding 1.5 and 3 m for regions of the BC coast (Table 5) are based on: (1) the average recurrence of long M_w~9 (530 ± 260 y) and southern Cascadia $M_w \geq 8$ (1000 ± 250 y) subduction zone ruptures (Frankel, 2011; Goldfinger et al., 2012); (2) the modelling of Cherniawsky et al. (2007) to estimate runup where applicable, and (3) the earthquake magnitude-tsunami runup empirical relations of Abe (1995; Equations 12-14; Table 2) for areas north of the model. Thus, long Cascadia ruptures could produce runup exceeding 1.5 m for all regions, and runup generally exceeding 3 m for all regions except Georgia Strait. Southern Cascadia ruptures are expected to produce runup generally exceeding 1.5 m (and with local maxima ≥ 3 m) only along the southern outer coast of Vancouver Island, with all other areas susceptible only to local maxima ≥ 1.5 m.

Explorer-North America plate boundary

The plate boundary further north along the Pacific coast may present an additional tsunami threat, but this potential is poorly understood. North of the Cascadia subduction zone, the plate boundary transitions from dominantly convergent to dominantly strike-slip (Fig. 6), with ongoing debate on how convergence is accommodated both at the Explorer-North America plate boundary (e.g., Mazzotti et al., 2003b; Rohr and Tryon, 2010) and in the region of the southern Queen Charlotte fault (e.g., Rohr et al., 2000; Bustin et al., 2007). The Explorer plate (Fig. 6) is an oceanic microplate that became detached from the Juan de Fuca plate at ~4 Ma with the formation of the left-lateral Nootka transform fault (Riddihough, 1984). The so-called Winona block may have acted as an independent microplate for a time (e.g., Davis and Riddihough, 1982), but is now generally assumed to be essentially part of the Explorer plate (e.g., Mazzotti et al., 2003b).

Debate is ongoing as to whether the Explorer plate is (1) essentially part of the North America plate, with relative Pacific-North America motion accommodated by distributed right-lateral shear (Rohr and Furlong, 1995; Kreemer et al., 1998) or (2) actively subducting beneath North America (Braunmiller and Nábělek, 2002; Mazzotti et al., 2003b). These end-member models have contrasting implications for the tsunamigenic potential of the region.

The Pacific-Explorer boundary (Fig. 6) may be evolving into a primarily transform boundary, with significant strike-slip motion accommodated along a fault zone within the western Explorer plate in a direction close to the Pacific-North America relative motion (e.g., Dziak, 2006). Similarly, earthquakes located to the northeast tend to exhibit a slip direction aligned with Pacific-North America motion (Ristau, 2004; Rohr and Tryon, 2010). High seismic deformation rates in the vicinity of the Revere-Dellwood-Wilson fault (Willoughby and Hyndman, 2005) suggest that a large portion of Pacific-North America motion is accommodated in this northern region, implying low rates of Explorer-North America convergence there. This is consistent with the plate models of Braunmiller and Nábělek (2002), and with Pleistocene sediment deformation in the Winona Basin (Davis and Riddihough, 1982) that suggests a decrease in convergence rate from southeast to northwest.

The existence of an Explorer microplate independent from North America is supported by GPS data from northern Vancouver Island (Mazzotti et al., 2003b), offshore earthquake slip vectors derived from moment tensor solutions (Braunmiller and Nábělek, 2002; Ristau, 2004), and deformation of offshore sediments (Davis and Hyndman, 1989). The presence of a subducted slab this far north, but not beneath northernmost Vancouver Island, is demonstrated by receiver function analysis (Cassidy et al., 1998; Audet et al., 2008), and by the occurrence of Episodic Tremor and Slip, which infers active subduction (e.g., Kao et al., 2009). Relative motion of ~20 mm/y between the Juan de Fuca and Explorer plates across the Nootka fault (Willoughby and Hyndman, 2005) suggests convergence of ~20-25 mm/y at the southern end of the Explorer-North America margin, consistent with strain accumulation rates inferred from GPS data (Mazzotti et al., 2003b). Lack of a slab beneath northernmost Vancouver Island implies that there has not been significant subduction of the Winona block; the top of a gently-dipping (~9°) subducting slab has been identified from seismic reflection beneath Winona Basin (Yuan et al., 1992), but the late onset of convergence north of Brooks Peninsula and the low convergence rates there suggest a maximum overall convergence of only 30 km (Braunmiller and Nábělek, 2002). GPS data from northernmost Vancouver Island cannot discriminate between strongly-oblique subduction of the Winona block and permanent crustal deformation (Mazzotti et al., 2003b).

For the purposes of this assessment, we assume subduction of the Explorer plate south of the Winona block at a rate of 20-25 mm/y, and a seismogenic and transition zone consistent with GPS and thermal data (Mazzotti et al., 2003b; Fig. 6); we also assume that earthquake rupture will taper to zero to the north by a linear decrease in both slip and locked zone width through the Winona block region from Brooks Peninsula to the Dellwood Knolls (Fig. 6; Table 6). Here we treat the Explorer subduction as an independent source, but it is possible that subduction could occur as an extension of a megathrust earthquake on the rest of the Cascadia system, i.e., along with subduction of the Juan de Fuca and Gorda plates to the south. Using the thrust earthquake magnitude-rupture area empirical relation of Strasser et al. (2010; Equation 6), we calculate that M_w 7.7 (7.4-8.0) earthquakes may occur (Table 6). Using Equations 7-9, we calculate an average recurrence interval of ~333 years (~112-1005 y; Table 6). We also assess a minimum rupture scenario that excludes the Winona block section; we calculate that M_w 7.4 ± 0.3 events could occur on the Explorer section alone, with an average recurrence of ~200 years (Table 6). Earthquakes of this size range have not been noted in the time of written history (~150 y).

Using the empirical relations between earthquake magnitude and near-field tsunami runup developed by Abe (1995; Equations 12-14; Table 2), we estimate that M_w 7.7 earthquakes on the Explorer megathrust could produce significant runup (up to ~7 m) on the west coast of northern Vancouver Island, but the southern part of the west coast as well as the northern mainland coast and southern Haida Gwaii would likely only experience local maxima of runup ≥ 1.5 m (Table 7). Larger events could produce runup consistently exceeding 1.5 m over these areas, while those as small as M_w 7.1-7.4 would have a much more localized impact.

Queen Charlotte margin

Pacific-North America relative motion along the Queen Charlotte margin (Fig. 6) is primarily transform, accommodated by strike-slip events on the near-vertical Queen Charlotte fault. The 1949 *M* 8.1 mainly strike-slip event, the largest historical earthquake in Canada, produced only a small tsunami. Peak-to-trough amplitudes of 7.5 cm and 10 cm were recorded on the Sitka, Alaska, and Honolulu tide gauges, respectively. Tide gauges on the Pacific coast of Canada did not record any waves. Newspapers reported a number of tsunami observations with amplitudes (likely above state of tide) of ~0.5 m at places on Haida Gwaii and on the adjacent BC and Alaska mainland. The highest reported amplitude of ~3 m was described in the Prince Rupert Daily News of August 27, 1949; from the description, this was likely a landslide-induced wave. The earthquake triggered many landslides on Haida Gwaii, and probably also triggered submarine landslides. Because the area is very sparsely populated, local tsunami waves or seiche action resulting from the earthquake were reported from only a few places.

Pacific-North America relative motion is increasingly oblique from north to south along the Queen Charlotte margin, with the component of convergence increasing from ~8 mm/y to ~15 mm/y from northern to southern Haida Gwaii (Mazzotti et al., 2003a). Two end-member models have been proposed for the accommodation of this convergence: (1) underthrusting of the Pacific plate beneath Haida Gwaii (e.g., Hyndman and Ellis, 1981); (2) distributed internal deformation of the Pacific and North America plates (e.g., Rohr et al., 2000). GPS data indicate that 5 ± 2 mm/y convergence is accommodated by internal shortening of the North America plate, but for the remaining 6-10 mm/y of convergence the data cannot distinguish between underthrusting and internal deformation of the Pacific plate (Mazzotti et al., 2003a). The subduction model is supported by the presence of a trench (Queen Charlotte trough) and accretionary prism (Queen Charlotte terrace) seaward of the Queen Charlotte transform fault,

and a dipping low-velocity slab beneath Haida Gwaii defined by receiver function analysis (Smith et al., 2003; Bustin et al., 2007). Gravity and heat flow data are also consistent with underthrusting (e.g., Hyndman and Hamilton, 1993). The main argument against active subduction involves the lack of deep Wadati-Benioff zone seismicity, but this may be precluded by the young age (high temperature) of subducting oceanic crust and the recent (~5 Ma) onset of transpression (Smith et al., 2003).

We assume orthogonal convergence accumulating at an average of 8 mm/y (6-10 mm/y; Mazzotti et al., 2003a) on a 250-km-long subduction fault with a dip of 28° (Bustin et al., 2007) and a thermally-constrained effective full rupture width of ~32 km (~22 km seismogenic zone 150-350 °C; ~20 km transition zone 350-450 °C where coseismic slip decreases linearly to zero downdip; Smith et al., 2003). Based on empirical relations between rupture area and thrust earthquake magnitude (Strasser et al., 2010; Equation 6), megathrust earthquakes of M_w 7.7 (7.5-8.0) may be expected (Table 8). We calculate an average recurrence for such events of ~713 years (266-1916 y; Table 8), based on the convergence rate above and Equations 7-9.

It must be noted that some of the parameters used in the above calculations are constrained over a relatively small area and likely do not apply uniformly along strike; thus, the quoted recurrence times have significant uncertainties. For example, the 28° dip is constrained only beneath central Haida Gwaii, but likely varies with the age of the Pacific plate along the margin. Convergence rates decrease to the north, and the northernmost extent of an underthrust slab is poorly constrained; a rupture length of 250 km corresponds to the most continuous bathymetric expression of the Queen Charlotte terrace (almost the full length of Haida Gwaii). A longer rupture of 400 km (the maximum potential extent of subduction north of the Tuzo Wilson triple junction; Smith et al., 2003) leads to the calculation of an M_w 7.9 (7.6-8.2) thrust event occurring approximately every 810 years (301-2174 y; Table 8). Also, the average convergence rate used implies that there is no significant internal deformation of the Pacific plate, i.e., that thrust earthquakes recorded in the region of the southern Queen Charlotte terrace (e.g., Ristau et al., 2007) solely reflect compression within accretionary sediments, without involvement of oceanic basement. Accommodation of even 2 mm/y convergence by shortening of the Pacific plate would increase these average recurrence intervals by ~30%.

Based on empirical relations between earthquake magnitude and near-field tsunami runup (Abe, 1995; Equations 12-14; Table 2), we estimate that the west coast of Haida Gwaii would be affected by tsunami runup exceeding 3 m for local megathrust earthquakes of M_w 7.8-8.2; M_w 7.5 earthquakes may result in local maxima of that size (Table 9). The west coasts of the northern mainland and northern Vancouver Island would not likely receive potentially damaging runup from M_w 7.5 earthquakes, but runup may exceed 1.5 m (and locally 3 m) for larger events. The southern west coast of Vancouver Island would likely only experience local maxima of runup ≥ 1.5 m for the largest events (M_w 8.2). Tsunami modelling is required to estimate potential tsunami runup on the east coast of Haida Gwaii; this region may be sheltered from such tsunamis, but at this stage we assume that runup similar to that on the northern mainland coast may occur.

An M_w 6.1 thrust earthquake that occurred near the southern portion of the Queen Charlotte fault in 2001 caused a tsunami with maximum recorded amplitudes on Vancouver Island of 23 cm (Rabinovich et al., 2008). The tsunami was not detected at tide gauges on eastern Haida Gwaii or the northern mainland, likely due to coastal sheltering; the Langara tide gauge (northern tip of Haida Gwaii) was not operational at the time (Rabinovich et al., 2008). The larger-than-expected tsunami for the moderate size of the earthquake demonstrates the significant potential hazard of tsunamis sourced from larger thrust earthquakes in this region.

Local crustal earthquakes

Tsunamis may be generated as a result of crustal earthquakes in the North America plate if the seafloor undergoes vertical displacement or if the shaking triggers mass movements that sufficiently disturb the water column (landslide tsunamis are discussed in the next section).

There is a relatively high level of crustal seismicity in the Cascadia forearc region extending from southern Puget Sound northwards to the southernmost Strait of Georgia. The area is under margin-parallel compression; GPS and paleoseismic data, as well as frequency-magnitude relations of crustal seismicity, indicate that long-term shortening of ~3 ± 1.0 mm/y is accommodated seismically within this region (e.g., Hyndman et al., 2003; Sherrod et al., 2008). Large earthquakes ($M \geq 7$) are expected in the overall region about every 400 years (Hyndman et al., 2003); none have occurred in the ~150-year historical period.

Tsunami deposits dating to about 1100 years ago (900-930 CE; Atwater, 1999) have been documented in central and northern Puget Sound, Washington (Atwater and Moore, 1992; Bourgeois and Johnson, 2001), coincident with regions of abrupt uplift and subsidence inferred to result from reverse faulting in an $M \geq 7$ earthquake on the Seattle fault (Bucknam et al., 1992; Fig. 7). The timing of this earthquake also approximately coincides with that of mass failures into nearby Lake Washington (Jacoby et al., 1992; Karlin et al., 2004) and in the Olympic Mountains ~75 km from the Seattle fault (Schuster et al., 1992). Evidence for smaller events since ~7 ka is documented by Sherrod et al. (2000). Modelling of an M_w 7.6 Seattle fault source results in a tsunami wave > 3 m reaching the nearby Seattle waterfront within 3 minutes (Koshimura et al., 2002), with waves less than 1 m in amplitude by the time they exit Puget Sound into the Canadian waters of Juan de Fuca Strait. Thus, future tsunamis from crustal earthquake sources in central and southern Puget Sound are unlikely to be hazardous to the BC coastline.

However, several lines of evidence suggest that tsunamigenic earthquakes may also be generated from sources in the northern Puget Lowland and eastern Juan de Fuca Strait. A number of active transpressional faults with documented surface offsets and Holocene displacements underlie the region, including the SE-NW-trending Southern Whidbey Island fault zone, and the E-W-trending Devil's Mountain fault zone, Utsalady Point fault and Strawberry Point fault (e.g., Johnson et al., 2001; Hayward et al., 2006; Fig. 7). Minimum rates of vertical displacement are estimated at 0.6 mm/y on the Southern Whidbey Island fault zone, and a composite of 0.5 mm/y on the latter three faults; the true rates may be higher (Johnson et al., 1996; 2001). Based on the mapped fault lengths, earthquakes of $M > 7.0$ on the Southern Whidbey Island fault, M 7.5 on the Devil's Mountain fault, and $M \geq 6.7$ on the Utsalady Point and Strawberry Point faults, are possible (Johnson et al., 1996; 2001; 2004).

The Holocene paleoseismic record of earthquakes on these faults is likely far from complete, and cannot be used to estimate the rates of earthquake recurrence (e.g., Johnson et al., 2001), but the effort has recently been aided by the use of LiDAR data to identify onshore fault scarps throughout the Puget Lowland (e.g., Haugerud et al., 2003). So far, significant Holocene displacements have been documented from one earthquake on the southern Whidbey Island fault zone (~3000 cal. y BP; Kelsey et al., 2004), and two on the Utsalady Point fault (~100-400 and ~1100-2200 cal. y BP; Johnson et al., 2004).

A number of tsunami deposits have been documented at two sites in the eastern Strait of Juan de Fuca: northern Whidbey Island (Williams and Hutchinson, 2000) and Discovery Bay (Williams et al., 2005). Some of these approximately correlate with Cascadia plate-boundary

tsunamis, but others may have a more local source such as one of the above faults, with several tsunami layers at Discovery Bay within the age range of the penultimate earthquake on the Utsalady Point fault (Johnson et al., 2004; Williams et al., 2005). The southern Whidbey Island fault earthquake predates the tsunami records of the above two sites, but a possible tsunami deposit was noted at a marsh on Whidbey Island that was uplifted during the event (Kelsey et al., 2004). Mathewes and Clague (1994) document evidence from southern Vancouver Island and the Vancouver region that suggests the occurrence of widespread vertical displacements during two earthquakes on crustal faults of unknown location within the last few thousand years (~2000 and ~3700 cal. y BP). Microfossil data indicating a marine incursion at an uplifted site near Vancouver suggest that the earlier event may have been accompanied by a tsunami (Mathewes and Clague, 1994).

In southern Georgia Strait, seismic reflection data show offsets of the seafloor indicating active faulting (Mosher et al., 2000). However, further north in the strait, surface displacements are less clear. A concentration of shallow (< 6 km depth) seismicity occurs ~30 km west of Vancouver, including two moderate felt earthquakes in 1975 (M 4.9) and 1997 (M 4.6) with mechanisms and aftershock sequences indicating thrust faulting on a north-dipping plane (Cassidy et al., 2000). No apparent surface offset is visible on a nearby seismic line (Mosher et al., 2000), but multibeam bathymetry data show evidence of surface disturbance to the southwest near the surface projection of the fault plane, as noted by Dash et al. (2007). Multibeam and seismic data provide evidence of active surface faulting in two other areas nearby to the south (Porlier Pass fault) and to the east (Fraser delta fault) (Barrie and Hill, 2004); however these faults are not apparently consistent with N-S compressional tectonics.

No confirmed tsunami deposits have yet been found around the Canadian Strait of Georgia (Clague et al., 2000; J. Clague, personal communication, 2010), suggesting that there have probably been no significant events within the last several hundred years. However, small events, or events that occurred more than a few hundred years ago, may not be preserved in the present-day stratigraphy. A study of tsunami deposits up to four years after the 2004 Indian Ocean tsunami suggests that initial deposits from tsunamis with a runup of less than 3 m are unlikely to be preserved, particularly in regions with high rainfall (Szczuciński, 2012). In southern Georgia Strait, just south of the U.S. border, a probable tsunami deposit is associated with paleoseismic evidence for an M~6-6.5 earthquake ~1.3-1.0 ka on one of three recently identified onshore-offshore Holocene faults (Birch Bay fault, Fig. 7; Kelsey et al., 2012).

Here we describe an approach that we use to approximate the tsunami hazard from crustal submarine faults. Based on a recurrence relation calculated from the seismicity of a ~80 km by 80 km region that covers eastern Juan de Fuca Strait, Haro Strait and the San Juan Islands, we calculate that M_w 7.5 earthquakes may be expected with an average recurrence of ~2830 years (878-9806 y). M_w 7.5 was chosen as it represents the estimated maximum magnitude on the mapped Devil's Mountain fault, which passes close to Canadian coastlines (Fig. 7). Assuming that such earthquakes may occur anywhere within the defined region with the same frequency per unit area, we estimate the potential tsunami impacts along the adjacent coastlines (Table 10). From the empirical tsunami runup-earthquake magnitude relations of Abe (1995; Equations 12-14; Table 2), an M_w 7.5 earthquake can produce mean local runup ≥ 1.5 m (and local maxima ≥ 3 m) up to 60 km from the source, with local maxima ≥ 1.5 m up to 120 km. Using 60 km as the radius of a circle centred on a coastal point of interest, where the circle is assumed to lie half underwater (potentially tsunamigenic earthquakes) and half on land (no tectonic tsunamis expected), we calculate the expected frequency of M_w 7.5 events sourced within half the area of

the circle; this is the approximate frequency of events that could produce mean local runup ≥ 1.5 m at the coastal site. Similarly, the frequency of M_w 7.5 events estimated over half the area of a circle with a 120-km radius is equivalent to the frequency of events that could produce local runup maxima ≥ 1.5 m. However, the maximum area in this case is encompassed by a 60-km radius (larger areas are either under land or outside of the seismicity zone); therefore we exclude the probability of local runup maxima from distances greater than 60 km. It should be noted that the resultant probabilities given in Table 10 (~1.6 and ~0.8% probability of runup exceeding 1.5 and 3 m, respectively, in 50 y) represent a range of maximum estimates that assume pure thrust faulting. Earthquake focal mechanisms imply a mixture of thrust and strike-slip faulting (e.g., Balfour et al., 2011); an M_w 7.5 earthquake with a significant strike-slip component would result in significantly smaller tsunami runup due to a smaller vertical displacement of the seafloor.

Compared with the area discussed above, seismicity rates in the northern and central Strait of Georgia and in western Juan de Fuca Strait are significantly lower, and no evidence of active faulting has been documented. Thus, we assume that these areas have a lower probability of potentially damaging tsunami runup, but we cannot discount it completely. We include the whole Strait of Georgia in this lower-hazard zone, because significant seismicity occurs only at the southernmost end. We assign an arbitrary range of low probabilities that are half those estimated for eastern Juan de Fuca Strait (Table 10).

A concentration of significant crustal seismicity also occurs in Hecate Strait (between Haida Gwaii and the northern BC mainland (Fig. 6); the few available earthquake focal mechanisms show a combination of thrust and strike-slip faulting (Ristau et al., 2007). Here, the rate of long-term deformation indicated by GPS data is significantly larger than the deformation rate inferred from recorded seismicity; possible reasons for the discrepancy include aseismic/postseismic deformation and infrequent large earthquakes on one or more faults that are currently locked (Bustin, 2006). Assuming the latter, a maximum fault area of 1500 km^2 and a convergence rate of 5 mm/y (Bustin, 2006), earthquakes up to M_w 7.1 (6.8-7.4) may be expected on crustal faults in Hecate Strait, with an average recurrence of ~728 years (271-1954 y; Table 11).

Taking a similar approach as described above for eastern Juan de Fuca Strait and southern Georgia Strait, we use the tsunami runup relations of Abe (1995; Equations 12-14; Table 2) to estimate the potential impact on the coasts of eastern Haida Gwaii and the adjacent mainland (Table 11). As noted above, the calculated probabilities represent a maximum, as they assume pure thrust faulting. The minimum values provided come from the recurrence relation of the actual earthquake catalogue (Bustin, 2006), thereby allowing for the possibility that the bulk of the ~5 mm/y convergence apparent from the GPS data is accommodated aseismically.

The approach outlined above provides an estimate of the maximum probability of potentially damaging tsunami runup from earthquakes on crustal submarine faults. However, many uncertainties remain, not least regarding the proportion of dip-slip motion that may occur on these faults. If fault motion has a significant strike-slip component, a far smaller tsunami will result than for a pure thrust earthquake of the same magnitude, and the M_w-runup relations of Abe (1995; Equations 12-14) will overpredict the tsunami runup for the magnitudes considered.

Landslide Tsunamis

Local landslides

Locally destructive tsunami waves are to be expected from subaerial and submarine landslides on the Pacific coast (e.g., Mosher, 2009). The 1946 M_s 7.3 crustal earthquake on central Vancouver Island (Fig. 1) did not offset the seafloor, but numerous subaerial and subaqueous failures were triggered, some of which generated locally dangerous waves (Hodgson, 1946; Rogers and Hasegawa, 1978; Mosher et al., 2004). Some damage and flooding occurred as a result, and one man drowned when his boat was tipped over by waves generated by a submarine failure of Mapleguard Spit, at Deep Bay on the east coast of Vancouver Island (Rogers, 1980; Table 1; Fig. 1).

Other historical landslide tsunamis have occurred in fjords along the mainland Pacific coast of North America. These areas are particularly at risk due to the potential failure of steep fjord walls or the fronts of submarine deltas with high sedimentation rates; high runup is possible from relatively small failures due to the confined nature of the long narrow basins. The most spectacular historical example occurred in Lituya Bay, Alaska (Fig. 1), in 1958. A subaerial rockfall (~30 million m^3) at the head of the inlet was triggered by near-epicentral shaking from an M_w 8.2 earthquake on the Fairweather fault; water displaced by the failure reached the global historical record runup elevation of 524 m on the opposite side of the inlet, destroyed forest over an area of ~10 km^2, and resulted in the deaths of two fishermen in the outer bay (Miller, 1960). A similar (but smaller) type of subaerial failure occurred in Knight Inlet, BC, probably in the 16th century (Table 1; Fig. 1). A rock avalanche (~3 million m^3) on the steep fjord wall entered the inlet to produce a tsunami that wiped out the village of Kwalate and its inhabitants on the other side of the inlet; modelling suggests wave amplitudes of 2-6 m prior to runup (Bornhold et al., 2007). ~15 km further north on the edge of Knight Inlet, tsunami waves resulted from a rockfall or rock slide in 1999; the Three Finger Peak landslide (~0.2-2 million m^3) ran out over gentle slopes for ~3.5 km before entering the inlet, where waves carried log boom equipment to the head of the inlet, 25 km to the northeast (van Zeyl, 2009).

An evaluation by van Zeyl (2009) concludes that the tsunami hazard from subaerial landslides is significantly less in Howe Sound (a more populated fjord north of Vancouver, Fig. 1) than in Knight Inlet, where submarine debris cones have been documented at six sites. However, submarine failures in Howe Sound must be considered a potential tsunami source. A large delta-front slide in 1955 caused the collapse of waterfront pulp mill facilities, although no damaging waves were documented (Terzaghi, 1956); side-scan sonar data reveal widespread evidence of mass movements in the delta region (Prior et al., 1981).

In 1975, a submarine slide in Kitimat Arm triggered a tsunami with coastal runup of up to 8.2 m, resulting in substantial damage at the head and on both sides of the ~4-km-wide inlet (Table 1; Fig. 1); oscillations across the inlet were observed for an hour after the event initiation (e.g., Skvortsov and Bornhold, 2007). The failure involved a total volume of ~55 million m^3, consisting of delta front and fjord wall sediments as well as fjord bottom sediments that became entrained in the ~1-km-wide debris flow as it travelled ~5 km down the fjord axis (Prior et al., 1982; Skvortsov and Bornhold, 2007). The slide was likely triggered by minor construction at low tide on marginally-stable delta sediments (Murty, 1979). Several previous landslides in Kitimat Arm had been documented since 1952, some of which resulted in low amplitude waves, with a more significant amplitude of 2.8 m observed for a landslide tsunami in 1974 (Murty, 1979). Construction (causing overloading of delta slope sediments) combined with an extreme

low tide was also the probable trigger for a submarine landslide in delta sediments and subsequent tsunami in Skagway, Alaska, in 1994, that caused one fatality and ~$20 million in damage to harbour and dock facilities (e.g., Kulikov et al., 1996; Table 1; Fig. 1).

The Strait of Georgia, including low-lying parts of greater Vancouver, is also potentially at risk from submarine landslide tsunamis, particularly from the foreslope of the Fraser River delta (Fig. 1). Shallow sediments (upper 10-20 m) over much of the subaerial and submarine delta have been identified as susceptible to seismic liquefaction (e.g., Mosher et al., 1997). There is evidence for mass failure at a multitude of scales, including extensive young (~150-1000 y) failure deposits at the base of the southern delta slope off Roberts Bank that may have resulted from one catastrophic failure or from a sequence of smaller flows (e.g., Christian et al., 1997). The Fraser delta, offshore of the main channel mouth, is the focus of ongoing extensive geophysical, geotechnical and other observations, largely with the aim of better understanding mechanisms of submarine sediment dispersal, including the potential for tsunamigenic failures (e.g., Lintern and Hill, 2010). Modelling of tsunamis from theoretical 0.23 and 0.75 km^3 failures of delta foreslope sediments can produce peak-to-trough wave amplitudes of up to 8 and 18 m, respectively, across the strait on the east coasts of Mayne and Galiano Islands; smaller waves (1-4 m) result for the mainland coast due to bathymetric reflection of the initial wave (Rabinovich et al., 2003). Dunbar and Harper (1993) modelled larger foreslope failures (2.5-7.5 km^3) as a number of independent, slow-moving slabs, resulting in maximum near-source coastal wave amplitudes of ~4 m.

With no frequency-size data available for potentially tsunamigenic local landslides on the Pacific coast, we cannot include these sources in the probabilistic tsunami analysis. However, all Pacific coastlines are considered at risk from locally-generated waves due to the high susceptibility of these areas to landslides, or proximity to high-susceptibility areas (Bobrowsky and Dominguez, 2010).

Continental slope landslides

There is evidence for numerous slope failures up to at least 5 km wide along the deformation front (frontal ridges) of the Cascadia subduction zone offshore Vancouver Island (e.g., Pohlman et al., 2008; Scholz et al., 2010; Fig. 1). Study of these failures is ongoing and as yet is far from providing a size-frequency relationship. A more detailed investigation of a 2-km-wide slide (likely a few thousand years old) reveals: a 300-m high headscarp; probable fault control with the failure bound by two margin-perpendicular normal faults; coincidence of the gas hydrate bottom-simulating reflector (BSR) with the glide plane of the slide suggesting that failure is concentrated at the strength contrast between underlying weak gas-charged sediments and overlying hydrate-cemented sediment (López et al., 2010). Slope failure is most likely during strong ground shaking; if coincident with megathrust seafloor displacement, such failures could contribute to locally amplified tsunamis as suggested for the 2004 Sumatra event (e.g., Tappin et al., 2007). Slope stability analysis is required to determine whether tsunamigenic failures may be triggered by smaller earthquakes offshore. The rare occurrence of much larger ("super-scale") slumps (dated at ~110, ~450, and ~1210 ka) has been documented further south along the margin, offshore southern Oregon, and may have resulted in very large tsunamis (Goldfinger et al., 2000; McAdoo and Watts, 2004).

If tsunamigenic continental slope failures were assumed to occur at a similar rate as we estimate for the Atlantic margin (see later section), the hazard is negligible compared to other Pacific tsunami sources. The frequency of large slumps appears to be significantly lower than

that of large earthquakes. Thus, we do not include them as a separate tsunami source, but we point out that future probabilistic tsunami hazard analyses of the Cascadia megathrust source should include such failures among the tsunami source variations.

Hawaiian Islands

Seafloor surveys have revealed the deposits of numerous large debris avalanches and slumps on the flanks of the Hawaiian ridge; 68 of these are longer than 20 km (e.g., Moore et al., 1994a). Possible tsunami deposits and evidence for soil stripping on the southeastern Hawaiian islands of Lanai and Hawaii suggest tsunami runup of up to 400 m or more, up to 6 km inland; the ages of these deposits are consistent with the ~125 ka Alika phase 2 debris avalanche off the western flank of Mauna Loa volcano on the island of Hawaii, and the runups are consistent with tsunami modelling of this deposit (Moore and Moore, 1984; McMurtry et al., 2004a, b). Similarly, the ages of possible tsunami deposits reported from Lanai and nearby Molokai correlate with the Alika phase 1 deposit offshore, dated at ~200-250 ka (Moore et al., 1994b; Rubin et al., 2000; Webster et al., 2007).

Based on tsunami modelling of a large deposit (~5000 km^3) off the northeastern flank of one of the islands, Ward (2001) suggests that a large volcanic flank collapse in Hawaii could generate tsunami runup on the Pacific coast of North America of up to ~20 m. However, dispersion effects were neglected in the modelling, and it is likely that significant attenuation would occur over the ~4000 km propagation distance (Pararas-Carayannis, 2002). This is demonstrated by more realistic models of flank collapses off the Canary Islands that result in wave amplitudes of ~1-3 m for similar propagation distances in the Atlantic (Mader, 2001; Gisler et al., 2006), or ~10% of the Ward (2001) model values. Without further constraints, but broadly consistent with the above models, we make the assumption that large flank collapses, as evidenced by giant failure deposits offshore the Hawaiian Islands, could result in local mean tsunami runup $\geq$ 1.5 m on the outer Pacific coast of Canada, but that local mean runup $\geq$ 3 m could only result from failures on the northeastern flanks, where the main tsunami energy would be directed towards Pacific Canada.

McMurtry et al. (2004b) present a compilation of age estimates for giant Hawaiian submarine landslides. The last nine giant failures have occurred on the flanks of the island of Hawaii, the largest, youngest, and most volcanically active in the island chain. The occurrence of eleven events in the last million years provides an average recurrence interval of ~91 ky. We take this as a minimum recurrence for local maximum runup $\geq$ 1.5 m on the Pacific coast of Canada (Table 12). Making the assumptions that future failures are equally likely on all three flanks of the island, and that failures on the western flanks are least likely to prove hazardous to Canada due to wave scattering to the northeast through the Hawaiian Islands, provides a best estimate of ~136 ky recurrence for local mean runup $\geq$ 1.5 m. We calculate a maximum recurrence of ~272 ky with the possibility that only failures on the northeastern flanks may present a tsunami hazard for Canada; we also choose this value as a minimum recurrence for local mean runup $\geq$ 3 m. Thus, the Pacific coast tsunami hazard from Hawaiian landslides is negligible. Without detailed tsunami modelling, we assume that Georgia Strait would be protected from potentially damaging waves, but we apply equal hazard to all other Pacific coastal zones (Table 12).

Aleutian Islands

Large submarine failures off the Aleutian margin (Fig. 2) are a potential source of damaging tsunami runup on the west coast of North America. Waythomas et al. (2009) modelled

eight hypothetical mass failures ranging in volume from 160 km^3 to 1440 km^3; their results suggest a threshold volume of ~400 km^3 for submarine landslides south of the Aleutian arc that may result in potentially damaging (≥ 1.5 m) tsunami runup on the Canadian Pacific coast; runup greater than ~3 m appears possible for mass failures greater than ~500 km^3 in the central Aleutian arc and ~800 km^3 in the west.

The region has not been surveyed at a resolution high enough to constrain either the size or possible frequency of large failures in the past; Waythomas et al. (2009) use a probabilistic approach developed by Watts (2004) to calculate an average recurrence interval of ~2000 years for failures with volume ≥ 100 km^3 that could be triggered by earthquakes of M_w 5.1-8.9. Return periods greater than 2000 years make a negligible contribution to the overall tsunami hazard of the outer coasts of British Columbia. Without further constraints (P. Watts, personal communication, 2011), we assume approximate best estimates of 3000 years (2500-5000 y) and 4000 years (3500-8000 y) for the recurrence of local mean tsunami runup exceeding 1.5 m and 3 m, respectively. In the absence of more detailed tsunami modelling, we assume that Georgia Strait would be protected from potentially damaging waves, but we apply equal hazard to all other Pacific coastal zones (Table 13).

ATLANTIC COAST

Unlike the Pacific coast, the Atlantic coast of Canada is a passive margin, located far from plate boundaries, and there are far fewer compressive plate boundaries around the Atlantic than around the Pacific Rim (Fig. 2). Consequently, far fewer tsunamis have been recorded in historical time. However, significant transoceanic tsunamis from convergent plate boundaries are possible, as illustrated by the 1755 Lisbon tsunami generated by a large thrust earthquake offshore southwestern Portugal and observed in Newfoundland (e.g., Roger et al., 2010a). Megathrust earthquakes in the northeastern Caribbean may present another threat, although further study is required to assess both their potential and their far-field hazard. The 1929 Grand Banks event demonstrated the potential for significant locally-generated landslide tsunamis on the east coast. We also consider far-field sources of landslide tsunamis in the eastern Atlantic Ocean.

Far-field tsunamis may be focussed towards the Canadian Atlantic coast by topographic steering to have a greater impact than otherwise anticipated. For example, during the 2004 Indian Ocean tsunami, the largest tsunami waves in the North Atlantic (~0.8 m) were recorded at Halifax, Nova Scotia, ~20,000 km from the source, due to the Mid-Atlantic Ridge acting as a waveguide (Rabinovich et al., 2006; Thomson et al., 2007).

Earthquake Tsunamis

Gibraltar-Cadiz

The catastrophic 1755 Lisbon earthquake, estimated at M_w 8.5 ± 0.3 (Solares and Arroyo, 2004) to M_w~9.0 (Muir-Wood and Mignan, 2009), triggered a damaging tsunami with many fatalities in western Europe and Morocco (e.g., Baptista et al., 1998). The tsunami was also observed on western Atlantic coasts in Brazil, the Caribbean, and Newfoundland, Canada. At Bonavista, Newfoundland, the harbour was drained for a period of ten minutes and then flooded,

along with the adjacent meadows (Tocque, 1846; Ruffman, 2006). An additional smaller transatlantic tsunami occurred in 1761 and may have been sourced from an aftershock of the 1755 Lisbon earthquake (e.g., Lander et al., 2002).

The source of the Lisbon earthquake is still under debate, but there is consensus that it must lie in the general region offshore southwestern Iberia (e.g., Baptista et al., 2003; Fig. 8). The plate boundary between Africa (Nubia) and Eurasia is diffuse (~200 km north to south) and little understood in this area between the Gloria transform fault to the west (Fig. 9) and the transpressive Rif-Tell fault zone to the east (e.g., Zitellini et al., 2009). Several faults (Fig. 8) have been proposed as the source of the Lisbon earthquake, including the Marques de Pombal thrust (Zitellini et al., 2001), Horseshoe fault (Stich et al., 2007), Gorringe fault (Johnston, 1996), Guadalquivir Bank (Baptista et al., 2003), and Gulf of Cadiz-Gibraltar Arc seismogenic zone (Gutscher et al., 2002). With the exception of the Gibraltar subduction fault, none of these faults are large enough to produce an M_w 8.5 earthquake, and various composite sources have been proposed (e.g., Baptista et al., 2003; Gràcia et al., 2003). Although large enough to produce an M_w 8.5-8.7 earthquake, the Gibraltar seismogenic zone alone cannot match all the tsunami observations; an additional source to the northwest may be necessary (Gutscher et al., 2006; 2009a).

We assess a range of possibilities where "Lisbon-type" large earthquakes occur on one or more dip-slip faults due to the Africa-Eurasia convergence or Gibraltar Arc motions of 3-5 mm/y (Argus et al., 1989; Fernandes et al., 2003; 2007; Serpelloni et al., 2007).

(1) For the Marques de Pombal-Guadalquivir composite source (connected by a décollement at depth), Baptista et al. (2003) estimate a rupture area of ~11,000 km^2, fault dips of 24-45º, and slip of 20 m (to match tsunami observations and earthquake size M_w 8.55). These estimates result in ~14-18 m northwest-southeast horizontal compression and an average recurrence of ~2800-3600 years at 5 mm/y convergence (~3500-4500 y at 4 mm/y; Table 14).

(2) Stich et al. (2007) propose that the 1755 earthquake could have been a compound event occurring mostly within the upper mantle on faults in high-rigidity old oceanic lithosphere beneath the Horseshoe plain, including the Horseshoe fault. Assuming a 50-km thick seismogenic zone, an average rigidity of 6 x 10^{10} N/m^2, fault dips of 55°, and slip of 5-10 m, a cumulative fault length of 175-350 km would be required to produce an earthquake of M_w 8.5 (Table 14). 10 m of fault slip would result from 5.75 m of accumulated horizontal strain, with an average recurrence of 1150-1450 years at 4-5 mm/y.

(3) The shallowly east-dipping Gibraltar seismogenic zone has dimensions estimated at 180 km x 210 km (Thiebot and Gutscher, 2006); 5 m slip results in an M_w 8.5 earthquake (Table 14; M_w 8.7 from 10 m slip). Evidence for active subduction (summarized in Gutscher et al., 2002; 2009a; Thiebot and Gutscher, 2006) includes: the presence of an eastward-thickening, actively-deforming accretionary prism in the Gulf of Cadiz; heat flow anomalies consistent with an active east-dipping thrust; seismic tomography showing an east-dipping slab beneath Gibraltar; earthquake hypocentres that deepen to intermediate depths below Gibraltar and the western Alboran Sea and to > 600 km depth beneath southern Spain; active extension in the Alboran Sea, interpreted as back-arc extension due to slab rollback, although others have attributed it to mantle delamination or slab break-off (e.g., Calvert et al., 2000). GPS data indicate motion to the west-southwest of a Gibraltar block relative to Eurasia at ~2.5-4.5 mm/y (Stich et al., 2006; Fernandes et al., 2007; Vernant et al., 2010). This motion is likely the result of extrusion due to transpression; slab rollback may also play a part, and was likely important in the past (Negredo et al., 2002). Subduction velocity is likely approximately equivalent to the

westward block motion, representing the motion of the upper plate toward the trench; however, this may be an underestimate if there is significant interseismic strain accumulation on the locked subduction fault. For 5 mm/y, average recurrence of an M_w 8.5 event (5 m slip) is 1000 years; for 3.5 and 2.5 mm/y, recurrence is ~1400 and 2000 years, respectively (Table 14).

Paleoseismic data provide important clues to the past recurrence of large earthquakes and tsunamis in the vicinity of the Iberian Peninsula. Tsunami deposits on the coasts of southwestern Spain (e.g., Luque et al., 2002; Morales et al., 2008) and Portugal (Scheffers and Kelletat, 2005) document several events in the last ~2000 years, all of which may correlate with events in the Portuguese historical tsunami catalogue (Baptista and Miranda, 2009). The most recent deposit correlates with the 1755 Lisbon tsunami; another widespread deposit that likely represents a similar tsunami impact has been dated at ~2000-2300 cal. yr BP, likely correlative with a tsunami documented in 218 BCE (e.g., Luque et al., 2002).

Offshore southwestern Iberia, turbidite deposits in separate deep sea basins (correlated over distances of up to ~175 km) are likely the product of shaking in large earthquakes (e.g., Gràcia et al., 2010). A few of the deposits are found only in localized basins, and probably result from smaller earthquakes, e.g., a thin turbidite found only in the Infante Don Henrique Basin (closest to the continental margin; Fig. 8) and dated at 1908 ± 8 CE correlates with the onshore 1909 Bonavente *M*~6.0 earthquake (no tsunami observed; Garcia-Orellana et al., 2006). Gràcia et al. (2010) found seven widespread events dating back to ~8850 cal. yr BP; within the last 7000 years, all widespread turbidite events may be correlated with tsunami deposits onshore, with the exception of the most recent widespread turbidite that has been precisely dated at 1971 ± 3 CE, likely representing the *M* 8.0 1969 Horseshoe earthquake, which triggered only a small tsunami. Assuming that the remaining four widespread earthquake-tsunami events since 6000-7000 cal. yr BP are equivalent to the *M*~8.5 Lisbon event, and that no events of this size are missing from the paleoseismic record, estimated interevent times range from ~1670 to ~3070 years. Incorporating the previous two widespread turbidite events (one of which may have had a climatic rather than seismic trigger) implies 5 or 6 events in the last ~9000 years and a mean recurrence of ~2170 or ~1730 years, respectively (uncertainty range ~870-2790 y; Table 14). Several of the proposed fault sources for the 1755 Lisbon earthquake, as described above, are compatible with these paleoseismic recurrence intervals.

Geist and Parsons (2009) apply an alternate approach to assess the possible frequency of Lisbon-type tsunamigenic events, based on convergence rates of 1-5 mm/y and global seismic moment distribution statistics from other oceanic convergent boundaries. They calculate a very long average recurrence interval of ~10,000 years (min. 8000 y) for M_w 8.5 earthquakes; however, the mean recurrence interval of ~3000 years (min. ~1700 y) for M_w 8.2 events is more in line with the paleoseismic and tectonic data above.

Roger et al. (2010a, b; 2011) modelled the Marques de Pombal-Guadalquivir composite source, as proposed by Baptista et al. (2003), to simulate far-field tsunami wave amplitudes and runup in the eastern Caribbean and in Newfoundland, for comparison with historical reports. One of the two main energy pathways of the teletsunami is directed towards Newfoundland, the other towards South America (Fig. 9). The use of high resolution bathymetric (and topographic) grids for the coast of southeastern Newfoundland allows for accurate modelling of propagation and inundation; the simulation produces runup exceeding 1.5 m along much of the coast, and up to 2.5 m or more on the Bonavista peninsula, in agreement with historical accounts of inundation (Roger et al., 2010a).

Barkan et al. (2009) carried out tsunami modelling for a number of theoretical thrust fault sources unconstrained by the locations of mapped faults. They conclude that to match far-field observations in 1755, including a lack of observations in the eastern U.S., the source must be located south of the Gorringe Bank in the Horseshoe Plain (Fig. 8); this allows Gorringe Bank, the Madeira-Tore Rise and the Azores (Fig. 9) to act as topographic scatterers to shield the U.S. east coast. Barkan et al. (2009) discount sources in the localities of the Marques de Pombal and Gulf of Cadiz faults as they produce relative far-field wave amplitudes that are too low in the Caribbean and/or too high in the southern U.S. compared with the observations. However, both sources can produce potentially damaging far-field wave amplitudes along the east coasts of both Newfoundland and Labrador. Conversely, Muir-Wood and Mignan (2009) propose that a source orientation of ~NNW-SSE (such as the Gulf of Cadiz fault) may have been necessary to produce the relatively high and low tsunami amplitudes in the Caribbean and eastern U.S., respectively.

We consider both the Marques de Pombal-Guadalquivir (Baptista et al., 2003) and Gulf of Cadiz (e.g., Thiebot and Gutscher, 2006) viable sources of past and future "Lisbon-type" events, capable of producing widespread runup in excess of 1.5 m, and possibly greater than 3 m along parts of Atlantic Canada, and for which we use the estimated paleoseismic recurrence intervals in our analysis (Tables 14-15). We assume that the inner Atlantic coastlines would be relatively sheltered, with only local runup maxima ≥ 1.5 m (Table 15).

NE Caribbean: the Puerto Rico trench and the Lesser Antilles

Subduction zone sources in the northeastern Caribbean are closer than the Lisbon earthquake source area to the Canadian Atlantic coast (minimum ~2600 km rather than 3700 km; Fig. 2) and may present a significant tsunami threat, but the potential hazard is poorly understood, requiring much further study. Several locally devastating tsunamis have occurred in the last 500 years of Caribbean history (e.g., O'Loughlin and Lander, 2003), but none have had significant far-field impacts recorded on the Atlantic coast of North America. However, the recurrence interval of events potentially damaging to Canada may be much longer than the historical record.

Relative to the Caribbean plate, Atlantic oceanic crust (North America and South America plates in the Greater and Lesser Antilles, respectively) is moving to the WSW at ~20 mm/y (Dixon et al., 1998; DeMets et al., 2000). Orthogonal convergence occurs at the Lesser Antilles subduction zone (Fig. 10), where the South America plate subducts westwards beneath the Caribbean plate with associated island arc volcanism, whereas along the Greater Antilles plate boundary, convergence is very oblique and arc volcanism has been absent since ~35 Ma (e.g., Jolly et al., 2008). No great megathrust earthquakes ($M \geq 8$) have occurred on the Antillean arc in the last 150 years, but several authors have recently drawn attention to their potential (e.g., Geist et al., 2006; Gutscher et al., 2008; Heuret et al., 2011).

At Hispaniola, plate motion is strongly partitioned between margin-normal and margin-parallel components. GPS data indicate that the Northern Hispaniola thrust fault accommodates 5.2 ± 2.0 mm/y of N-S convergence between the Caribbean plate and the Bahama carbonate platform (on the North America plate), and the onland Septentrional and Enriquillo faults accommodate 12.8 ± 2.5 and 9.0 ± 9.0 mm/y, respectively, of ~E-W left-lateral strike-slip motion (Calais et al., 2002). A series of large thrust earthquakes occurred on the Northern Hispaniola fault in 1946-1953; up to 5-m tsunami waves triggered by an M_s 8.1 earthquake in 1946 killed 1790 people in the Dominican Republic, and a further 75 died in a tsunami generated by an M_s 7.9 aftershock a few days later (Lander et al., 2002); both tsunamis were also recorded at Daytona Beach, Florida, and Atlantic City, New Jersey (Bodle and Murphy, 1948).

Further east, there is oblique subduction of old oceanic crust of the North America plate beneath the Puerto Rico-Virgin Islands block, which moves in the same direction as the Caribbean plate, but slightly slower at ~17 mm/y (Jansma et al., 2000). Strain partitioning is less apparent here (e.g., ten Brink and Lin, 2004; Manaker et al., 2008), although some left-lateral slip is likely accommodated on the offshore east Septentrional, Bowin, and Bunce faults (e.g., LaForge and McCann, 2005). Slip vectors of thrust events on the interface tend to be more oblique (closer to the ENE plate motion vector) than on the Northern Hispaniola fault to the west, but some events, including an M_w 7.8 earthquake in 1943, exhibit more orthogonal slip to the north-northeast (Doser et al., 2005). The 1943 event involved oblique thrusting on the plate interface, but it did not produce an observable tsunami, and neither did an estimated M~8 event in 1787 that likely occurred on the Puerto Rico trench, although it is possible that the source was the Bowin strike-slip fault (McCann, 1985; Dolan and Wald, 1998).

The 1943 earthquake rupture coincides with the occurrence of a subducted high-standing carbonate bank (Mona Bank), similar to the 1946-53 sequence on the Northern Hispaniola fault further west, where rupture coincided with the Navidad and Silver banks (Dolan and Wald, 1998; Mann et al., 2002; Fig. 10). This suggests that seismic rupture tends to be isolated to these strongly locked collisional asperities, with only partial locking of the remainder of the interface; thus, the occurrence of an M~9.0 megathrust event may be unlikely because a smooth interface may be necessary to promote large ruptures (e.g., Hyndman, 2007). In addition, modelling of GPS data from Puerto Rico and the Virgin Islands suggests little or no trench-perpendicular compressional strain accumulation (ten Brink and López-Venegas, 2012). However, large subduction earthquakes cannot yet be discounted, especially in light of the occurrence of the last two global $M \geq 9.0$ earthquakes (Sumatra 2004 and northeastern Japan 2011) on subduction faults where such large events were not previously considered possible due to factors relating to the obliquity of convergence (northern Sumatra) and low apparent coupling with frequent moderate events (Japan trench; e.g., Gutscher and Westbrook, 2009).

LaForge and McCann (2005) suggest that the Puerto Rico trench can be divided into western and eastern zones with respectively high and low degrees of seismic coupling (80% or ~12 mm/y vs. 20% or ~3.5 mm/y seismic slip). Using Gutenberg-Richter seismicity relations and an estimated maximum magnitude of 8.2 for each zone, they estimate recurrence intervals for an M 8.0 earthquake of 1400 and 3000 years for the western and eastern zones, respectively. Combining the recurrence of M 8.0 events in both zones gives 950 years if both zones follow a Gutenberg-Richter relation or 510 years if characteristic events occur in the eastern zone. Earthquakes of this size would be unlikely to produce tsunami waves damaging to Atlantic Canada, particularly if slip is very oblique.

Geist and Parsons (2009) take a different approach based on tectonic slip rates, full locking, the frequency-magnitude statistics of global subduction zone earthquakes, and a seismogenic zone between 5 and 30 km depth, dipping at 20°. On the combined 1100 km length of the Puerto Rico trench and northern Hispaniola fault, they calculate that earthquakes of magnitude 8, 8.5, and 9 may occur with average recurrence intervals of ~300, 1000, and ~3000-7000 years, respectively.

Detailed tsunami modelling is required to determine the magnitude threshold of earthquakes on the Puerto Rico trench that could result in potentially damaging tsunami runup in Canada. An examination of the historical global tsunami runup database of the NGDC suggests that, at distances greater than 2000 km from the source, runups exceeding 1.5 m are very unlikely, at any sites, for events of $M < 8.5$. Therefore, we assume that only earthquakes of $M \geq$

8.5 could produce runup ≥ 1.5 m on most of the Atlantic coast of Canada; we make the further assumption that large events could result in tsunami runup that exceeds 3 m in places (Table 16). We assume that the northeastern Atlantic coast would be relatively sheltered, but that local runup maxima exceeding 1.5 m may occur. Based on the recurrence of *M* 8.5-9 earthquakes estimated by Geist and Parsons (2009), we choose 1000 years as the minimum recurrence of runup ≥ 1.5 m, and 7000 years as the maximum; as a best estimate, we choose the median value of 4000 years.

The ~N-S-trending Lesser Antilles subduction zone (Fig. 10), where convergence is near-orthogonal to the trench, may present an additional tsunami threat to the Atlantic coast of Canada. Preliminary thermal modelling indicates that the seismogenic zone of the megathrust increases in width from north to south (from a minimum of 80 km north of 16°N to 230 km at 13°N) due to the increasing width of the accretionary wedge (Gutscher et al., 2009b; 2010). Moderate to large (up to *M*~7.5) thrust earthquakes on the subduction interface have been recorded in the northern Lesser Antilles, but there is a complete absence of instrumentally recorded thrust earthquakes south of 14.5°N, suggesting that the fault may be fully locked there (Gutscher et al., 2010), or that convergence is aseismic. Gutscher et al. (2010) suggest that earthquakes up to *M*~8.0 are possible in the north, but with such a wide seismogenic zone in the south a rupture length of ~500 km may be capable of producing great earthquakes up to *M*~9.0 in the Lesser Antilles. The potential for *M* ≥ 8.5 events is also noted by Heuret et al. (2011). During these events, slow slip beneath the wide zone of shallow accretionary sediments may contribute significantly to tsunamigenesis as was observed in the similar setting of the Andaman trench during the 2004 Sumatra earthquake (Gutscher and Westbrook, 2009).

There are no published estimates on the possible recurrence of great earthquakes in the Lesser Antilles, and no far-field tsunami modelling has yet been carried out. In the absence of further constraints, we assume a range of recurrence intervals based on a comparison with the Cascadia subduction zone, where paleoseismic data infer that *M*~9 earthquakes occur with an average recurrence of ~530 ± 260 years (Goldfinger et al., 2012). The 20 mm/y convergence rate at the Lesser Antilles (e.g., DeMets et al., 2000) is approximately half that at Cascadia, and thus we assume a range of recurrence intervals for *M*~9 events that are twice as long (1060 ± 520 y). We further assume that such events will produce runup ≥ 1.5 m (but only locally ≥ 3 m) along the outer coasts of Nova Scotia, southern Newfoundland, and New Brunswick (Table 17). For southeastern Newfoundland and the inner southern Atlantic coasts, we assume that runup ≥ 1.5 m is possible but less likely, and that the northeastern Atlantic coast is sheltered from potentially damaging waves. We emphasise that modelling is required to determine whether or not the Lesser Antilles subduction zone represents a significant source of tsunami hazard for the Atlantic coast.

Additional historical tsunami sources in the northeastern Caribbean have included extensional earthquakes as well as volcanic eruptions and related mass movements (in the Lesser Antilles, e.g., Mount Pelée and Soufrière volcanoes). Damaging local tsunamis have been triggered from an *M*~7.5 probable transtensional earthquake in the Anegada Passage, Virgin Islands, in 1867 (e.g., Zahibo et al., 2003), and an M_w 7.3 extensional earthquake in 1918 in the N-S-trending Mona Passage (e.g., Mercado and McCann, 1998; Jansma et al., 2000; Fig. 10); the 1918 tsunami was recorded at Atlantic City, New Jersey, as 3-6 cm waves (Reid and Taber, 1919). None of these tsunami sources are expected to result in potentially damaging far-field effects on the Atlantic coast of North America (AGMTHAG, 2008).

Paleoseismic studies in the region have so far provided little insight into the history of large tsunamis in the northern and eastern Caribbean through the Holocene. Turbidite deposits

that may indicate the past occurrence of large plate-boundary earthquakes are present in the floor of the Puerto Rico trench; the largest of these, known as the "giant turbidite", extends for at least 300 km along the margin and has five separate entry points indicative of widespread simultaneous shaking (Pilkey, 1988). Unfortunately, these deposits have not been dated (O.H. Pilkey, personal communication, 2011). The 1918 Mona Passage tsunami is the only historical event in the region with a proven tsunami deposit (e.g., Scheffers et al., 2005). A possible prehistoric tsunami deposit on an island in Mona Passage is dated at maximum 4200 years old (Taggart et al., 1993). A south-directed overwash deposit recently described on Anegada Island (Fig. 10) occurred between about 1650 and 1800 CE (Atwater et al., 2010). The deposit is of likely tsunamigenic origin (Watt et al., 2011); it may have resulted from the 1755 Lisbon tsunami, but modelling suggests that a local origin is more probable (Buckley et al., 2011), possibly the 1690 Antilles earthquake and tsunami (exact source unknown) or a previously unknown event (Atwater et al., 2010). In the Lesser Antilles, the only clearly identified Holocene tsunami deposits are found on the east coast of Guadeloupe in the north-central part of the arc; radiocarbon dating implies an event age of ~2400-2700 years BP, and a submarine slide may be the most likely source (Scheffers et al., 2005). The apparent lack of tsunami deposits in the Caribbean is likely a consequence of poor preservation in the tropical climate and difficulty in distinguishing the source as tsunamis rather than the more frequent hurricanes (e.g., Day et al., 2008). Studies of recent tsunamis elsewhere suggest that tsunamis with runup less than 3 m are unlikely to be preserved, and for larger tsunamis, only 50-60% of the inundation distance is represented by sand deposits 1-4 years after the event (Goto et al., 2011; Szczuciński, 2012).

The ~E-W orientation of the Puerto Rico trench makes it the Caribbean source most potentially hazardous to the Canadian Atlantic coast; tsunami energy from a great subduction earthquake would be directed largely to the north, orthogonal to the Canadian continental margin (e.g., Geist and Parsons, 2009). An all-source tsunami gain map for Halifax, Nova Scotia (Fig. 11; Xu, 2007) shows that a tsunami sourced in the region of the Puerto Rico trench would propagate more efficiently to Halifax than from any other potential far-field location in the Atlantic. Tsunami simulations show that an *M*~9.0 thrust earthquake on the Puerto Rico trench (including the northern Hispaniola fault) could produce damaging waves along the U.S. Atlantic coast, with amplitudes of ~0.5-3.0 m at the shelf edge and significantly higher runup expected (Knight, 2006; AGMTHAG, 2008; Geist and Parsons, 2009). Similar or higher values are likely in Atlantic Canada, although tsunami amplitudes have yet to be modelled.

Although most far-field energy from a megathrust-triggered tsunami in the Lesser Antilles would likely be directed eastwards rather than northwards, the possibility of damaging far-field tsunami waves from this source warrants further investigation. In the Pacific Ocean, edge waves from the 1960 Chilean tsunami caused damage in Vancouver Island coastal inlets, although the main energy was directed elsewhere. The Mid-Atlantic Ridge may also act to steer tsunami waves towards Atlantic Canada, as it did during the 2004 Sumatra tsunami when Halifax, Nova Scotia recorded the largest tsunami waves (~80 cm) in the North Atlantic, ~20,000 km from the source (Rabinovich et al., 2006; Thomson et al., 2007). This topographic steering effect is apparent in the tsunami gain map for Halifax (Fig. 11).

St. Lawrence Estuary crustal earthquakes

The banks of the St. Lawrence Estuary, Quebec (Fig. 1), along with their population of at least a million, are considered to be at risk from local waves generated by seismic displacements or failures of the widespread Quaternary sediments (e.g., Poncet et al., 2010). Seismicity along

the St. Lawrence valley likely occurs as a result of compressional reactivation of Paleozoic normal faults (Iapetan rift zone) under the present-day stress field, which is dominated by postglacial rebound (Mazzotti and Adams, 2005; Mazzotti et al., 2005). Numerous mass movements have been noted along the banks and submarine slopes of the estuary; many of these have been linked to the *M*~7-7.5 Charlevoix earthquake of 1663 CE (e.g., Locat et al., 2003; Ebel, 2011). In the Betsiamites delta region of the lower St. Lawrence, at least three large failures have occurred in the last ~10,000 years, one of which correlates with the 1663 event (Cauchon-Voyer et al., 2008; 2011), suggesting an average recurrence equivalent to that of *M*~7.2-7.8 events in the Charlevoix seismic zone (Mazzotti et al., 2005). Liquefaction features of similar age have been found along three rivers in the Charlevoix seismic zone, but not further southwest in the Quebec City-Trois-Rivieres area (Tuttle and Atkinson, 2010).

Focal mechanisms of earthquakes sourced in the St Lawrence valley mostly reflect thrust faulting with a minor oblique component (Mazzotti et al., 2005); a tectonic tsunami could result from displacement of the river/estuary floor. However, we cannot take an approach similar to that used for crustal earthquake sources on the Pacific coast. Only a small part of the seismicity area underlies water; also, the earthquake-tsunami relations of Abe (1995) cannot be applied to such a confined water body, where even a small displacement may have a relatively large effect. Landslide tsunamis may also result. However, the relationship between seismicity and mass movements can be complex, other factors may be responsible for large failures (Lamontagne, 2009), and even small failures may produce locally damaging waves; thus we do not quantify the probability of landslide tsunamis in the St. Lawrence estuary, but highlight it as an area susceptible to landslide-triggered waves.

Tsunami modelling of seismic displacement and landslide sources in the St Lawrence estuary suggests that local wave amplitudes up to 5 m or more are possible, with larger sources (e.g., blocky landslide with volume of 50 million m^3) leading to waves of 1-2 m propagating at least 30 km up and downstream (El-Sabh et al., 1988; Chassé et al., 1993; Poncet et al., 2010).

With few constraints, we assume that the tectonic tsunami hazard in the St. Lawrence estuary (inner Atlantic zone) is negligible, but we take a conservative approach. For the maximum level of hazard we assume that runup ≥1.5 m (locally exceeding 3 m) may occur with a return period of ~3300 years (equivalent to the return period of large failures, and presumably large earthquake regional ground motions, in the lower St. Lawrence).

Landslide Tsunamis

Continental slope landslides

The only historical landslide-triggered tsunami documented on the east coast of North America occurred in November 1929 and resulted in 28 deaths in Newfoundland, Canada (Table 1). An M_s 7.2 earthquake at the edge of the Grand Banks south of Newfoundland (Fig. 12) triggered a large submarine landslide-turbidity current on the continental slope that broke 12 seafloor telegraph cables (e.g., Heezen and Ewing, 1952). The landslide triggered a tsunami that traversed the continental shelf to strike southern Newfoundland; most damage and all fatalities occurred on the Burin Peninsula, where wave amplitudes of 3-8 m and runup up to 13 m were documented (e.g., Ruffman, 2001; Fine et al., 2005). Future submarine landslides along the Atlantic continental slope may also trigger destructive tsunamis; mapping has revealed that mass

failures much larger than the 1929 slide have occurred in the past (e.g., Piper and Ingram, 2003; Piper and McCall, 2003; Mosher et al., 2010).

Not all submarine mass failures are tsunamigenic. For the purposes of tsunami hazard analysis, it is then necessary to address the question of what threshold characteristics of a submarine failure are necessary to trigger a tsunami with the potential to cause damage at coastal sites. Landslide volume is a primary control on tsunamigenesis, but several other important factors include failure initial acceleration, velocity and duration, density, viscosity, slope angle, displacement relative to area, retrogressive behaviour, and water depth (e.g., Fine et al., 2003; Trifunac and Todorovska, 2003; Harbitz et al., 2006). During tsunami propagation from the source, the bearing of coastal sites relative to the direction of slide motion will determine the most affected areas, e.g., the Burin Peninsula, located across the continental shelf directly updip from the Grand Banks landslide (Fig. 12), experienced much greater tsunami wave amplitudes and runup than all other locations at an angle from the slide direction (e.g., Murty, 1977). Other factors to consider that influence the trade-off between attenuation (radial spreading and/or dispersion) and amplification over the tsunami's travel path include distance, bottom friction, nearshore bathymetry, and resonance effects in inlets, as well as the position of the failure on the continental slope – a lower position allows for greater amplification by shoaling as the back-going (shoreward) wave propagates up the slope (e.g., Harbitz et al., 2006; Geist et al., 2009b; Imamura, 2009; Liu, 2009). Thus, complex modelling is required to assess the potential tsunamigenic impact of submarine failures at coastal sites. The historical Grand Banks event also provides important ground-truthing data.

Landslide tsunamigenesis

Tsunami modelling that has been carried out for the Atlantic margin of North America provides some insight into the threshold size for damaging tsunamigenic failures. For the Currituck slide offshore North Carolina, Geist et al. (2009b) assessed slide volumes of 57, 108, and 165 km^3; modelled coastal runup is ~3 ± 1, ~4 ± 2, and ~6 ± 3 m, respectively. The largest slide is similar in volume to the Grand Banks slide, where maximum wave amplitudes were 3-8 m, and runup up to 13 m (e.g., Fine et al., 2005), the higher runup due to resonance amplification (e.g., Murty, 1977). At Cape Fear (also offshore North Carolina), for slide volumes of ~8 and 60 km^3, Hornbach et al. (2007) modelled respective maximum wave amplitudes at 100 m depth of 0.7 and > 2 m (for 50 km along strike).

The Canadian continental margin is far from uniform along strike (Fig. 12), and complex modelling is needed to approximate the effects at different coastal locations of a wide range of landslide parameters from different sources along the continental slope. An example is given by Grilli et al. (2009) who used a probabilistic Monte Carlo simulation approach to model a wide range of landslide and tsunami parameters (dependent on seismic hazard) on the continental shelf offshore the New Jersey/New York coast; a 100-year tsunami would produce waves < 1 m, whereas a 500-y tsunami could result in 1-4 m waves. However, this approach appears to significantly overestimate the frequency of landslides mapped offshore (e.g., Chaytor et al., 2009); uniform shaking will generally not result in uniform failure, even on slopes of apparent uniform susceptibility (e.g., Jibson et al., 2000).

Mosher et al. (2010) simulated a tsunami resulting from a deep-seated landslide on the western Scotian Slope comparable in scale to the Pliocene Shelburne mass-transport deposit identified in seismic data (location in Fig. 12), i.e., a minimum volume of 862 km^3 or about five times larger than the Grand Banks landslide, with thicknesses of ~130-450 m. As the deposit

consists of slump and debris flow portions, Mosher et al. (2010) tested two scenarios for their impact on Halifax, Nova Scotia, located ~200 km north of the source across the continental shelf. In the first scenario, only the 117 km^3 slump portion is modelled, resulting in a maximum wave amplitude of 13 m (above the state of tide) at Halifax; modelling of a simultaneous 862 km^3 failure incorporating both the slump and debris flow produces a 25 m wave at Halifax. However, the use of instantaneous vertical displacements may have overestimated the amplitudes.

The 1929 landslide, triggered by an *M* 7.2 earthquake beneath the continental slope of the Grand Banks, Newfoundland (Fig. 12), involved a 150-200 km^3 volume of sediment. The most damaging waves of the resulting tsunami were those that travelled directly north across the continental shelf, orthogonal from the headwall of the slide, to devastate the Burin Peninsula, ~250 km from the tsunami source. It seems likely that the location of Halibut Channel played a significant role in directing tsunami energy directly from the site of greatest sediment failure (most efficient tsunamigenesis) to the Burin Peninsula (Fig. 12). Severe damage occurred in over 40 communities along a ~75-km (straight line distance) stretch of coastline (white line in Fig. 12), and loss of life (28 people) occurred in six communities (e.g., Berninghausen, 1968; Ruffman and Hann, 2006). Minor tsunami damage occurred on the outer coasts of Nova Scotia and Newfoundland extending from the most severely affected area up to ~425 km to the southwest, as far as Canso, Nova Scotia, where runup of ~60 cm damaged wharves and boats, and up to ~160 km to the east, as far as the southern tip of the Avalon Peninsula, Newfoundland (e.g., Berninghausen, 1968). Northeastern Newfoundland was also slightly affected in the Bonavista area (e.g., Ruffman, 2006). Wave amplitudes on the Burin Peninsula are estimated at 3-8 m, with runup of up to 13 m, highest at the heads of long bays (e.g., Ruffman, 2001; Fine et al., 2005). Few wave amplitude estimates are available outside of the Burin Peninsula, but a runup of 1.5 m was reported at Sydney, Nova Scotia, located ~330 km southwest of the Burin Peninsula. The tide gauge at Halifax, Nova Scotia, ~640 km southwest of Burin, recorded a maximum peak-to-trough wave amplitude of ~1.25 m (Fine et al., 2005). Small tsunami waves were measured by tide gauges as far away as South Carolina (Charleston), the Azores, the Antilles, and the west coast of Portugal (Berninghausen, 1968, and references therein; Ruffman, 1994).

The observations of the 1929 Grand Banks tsunami suggest that a tsunami generated by a 1929-type submarine landslide with 150-200 km^3 volume could result in runup that exceeds 1.5 m along a stretch of coastline up to ~700 km or more in straight-line length (~100 km for severe damage, with minor damage possible for ~300 km on either side). Tsunamis resulting from smaller landslides closer to the threshold volume are expected to affect a considerably shorter length of coastline.

We estimate threshold volumes for damaging tsunamigenic failures on the Atlantic continental slope based on the modelling studies and the effects of the Grand Banks event discussed above. We estimate that damaging tsunami runup that exceeds 1.5 and 3 m may result from failures that exceed volumes of 40 and 55 km^3, respectively. We stress that these values are an approximation – the threshold may well vary along the coast, due to factors such as differences in width of the continental shelf or the presence of inlets where resonance amplification may occur. Also, as outlined above, tsunamigenesis is influenced by many factors, but landslide volume is the only one that can be approximated from the available data on slide deposits. Future studies should entail more detailed modelling of a wide range of failures to ascertain coastal locations that may be particularly susceptible to damaging waves from relatively small failures.

Event recurrence

Three main styles of sediment failure have been recognized on the Atlantic continental slope (e.g., Piper, 2005): (1) glaciogenic debris flow deposits, generally located seaward of shelf-crossing glacially-excavated troughs, forming trough-mouth fans; (2) deep-seated mass movements involving failure on a décollement surface and resulting in deposits made up of blocks up to hundreds of metres thick; (3) shallow retrogressive failures, typically 10-20 m in thickness, e.g., the 1929 Grand Banks failure.

Each of these failure styles is likely the result of different trigger mechanisms and/or preconditioning to failure, and therefore they are not expected to plot on the same frequency-size relation. (1) Glaciogenic sediments in trough-mouth fans are thought to result from very high-viscosity debris flows made up of glacial till that move too slowly to be tsunamigenic (e.g., Tripsanas and Piper, 2008). Also, such flows occurred at times of meltwater discharge from their parent ice streams, and are not expected to occur at the present day. However, the other two styles certainly have tsunamigenic potential. (2) Evidence for only a few large deep-seated failures has been identified on the margin (e.g., the Hopedale-Makkovik failure complex offshore Labrador, Deptuck et al., 2007; the Shelburne mass-transport deposit on the western Scotian Slope, Mosher et al., 2010; locations in Fig. 12). These deposits represent catastrophic slides that would undoubtedly have produced large tsunamis; however, with very long recurrence intervals their probabilistic contribution to the tsunami hazard of the east coast is low.

(3) Most failures are of the shallow, retrogressive type similar to the 1929 Grand Banks event. On the Atlantic continental slope, small failures (up to ~10 km^3) are common on steep slopes, e.g., canyon walls, but large, potentially tsunamigenic slides occur on lower angle slopes where the regional gradient is typically 2-6° (Piper et al., 2003; Twichell et al., 2009). Piper et al. (2011) make the assumption that slopes with a mean gradient exceeding 2° have local slopes where the gradient exceeds 6° and where failure is relatively easily initiated under strong ground shaking (e.g., ten Brink et al., 2009a) and could retrogress to lower-angle slopes. The slope stability analysis of Mosher et al. (1994) shows that under static conditions, the Scotian Slope seabed is stable (with the exception of canyon walls, etc.). Failure would require elevated pore pressure and/or earthquake shaking, as occurred on the Grand Banks in 1929. Other factors such as shallow salt deformation, seaward-dipping faults, and the presence of gas-charged sediments (e.g., due to gas hydrate dissociation) may play a role, but it is likely that ground shaking is necessary to precipitate failure (e.g., Giles et al., 2010).

The recurrence of large (potentially tsunamigenic) submarine landslides on the Atlantic continental slope is poorly known and difficult to estimate (e.g., Lee, 2009; ten Brink et al., 2009a). Individual failures must be identified and dated using detailed mapping and sampling of the seafloor and sub-seafloor. The recurrence of large submarine failures has likely varied through the Quaternary depending on glacial cycles; mass failures are more frequent during and after glaciation/deglaciation due to increased sedimentation on the upper continental slope during sea level low stands and increased seismicity caused by isostatic adjustments to glacial loading/unloading (e.g., Piper et al., 2003; Lee, 2009).

Published estimates of the return periods of large (regional) failures on parts of the continental slope off Nova Scotia and Newfoundland range from ~10,000 years (Piper and Gould, 2004) to a few hundred thousand years, based mainly on the number of stacked mass-transport deposits above marker horizons in seismic data on the continental rise (Piper et al., 2003). Piper (2005) estimates a crude size-frequency relationship for the eastern Canadian margin, with a recurrence interval of ~5 ky for small failures and > 200 ky for large failures, without a clear

definition of "small" and "large". However, the record in any one area is dependent on the resolution and quality of available data; e.g., based on morphology alone the large (150-200 km^3) 1929 Grand Banks tsunamigenic slide may not have been identified as it did not produce an easily identifiable bathymetric signature (Mosher and Piper, 2007). The record of smaller failures, closer to the estimated threshold size, is certainly incomplete in most areas, so that individual size-frequency relations cannot be estimated for most of the margin. In many cases it is also difficult to estimate the failure volume, when the original scar has long since been eroded or obscured by subsequent sedimentation and any corresponding mass-transport deposits are likely incompletely mapped and/or much of the failed sediment may have bypassed the slope to be deposited on the abyssal plain.

A chronology of regional failures identified along the southeastern Canadian margin was presented by Piper et al. (2003) and updated by Piper (2005). Subsequent studies have increased the number of failures recognised in several areas including Flemish Pass (Huppertz and Piper, 2009) and Orphan Basin (Piper et al., 2011), illustrating the incompleteness of the record along the rest of the margin. The record is especially incomplete for the Labrador margin; preliminary studies indicate that the distribution of failures is generally similar to the Scotian Slope and Orphan Basin, and the frequency of dated failures is comparable to these areas at a time when the level of knowledge was similar (Piper, 2007). Seismic reflection data from eastern Hudson Strait reveal a number of debris-flow scars (up to 10 km wide) and associated deposits that appear to postdate glaciomarine sedimentation in the region, i.e., such failures are likely younger than ~8 ka (MacLean et al., 2001). Preliminary data from a recent seismic cruise off northeastern Newfoundland suggests a relatively high frequency of failures in the region of the Notre Dame trough-mouth fan, coinciding with steep fault scarps along the extension of the Charlie Gibbs fracture zone (Campbell and Saint-Ange, 2012; Fig. 12).

Piper et al. (2011) provide the most complete record of shallow failures anywhere on the margin over the last ~90 ky for Orphan Basin, off northeastern Newfoundland (Fig. 12). Mass-transport deposits identified with ultra-high resolution seismic reflection data are correlated with slump-generated turbidites cored on the basin floor. Fifteen failures are recognized that affected along-slope extents of at least 10 km; seven of these affected the slope for at least 100 km. The record from Orphan Basin can be used to approximate a size-frequency relationship, using along-slope extent as a proxy for failure size (Fig. 13; Piper et al., 2011).

A size-frequency relation can be calculated in a similar way for failures in the relatively small source area of Flemish Pass (Figs. 12 and 13). This relation is based on amalgamating data for large failures (extent ≥ 90 km) over the last ~400 ky identified from seismic profiles (Piper and Campbell, 2005) with higher-resolution data for smaller failures (extent ≥ 40 km) over the last ~165 ky (Huppertz and Piper, 2009).

To calculate the expected frequency of failures of a threshold size for potentially damaging tsunami waves, it is necessary to estimate the corresponding failure extent for a 40 km^3 volume. We assume that failures in Orphan Basin and Flemish Pass are similar in style to the Grand Banks failure, for which the dimensions are approximately known. Shallow retrogressive failures typically involve the upper 10-20 m of sediment, and downdip extent likely scales with along-slope extent. For an extensive catalogue of slides on the U.S. Atlantic margin, Chaytor et al. (2009) estimate the following relation between failure volume V and area A:

$$V = 0.0163A^{1.1} \quad (15)$$

The volume of the Grand Banks slide is estimated at 150-200 km^3 and its area at ~10,000 km^2 (Fine et al., 2005; Mosher and Piper, 2007), suggesting the relation:

$$V = 0.02A \quad (16)$$

similar to the relation of Chaytor et al. (2009). Relating the volume to the ~250 km length (L) of the Grand Banks failure provides the relation:

$$V = 0.8L; \quad (17)$$

thus a shallow failure with a volume of 40 km^3 is expected to have an along-slope extent of ~50 km, and a 55 km^3 failure an extent of ~70 km.

In Orphan Basin, the expected frequency of landslides with an extent ≥ 50 km is ~0.1/ky (0.06-0.15/ky), equating to an average recurrence interval of ~10 ky (6.5-17 ky). In Flemish Pass, such threshold landslides are expected to occur with an average recurrence interval of ~21 ky (15-32.5 ky). Continental slope failures with extents ≥ 70 km are expected approximately every ~11.5 ky (7-20.5 ky) in Orphan Basin and ~45 ky (27-78 ky) in Flemish Pass. The average recurrence interval for 1929-size failures in Orphan Basin is ~31 ky (16-76 ky).

In the absence of robust size-frequency data elsewhere along the margin, we assume that the frequency of threshold events estimated for Orphan Basin is approximately representative of the entire Canadian Atlantic margin. In most cases, for events close to threshold size, a coastal location is assumed to be at risk from only one source section of the continental slope. However, due to the bend in the shape of the continental margin off southeastern Newfoundland and the likely main tsunami travel paths, this coastal area must be assumed to be at risk from landslide-generated tsunamis from three source areas: Orphan Basin, Flemish Pass, and the Salar Basin on the southeastern Grand Banks (Fig. 12). Tsunami modelling is required to test this assumption, but at this stage the probability of a damaging landslide-triggered tsunami is considered to be significantly higher here than elsewhere along the margin.

For the outer Atlantic coast then, we assume that mean local runup ≥ 1.5 m could result from failures with an along-slope extent ≥ 50 km, and mean local runup ≥ 3 m may be produced from failures ≥ 70 km (Table 18). The inner Atlantic coastlines (zones given in Table 18) are assumed to be susceptible to only local runup maxima ≥ 1.5 m and ≥ 3 m for slides exceeding 50 and 70 km in length, respectively.

Canary Islands

Large landslide deposits offshore the western Canary Islands (off northern Africa; Fig. 2) suggest that major volcanic flank collapses of these young oceanic hot spot islands have occurred periodically over the last ~1 million years (e.g., Carracedo et al., 1999). Modelling by Ward and Day (2001) of a western flank failure of Cumbre Vieja volcano on the island of La Palma implies that potentially catastrophic tsunami waves could impact the North American Atlantic coast (10-25 m wave amplitudes for a 500 km^3 failure). However, the presence of stacked sub-units within turbidite deposits led Wynn and Masson (2003) to suggest that each major failure deposit may represent several stages of collapse spread over days, each involving a smaller volume (as low as 10-25 km^3) with a consequently lower tsunami hazard. Moreover, subsequent studies (e.g., Pararas-Carayannis, 2002) point out that Ward and Day (2001) failed to account for the effects of dispersion, which would be very significant for the short-period, short-wavelength waves expected, drastically reducing the far-field wave amplitudes. Subsequent, more realistic models by Mader (2001) and Gisler et al. (2006) can produce far-field waves on the east coast of North America of no more than 3 m and 1 m, respectively, with damaging runup possible in both cases.

Thus, we do consider Canary Islands volcanic collapses to be a potential source of infrequent damaging tsunamis for the east coast of Canada. Masson et al. (2002) present data on large submarine landslide deposits offshore the western Canary Islands, dating back to ~1 Ma. A

total of twelve flank failures are documented over that time period from the islands of El Hierro, La Palma, and Tenerife, most recently at ~15 ka, ranging in estimated volume from < 50 to ~650 km^3; the data are plotted as cumulative volume versus frequency in Figure 14. A 500 km^3 failure, as modelled in the three studies above, is expected approximately every 590 ky. We take 150 km^3 as the lowest possible slide volume to produce tsunami waves damaging to the Canadian Atlantic coast; Ward and Day (2001) estimate 3-8 m amplitudes for such a failure, but we assume that a more realistic model would produce waves an order of magnitude smaller, that with runup may reach 1.5 m. Based on the frequency-volume relationship in Figure 14, such failures are expected approximately every 160 ky (97-313 ky assuming a range of maximum volumes).

Although the study of Ward and Day (2001; 2005) significantly overestimates tsunami wave amplitudes, their far-field modelling results are useful in illustrating variations due to bathymetry in the relative impact of far-field tsunamis along the Canadian Atlantic coast. For example, as a result of focussing by the Laurentian Channel, the eastern coasts of Prince Edward Island and New Brunswick may experience wave amplitudes as large as those on the outer coasts of Nova Scotia, Newfoundland and Labrador (Fig. 15). Thus, we apply equal hazard to all susceptible Atlantic coastal zones, assuming that events with a 160 ky recurrence interval could result in local mean runup ≥ 1.5 m, 313 ky events could produce local mean runup ≥ 3 m, and 97 ky events could produce only local maxima ≥ 1.5 m (Table 19). The Canary Islands source provides a negligible contribution to the tsunami hazard of Atlantic Canada.

Storegga

Massive submarine landslides have occurred off the coast of Norway in the past, the largest being the Storegga slide complex (Fig. 2), which has failed approximately every 100 ky, most recently at ~8100 cal. yr BP (Solheim et al., 2005). In the absence of far-field modelling studies, we assume that northern Newfoundland and southern Labrador could potentially be affected by tsunami waves from a slide similar to those in the Storegga complex. For the latest and largest slide (estimated volume 2500-3500 km^3; Haflidason et al., 2004; Solheim et al., 2005), runup of 3 to > 20 m is reported from tsunami deposits in coastal areas within ~900 km of the slide (western Norway, eastern Scotland, the Faroe and Shetland Islands; e.g., Bondevik et al., 2005). However, coastal wave runup in the western Atlantic would not likely exceed 1.5 m due to attenuation over the > 3000 km distance and wave scattering by Iceland and the Faroe Islands. Also, it is thought that the Storegga area is currently stable, and that another glacial cycle would be required to lead to the next failure (Bryn et al., 2005). Thus, we do not include this source in the tsunami hazard assessment for eastern Canada.

ARCTIC COAST

The tsunami hazard of the sparsely-populated Arctic region of Canada is poorly known. Tide gauge stations have only recently been installed in the Arctic, the region has only a very short written history and poorly-recorded oral history (e.g., Ruffman and Murty, 2006), and there have been no targeted geoscience studies to document coastal evidence for past tsunamis. It is likely that tsunami hazard is significantly lower for the margins of the Arctic Ocean than for both the Pacific and Atlantic, given the lack of subduction plate boundaries and the expected attenuating effect of extensive sea ice cover, especially in winter (e.g., Murty, 1983; Hill et al.,

2001). However, as on the other coasts, there is a real possibility of locally-damaging tsunamis generated by submarine or subaerial landslides; an additional hazard in some areas relates to iceberg calving and/or jökulhlaups, and we also consider a possible tectonic source beneath the Mackenzie delta.

Ruffman and Murty (2006) report local oral history from the coast of southern Baffin Island regarding a large Inuit hunting party that disappeared at the time of a major felt earthquake in the early 1860s, suggesting the occurrence of a damaging local tsunami. No tsunami waves have been reported along the coast of the Beaufort Sea (Fig. 1). However, several studies have identified storm surge deposits in the coastal sedimentary environment, many of them suggesting surges of up to ~3 m or more in observed storm events in 1944 and 1970 (e.g., Henry and Heaps, 1976; Reimnitz and Maurer, 1978; Harper et al., 1988; Jenner and Hill, 1998; Pisaric et al., 2011). In the absence of other evidence, it is often impossible to distinguish between tsunami and storm surge deposits (e.g., Peters et al., 2003; Bourgeois, 2009); thus, it is possible that some of these could be tsunami deposits, but there is currently no supporting evidence for such a hypothesis.

Earthquake Tsunamis

The Canadian Arctic margins are located far from subduction plate boundaries; potentially damaging far-field subduction tsunamis are extremely unlikely. Tectonically-generated tsunamis related to known Arctic concentrations of seismicity are also unlikely, as there is no evidence that this seismicity defines any tectonic structures that are tsunamigenic. Earthquakes beneath the continental slope of the Beaufort Sea (Fig. 16) have been interpreted as deep extensional faulting due to sediment loading (Hasegawa et al., 1979); seismicity appears to be confined to an area underlain by oceanic crust on this rifted margin (Lane, 2002). Other earthquake concentrations relate to postglacial extensional faulting on eastern Baffin Island, and mainly strike-slip faulting in Baffin Bay (Basham et al., 1977; Bent, 2002).

Mackenzie thrust

The potential for large thrust earthquakes beneath the Mackenzie delta in the Beaufort Sea region was suggested by Hyndman et al. (2005). GPS data from Yukon Territory reveal a north-northeastward motion of the northern Canadian cordillera relative to the stable North America craton to the east; resultant compressive strain occurs in northeastern Yukon as thrust faulting in the Mackenzie Mountains and ~N-S right-lateral strike-slip faulting in the Richardson Mountains (e.g., Leonard et al., 2007; Mazzotti et al., 2008; Fig. 16). In the Mackenzie delta region there is likely a residual ~2 mm/y northward motion; the lack of recorded seismicity indicates that the north-south compression is accommodated either by aseismic deformation or by infrequent large thrust earthquakes on one or more currently locked faults. A thin-skinned fold-and-thrust belt was formed in the area in response to late Paleocene-middle Eocene north-south compression; more distal east-west-striking folds formed in the Miocene, and Holocene deformation is also apparent locally (e.g., Lane, 2002; Houseknecht and Bird, 2011). Hyndman et al. (2005) suggest that one outcome of the current north-south compression could be ongoing thrusting of the Mackenzie delta sediments and underlying continental crust over the oceanic crust to the north along a décollement.

We assume that large tsunamigenic earthquakes may occur on such a locked thrust fault (shown schematically in Fig. 16), and estimate the range of potential earthquake magnitudes and resultant tsunami impacts. With very few constraints available, we assume a fault length of 200-300 km and an arbitrary range of rupture widths (30-80 km); empirical relations between fault area and moment magnitude (Strasser et al., 2010; Equation 6) suggest that M_w 7.9 (7.4-8.4) events may occur, the large range reflecting the very large uncertainties (Table 20). Using a convergence rate of 2 mm/y and Equations 7-9, we estimate average recurrence intervals for these events of ~3300 years (~980-10,300 y).

Sediment cores from the southern Canada Abyssal Plain contain four distal turbidites (1-5 m in thickness) interbedded with pelagic deposits dating back to ~8 ka (Grantz et al., 1996). Turbidite composition is consistent with a provenance of Pleistocene and Holocene sediments on the outer continental shelf and upper slope of the Mackenzie delta; Grantz et al. (1996) suggest an origin of shallow submarine slides triggered by earthquake shaking. An average turbidity current recurrence of ~2000 years is consistent with our recurrence estimates for hypothetical Mackenzie thrust earthquakes, but is also consistent with the recurrence of M~7 earthquakes predicted by the recurrence relation of historical Beaufort Sea seismicity (northeast of the Mackenzie thrust in Fig. 16).

Using empirical relations between M_w and tsunami runup (Abe, 1995; Equations 12-14; Table 2), an M_w 8.4 thrust earthquake beneath the Mackenzie delta could result in tsunami runup $\geq$ 3 m along the northern coasts of Yukon and western Northwest Territories, with localized runup $\geq$ 1.5 m possible along parts of Banks Island, Victoria Island, and as far east as northwestern Nunavut (Table 21; Fig. 1). Smaller earthquakes would likely result in only localized potentially damaging runup. It is important to note that these calculations do not take ice cover into account. It is possible that breakup and transport of ice could increase the potential for damage close to the source, but would likely also significantly reduce tsunami runup further afield, based on the contrasting phenomena observed during storm surge events in periods of low versus high ice cover (e.g., Henry and Heaps, 1976; Reimnitz and Maurer, 1978).

Given the extremely poor constraints on a potential Mackenzie thrust event, and the possibility that convergence is aseismic and therefore non-tsunamigenic, it should be stressed that further investigation is required before this can be considered as a known hazard. Therefore we exclude this source from the cumulative tsunami hazard calculation for the Arctic coastline.

Landslide Tsunamis

Local landslides

Much of the Arctic coastline is at risk from locally destructive waves triggered by subaerial and submarine failures. As on the Pacific coast, fjords are particularly susceptible due to the combination of steep slopes, active delta fronts, and the potential for high runup on the banks and at the heads of confined inlets, where human settlements are common. Fjords are common along eastern Baffin Island, and along the coasts of other islands in the High Arctic. Although landslide tsunamis have not been reported, several failures have been noted (Syvitski et al., 1987, and references therein), and landslide tsunamis have been documented from similar environments in the Disko Island region off western Greenland (Ruffman and Murty, 2006; Fig. 1). Iceberg calving from coastal glacier termini and ice shelves present a similar local tsunami hazard in Arctic fjords; damaging waves have been reported from such events in Greenland (e.g.,

Amundson et al., 2008; Macayeal et al., 2011). Jökulhlaup events (catastrophic release of water from a glacier; "glacier burst" in Icelandic) could also produce locally damaging waves, where glacier termini are near sea level (e.g., Lewis et al., 2007).

Continental slope landslides

Similar to the Atlantic margin, the Beaufort continental slope is underlain by stacked mass-transport deposits and there is evidence for widespread retrogressive failures and slumps (e.g., Hill et al., 1982; Kayen and Lee, 1991). Canada Basin is filled with turbidites that were likely derived from stacked mass-transport deposits along the Beaufort and Arctic Archipelago margins (Mosher et al., 2012). The stratigraphy of the Mackenzie delta fan is dominated by mass-transport deposits (Mosher et al., 2012); with ongoing high sedimentation rates on the delta, this could be a source of tsunamigenic failures. A large submarine landslide scar has been imaged at the shelf-slope interface in the southern Beaufort Sea (Hill et al., 1982; Bennett et al., 2008; Paull et al., 2011; location in Fig. 16). Based mainly on a reticulate morphology of the headwall area, Hill et al. (1982) speculated a creep failure mode for this landslide, which would have no significant implications for tsunami generation. However, other mass failure modes are possible; e.g., other authors (e.g., Kayen and Lee, 1991; Nixon and Grozic, 2007) have raised the possibility of failure at the Beaufort shelf edge along a weak gassified layer caused by gas hydrate dissociation. Mosher (2009) suggested that the slide could have been tsunamigenic. Unfortunately, since none of the failures have been dated, a size-frequency relationship cannot be approximated. As mentioned above, cores from the southern Canada Abyssal Plain indicate an average Holocene turbidity current recurrence of ~2000 years (Grantz et al., 1996); it is likely that these turbidites resulted from slope failures on the outer continental shelf/upper slope of the Mackenzie delta, but the size and tsunamigenic potential of such failures remain unknown.

The Baffin slope area also requires much further study, particularly to determine whether the widespread debris flow deposits on the lower slope (e.g., Aksu and Piper, 1987; Aksu and Hiscott, 1989) are the result of glaciogenic processes or more catastrophic potentially tsunamigenic failures. A number of turbidite layers have been cored on the abyssal plain of Baffin Bay; the record from one site offshore southern Baffin Island suggests a minimum of eight turbidity currents in the last ~50,000 years (Benetti, 2006). However, turbidity currents may be initiated by a number of different processes (Piper and Normark, 2009), and further studies are required to constrain the history of failures on the Baffin slope. A recent survey found no evidence for slope failures in the epicentral region of the 1933 M_w 7.4 Baffin Bay earthquake (Li et al., 2010).

It is generally thought that earthquake shaking is necessary to trigger large failures on the continental slope (e.g., Mosher et al., 1994); the Canadian national seismic hazard maps (Halchuk and Adams, 2008) show generally similar levels of seismic hazard for the Arctic and Atlantic continental margins. The presence of numerous gas escape structures on the outer shelf and slope in the Beaufort Sea raises the possibility that gas escape is another mechanism that may contribute to slope instability in this region. However, given the weak level of understanding of slope failure mechanisms and timing, further investigations are required before the recurrence intervals can be stated with confidence. In the absence of better constraints, we assume that potentially damaging coastal tsunami runup due to continental slope landslides may be expected along the margins of Canada Basin and Baffin Bay with a similar frequency to that calculated for the Atlantic margin, i.e., with an average recurrence interval of ~10 ky (6.5-17 ky). Further, without any constraints on how much of the Arctic coast may be affected by such

tsunamis, we apply a uniform hazard to the entire zone. However, we note that some Arctic coastlines are undoubtedly sheltered from slope failure tsunamis, particularly throughout most of the year when ice cover is high, and that hazard will be highest during times of lowest ice extent.

CUMULATIVE TSUNAMI HAZARD OF THE CANADIAN COASTLINE

The previous sections of this report assess the hazard presented by individual tsunami sources to the coasts of Canada. Here, we combine the relative hazard from each source to calculate the overall hazard for each section of the coastline. For each region, the annual frequencies of occurrence of potentially damaging runup $Hr \geq 1.5$ m from different sources are added together to provide an estimate of the cumulative annual frequency of $Hr \geq 1.5$ m resulting from any source (Equations 3-5). The cumulative frequencies are then used to calculate cumulative probabilities (Equation 2), i.e., the probability that the coastline in question will experience potentially damaging tsunami runup of 1.5 m or more within a 50-year period, from any source (Tables 22-24). In each case, a "best estimate" is presented, as well as a minimum and maximum possible value of the probability, taking into account the uncertainties of the various sources. The probabilities are also presented in the form of equivalent recurrence intervals. Tables 22-24 also include the probability of each region experiencing a more severe ("significant") tsunami runup of 3 m or more in a 50-year period. Tables 25-27 provide the maximum runup expected to occur various time periods (50-2500 years).

Figures 17 and 18 present the best estimate of the overall tsunami hazard for the coastlines of Canada, for runup exceeding 1.5 and 3 m, respectively, in 50 years (maximum runup levels expected within longer time periods are shown in Appendix D). Coastline sections are coloured according to their probabilities. We stress that regions with an apparent negligible probability (< 2% in 50 years) of tsunami runup from the sources assessed may be vulnerable to locally-damaging waves triggered by mass movements. Such hazards could not be quantified for this assessment, but susceptible coastlines are highlighted in Figure 19.

The cumulative estimates in Tables 22-24 (also shown for representative regions in Fig. 20) indicate that the tsunami hazard (runup exceeding 1.5 m) of the outer Pacific coastline (~40-80% probability of exceedance in 50 y) is an order of magnitude greater than that of the outer Atlantic coastline (~1-15%), which in turn is an order of magnitude greater than the Arctic coastline (< 1%). These numbers are equivalent to an expected recurrence of 1.5 m+ runup of ~30-100 years for the outer Pacific coast, and ~300-1700 and ~6500-17,000 years for the outer Atlantic and Arctic coasts, respectively. For runup exceeding 3 m, the Pacific hazard (~10-30% probability of exceedance in 50 y; equivalent recurrence of ~150-500 y) is significantly higher than both the Atlantic (~1-5%; ~650-4000 y) and the Arctic (< 1%; ~7000-20,000 y).

Figure 21 illustrates the source contributions to the overall tsunami hazard (also see Tables 22-24, and Appendix E). On the outer Pacific coastline, the 1.5 m+ tsunami runup hazard is dominated by far-field subduction zone sources, whereas the more severe 3 m+ tsunami hazard is almost entirely contributed by local plate boundary subduction zone sources. For the more sheltered inner Pacific coasts of Juan de Fuca and Georgia Straits, the hazard at both levels is contributed mostly by the Cascadia subduction zone. Tsunami hazard on the Atlantic coastline is dominated by quite poorly-constrained far-field subduction zone sources at both the 1.5 m+ and 3 m+ runup levels. Tsunami hazard on the Arctic coastline remains uncertain, but these regions are assumed to be sheltered from far-field tsunamis, so the hazard is provided by local landslide sources.

Regional Recommendations

This report presents a preliminary assessment of the tsunami hazard of the Canadian coastline, by identifying potential tsunami sources and quantifying their hazard in a probabilistic way, wherever the available data allow. For each region, we calculate probabilities of damaging tsunami runup at two levels (exceeding 1.5 and 3 m), but we do not present the maximum runup likely to occur within given time periods. The current state of knowledge precludes a complete probabilistic tsunami hazard assessment. This would require quantification of a wide range of possible scenarios for each tsunami source, coupled with tsunami modelling that incorporates fine-resolution bathymetry and onland topography to adequately assess potential tsunami runup at the coast.

Pacific Coast

The Cascadia subduction zone clearly presents the highest overall tsunami hazard to the Pacific coast, and the most extreme potential runup; more tsunami modelling is needed, with improvements in both the range of source models and in the use of detailed bathymetric and topographic data to provide accurate assessments of coastal runup, especially for populated areas. At near-field locations, variations in rupture on the fault have a large impact on tsunami runup at the coast, e.g., for Cascadia, a narrower rupture would produce a larger tsunami than a wider rupture for the same earthquake size, due to the concentration of fault slip at shallower depth (closer to the trench) and beneath relatively deep water (Geist, 2002; 2005). Splay fault rupture and local landslides also influence local tsunami runup (e.g., as documented/suggested for the 1964 Alaska and 2004 Sumatra earthquakes, e.g., Plafker, 1967; DeDontney and Rice, 2011; Suleimani et al., 2011). Thus, improved constraints on the geology and geometry of the subduction zone to assess the range of possible rupture scenarios are critical. Hazard analysis will also benefit from comparisons with other subduction zones where historical events can be better studied. A useful case study is presented by Priest et al. (2009), who carried out a probabilistic analysis to assess potential tsunami runup at Cannon Beach, Oregon (location in Fig. 4), from Cascadia subduction zone sources. Their deterministic approach involves a wide range of rupture scenarios that are consistent with available data and weighted according to their estimated likelihood. Variations include local/regional high-slip patches and the inclusion of splay fault rupture; earthquakes of M_w 8.3-9.4 involving fault slip of ~8-38 m result in maximum tsunami runup (at Cannon Beach) of 9-30 m, with the preferred scenario producing runup of ~10 m. Additional scenarios could incorporate the potential for large submarine mass failures at the deformation front, coincident with megathrust rupture, and rupture that extends northward to include subduction of the Explorer plate.

This preliminary analysis indicates that, although no historical events have occurred, potential thrust sources along the Explorer and Queen Charlotte margins may contribute a significant proportion of the tsunami hazard for the northern BC coastline (Table 22; Fig. 21). Future work needs to provide better constraints on the extent and nature of subduction along both the Queen Charlotte and Explorer margins, and to seek paleoseismic evidence for tsunamigenic earthquakes in the past (e.g., tsunami deposits, offshore turbidites, landslide deposits, and indicators of vertical coseismic displacements). Modelling should also be undertaken to assess

the tsunamigenic potential of megathrust earthquakes generated in these regions, and to better constrain the potential impacts at the coastline.

The inner Pacific coasts, particularly Georgia Strait, are sheltered from most tsunami sources included in this assessment. However, these areas are at risk from locally-damaging waves triggered by crustal earthquakes or landslides. For many areas, especially fjords, landslide tsunamis likely present the greatest hazard, but are difficult to quantify (susceptible areas are shown in Fig. 19). A probabilistic analysis will require (1) the identification of potential sources; (2) evidence for past tsunamigenic events to establish frequency-size relationships and/or slope stability analyses that incorporate expected earthquake shaking levels; (3) probabilistic tsunami modelling of a wide range of possible failures.

Atlantic Coast

Analysis of the Atlantic coast tsunami hazard (Table 23; Fig. 21) indicates that far-field subduction zone sources may be very significant, but the hazard is poorly constrained. Tsunami modelling is critically needed to identify which sections of coastline are at risk from each potential source, e.g., the tsunami gain map of Xu (2007; Fig. 11) indicates that Halifax, Nova Scotia, is relatively sheltered from Gibraltar-Cadiz sources, with a higher hazard presented by the northeastern Caribbean. The frequency of events similar to the 1755 Lisbon tsunami, which was observed in Bonavista, Newfoundland, is relatively well constrained, but much further research is required to constrain potential events on the Puerto Rico trench and the Lesser Antilles subduction zone.

Continental slope failures similar to the 1929 Grand Banks event also present a significant hazard to the Atlantic coast. Our assessment involves a number of simplistic assumptions that need to be tested with modelling and with the collection of more data. These assumptions include: (1) the size-frequency relationship of failures in Orphan Basin can be applied to other parts of the margin; (2) the threshold volume of tsunamigenic failures is 40 km^3, and this value applies along the whole Atlantic margin; (3) with the exception of southeastern Newfoundland, a coastal location is at risk from only one slope failure source area directly offshore.

As with the Pacific coast, inner coastal areas that may be relatively sheltered from most tsunami sources, e.g., the St. Lawrence Estuary, have a potentially higher hazard from local landslide tsunami sources (Fig. 19). Similar recommendations apply as for the Pacific. The possibility of tectonic tsunamis in the St. Lawrence Estuary also merits further study.

Arctic Coast

The tsunami hazard of the Arctic coast (Table 24; Fig. 21) is the most poorly constrained. For the coasts of Yukon and Northwest Territories, the hypothetical Mackenzie thrust may present the highest potential tsunami hazard, although at present we consider the uncertainties too great to include this source in the national hazard map. Much further work is required to constrain the potential rupture dimensions and tsunamigenic potential of this fault, and to search for paleotsunami deposits. Data collection is also required to test the simplistic assumption that continental slope failures have a size-frequency relationship similar to Orphan Basin on the Atlantic margin. Similar to the Pacific and Atlantic coasts, the Arctic is also at risk from local landslide tsunamis; additionally, locally-damaging waves are likely from glacial sources, a hazard that may increase with climatic warming (Fig. 19). Tsunami modelling of sources in the Arctic should also account for the presence of sea ice, which may increase the potential for

damage locally, but would likely decrease the hazard further afield. Tsunami hazard is likely to vary seasonally with changes in ice extent.

NOTE ADDED IN PROOF: OCTOBER 27 2012 HAIDA GWAII EVENT

On October 27, 2012 at 8:04 p.m. local time an earthquake of M_w 7.7 occurred off southern Moresby Island in Haida Gwaii; the mechanism was predominantly thrust on a northwest-striking, eastward-dipping fault plane. Such an event is expected to generate a tsunami with the greatest energy (highest amplitudes) directed perpendicular to the fault, i.e., to the northeast towards the unpopulated (and un-instrumented) west coast of Moresby Island, and out to sea to the southwest. Smaller amplitudes would be expected to the northwest and southeast of the rupture.

A maximum peak-to-trough tsunami amplitude of ~52 cm (~26 cm amplitude above the state of tide) was recorded at the nearest tide gauge station (Langara Island; ~160 km northwest of the rupture). Maximum peak-to-trough amplitudes recorded on Vancouver Island (>300 km southeast of the rupture) were ~46 cm (~21 cm peak amplitude above state of tide) at Winter Harbour, ~26 cm (16 cm) at Port Alberni, and ~20 cm (9 cm) at Tofino. It is hoped that post-event studies will help to constrain the fault source and contribute to a better understanding of the tsunami hazard of the Pacific coastline of Canada.

ACKNOWLEDGMENTS

Many people provided critical input to this report through contributing data and discussion. In particular, we thank Calvin Campbell, Josef Cherniawsky, Scott Dallimore, Phil Hill, Sabine Hippchen, Roy Hyndman, Carmel Lowe, Brian MacLean, David Mazzucchi, David Mosher, David Piper, Alexander Rabinovich, Alan Ruffman, Franck Saint-Ange, Fred Stephenson, and Kelin Wang. The manuscript was much improved thanks to an internal review by John Adams, and informal review comments by Josef Cherniawsky and Isaac Fine. Several figures in this report were prepared with the aid of GMT software (Wessel and Smith, 1995).

REFERENCES

Abe, K., 1979, Size of great earthquakes of 1837-1974 inferred from tsunami data, Journal of Geophysical Research, v. 84, B4, p. 1561-1568, doi:10.1029/JB084iB04p01561.

Abe, K., 1995, Estimate of tsunami run-up heights from earthquake magnitudes, In: Tsuchiya, Y., and Shuto, N. (eds.), Tsunami: progress in prediction, disaster prevention and warning, Advances in Technological Hazards Research, v. 4, Kluwer Academic Publishers, Dordrecht, the Netherlands, v. 4, p. 21-35.

Aksu, A.E., and Hiscott, R.N., 1989, Slides and debris flows on the high-latitude continental slopes of Baffin Bay, Geology, v. 17, no. 10, p. 885-888, doi:10.1130/0091-7613(1989)017<0885:SADFOT>2.3.CO;2.

Aksu, A.E., and Piper, D.J.W., 1987, Late Quaternary sedimentation in Baffin Bay, Canadian Journal of Earth Sciences, v. 24, no. 9, p. 1833-1846, doi:10.1139/e87-174.

Amundson, J.M., Truffer, M., Lüthi, M.P., Fahnestock, M., West, M., and Motyka, R.J., 2008. Glacier, fjord, and seismic response to recent large calving events, Jakobshavn Isbræ, Greenland, Geophysical Research Letters, v. 35, no. 22, L22501, doi:10.1029/2008GL035281.

Argus, D.F., Gordon, R.G., DeMets, C., and Stein, S., 1989, Closure of the Africa-Eurasia-North America plate motion circuit and tectonics of the Gloria fault, Journal of Geophysical Research, v. 94, B5, p. 5585-5602, doi:10.1029/JB094iB05p05585.

Atlantic and Gulf of Mexico Tsunami Hazard Assessment Group (AGMTHAG), 2008, Evaluation of tsunami sources with the potential to impact the U.S. Atlantic and Gulf coasts – a report to the Nuclear Regulatory Commission, U.S. Geological Survey Administrative Report, 300 p.

Atwater, B.F., 1999, Radiocarbon dating of a Seattle earthquake to A.D. 900-930, Seismological Research Letters, v. 70, no. 2, p. 232.

Atwater, B.F., and Griggs, G.B., 2012, Deep-sea turbidites as guides to Holocene earthquake history at the Cascadia subduction zone – alternative views for a seismic-hazard workshop, U.S. Geological Survey Open-File Report 2012-1043, 58 p.

Atwater, B.F., and Moore, A.L., 1992, A tsunami about 1000 years ago in Puget Sound, Washington, Science, v. 258, no. 5088, p. 1614-1617, doi:10.1126/science.258.5088.1614.

Atwater, B.F., Tuttle, M.P., Schweig, E.S., Rubin, C.M., Yamaguchi, D.K., and Hemphill-Haley, E., 2004, Earthquake recurrence inferred from paleoseismology, In: Gillespie, A.R., Porter, S.C., and Atwater, B.F. (eds.), The Quaternary Period in the United States, Elsevier Science, New York, p. 331-350.

Atwater, B.F., Musumi-Rokkaku, S., Satake, K., Tsuji, Y., Ueda, K., and Yamaguchi, D.K., 2005, The orphan tsunami of 1700 – Japanese clues to a parent earthquake in North America, U.S. Geological Survey Professional Paper 1707, 144 p.

Atwater, B.F., ten Brink, U.S., Buckley, M., Halley, R.S., Jaffe, B.E., López-Venegas, A.M., Reinhardt, E.G., Tuttle, M.P., Watt, W., and Wei, Y., 2010, Geomorphic and stratigraphic evidence for an unusual tsunami or storm a few centuries ago at Anegada, British Virgin Islands, Natural Hazards, doi:10.1007/s11069-010-9622-6.

Audet, P., Bostock, M.G., Mercier, J.-P., and Cassidy, J.F., 2008, Morphology of the Explorer-Juan de Fuca slab edge in northern Cascadia: imaging plate capture at a ridge-trench-transform triple junction, Geology, v. 36, no. 11, p. 895-898, doi:10.1130/G25356A.1.

Balfour, N.J., Cassidy, J.F., Dosso, S.E., and Mazzotti, S., 2011, Mapping crustal stress and strain in southwest British Columbia, Journal of Geophysical Research, v. 116, B03314, doi:10.1029/2010JB008003.

Baptista, M.A., and Miranda, J.M., 2009, Revision of the Portuguese catalog of tsunamis, Natural Hazards and Earth System Sciences, v. 9, no. 1, p. 25-42, doi:10.5194/nhess-9-25-2009.

Baptista, M.A., Heitor, S., Miranda, J.M., and Mendes Victor, L., 1998, The 1755 Lisbon tsunami: evaluation of the tsunami parameters, Journal of Geodynamics, v. 25, no. 2, p. 143-157, doi:10.1016/S0264-3707(97)00019-7.

Baptista, M.A., Miranda, J.M., Chierici, F., and Zitellini, N., 2003, New study of the 1755 earthquake source based on multi-channel seismic survey data and tsunami modeling, Natural Hazards and Earth System Sciences, v. 3, no. 5, p. 333-340, doi:10.5194/nhess-3-333-2003.

Barkan, R., ten Brink, U., and Lin, J., 2009, Far field tsunami simulations of the 1755 Lisbon earthquake: implications for tsunami hazard to the U.S. east coast and the Caribbean, Marine Geology, v. 264, no. 1-2, p. 109-122, doi:10.1016/j.margeo.2008.10.010.

Barrie, J.V., and Hill, P.R., 2004, Holocene faulting on a tectonic margin: Georgia Basin, British Columbia, Canada, Geo-Marine Letters, v. 24, p.86-96, doi:10.1007/s00367-003-0166-6.

Basham, P.W., Forsyth, D.A., and Wetmiller, R.J., 1977, The seismicity of northern Canada, Canadian Journal of Earth Sciences, v. 14, no. 7, p. 1646-1667, doi:10.1139/e77-140.

Becker, D., and Meier, T., 2010, Seismic slip deficit in the southwestern forearc of the Hellenic subduction zone, Bulletin of the Seismological Society of America, v. 100, no. 1, p. 325-342, doi:10.1785/0120090156.

Benetti, S., 2006, Late Quaternary sedimentary processes along the western North Atlantic margin, Ph.D. thesis, University of Southampton, Southampton, U.K., 188 p.

Ben-Menahem, A. and Rosenman, M., 1972, Amplitude patterns of tsunami waves from submarine earthquakes, Journal of Geophysical Research, v. 77, no. 17, p. 3097-3128, doi:10.1029/JB077i017p03097.

Bennett, R., Rochon, A., Schell, T., Bartlett, J., Blasco, S., Hughes-Clarke, J., Scott, D., MacDonald, A., and Rainey, W., 2008, Cruise Report Amundsen 2004-804: Beaufort Sea / Amundsen Gulf / Northwest Passage, June 23 – August 27, 2004, Geological Survey of Canada, Open File 5798, 111 p.

Bent, A.L., 2002, The 1933 Ms=7.3 Baffin Bay earthquake: strike-slip faulting along the northeastern Canadian passive margin, Geophysical Journal International, v. 150, p. 724-736, doi:10.1046/j.1365-246X.2002.01722.x.

Berninghausen, W.H., 1968, Tsunamis and seismic seiches reported from the western north and south Atlantic and the coastal waters of northwestern Europe, U.S. Naval Oceanographic Office Informal Report 68-85, 48 p.

Bilek, S.L., and Lay, T., 1999, Rigidity variations with depth along interplate megathrust faults in subduction zones, Nature, v. 400, p. 443-446, doi:10.1038/22739.

Bobrowsky, P.T., and Dominguez, M.J., 2010, Landslide susceptibility map of Canada, Geological Society of America Abstracts with Programs, v. 42, no. 5, p. 275.

Bodle, R.R., and Murphy, L.M., 1948, United States earthquakes, 1946, no. 714, U.S. Dept. of Commerce, Coast and Geodetic Survey, 48 p.

Bondevik, S., Løvholt, F., Harbitz, C., Mangerud, J., Dawson, A., and Svendsen, J.I., 2005, The Storegga Slide tsunami – comparing field observations with numerical simulations, Marine and Petroleum Geology, v. 22, no. 1-2, p. 195-208, doi:10.1016/j.marpetgeo.2004.10.003.

Bornhold, B.D., Harper, J.R., McLaren, D., and Thomson, R.E., 2007, Destruction of the First Nations village of Kwalate by a rock avalanche-generated tsunami, Atmosphere-Ocean, v. 45, no. 2, p. 123-128, doi:10.3137/ao.450205.

Bourgeois, J., 2009, Chapter 3: Geologic effects and records of tsunamis, In: Bernard, E.N., and Robinson, A.R. (eds.), The Sea, v. 15: Tsunamis, Harvard University Press, Cambridge, Massachusetts, p. 55-91.

Bourgeois, J., and Johnson, S.Y., 2001, Geologic evidence of earthquakes at the Snohomish delta, Washington, in the past 1200 yr, Geological Society of America Bulletin, v. 113, no. 4, p. 482-494, doi:10.1130/0016-7606(2001)113<0482:GEOEAT>2.0.CO;2.

Braunmiller, J., and Nábělek, J., 2002, Seismotectonics of the Explorer region, Journal of Geophysical Research, v. 107, B10, 2208, doi:10.1029/2001JB000220.

Bryn, P., Berg, K., Forsberg, C.F., Solheim, A., and Kvalstad, T.J., 2005, Explaining the Storegga Slide, Marine and Petroleum Geology, v. 22, p. 11-19, doi:10.1016/j.marpetgeo.2004.12.003.

Buckley, M.L., Wei, Y., Jaffe, B.E., and Watt, S.G., 2011, Inverse modeling of velocities and inferred cause of overwash that emplaced inland fields of boulders at Anegada, British Virgin Islands, Natural Hazards, doi:10.1007/s11069-011-9725-8.

Bucknam, R.C., Hemphill-Haley, E., and Leopold, E.B., 1992, Abrupt uplift within the past 1700 years at southern Puget Sound, Washington, Science, v. 258, no. 5088, p. 1611-1614, doi:10.1126/science.258.5088.1611.

Burbidge, D., Cummins, P.R., Mleczko, R., and Thio, H.K., 2008, A probabilistic tsunami hazard assessment for western Australia, Pure and Applied Geophysics, v. 165, no. 11-12, p. 2059-2088, doi:10.1007/978-3-0346-0057-6_6.

Bustin, A.M.M., 2006, The crustal structure, deformation from GPS, and seismicity related to oblique convergence along the Queen Charlotte margin, British Columbia, Ph.D. thesis, University of Victoria, Victoria, Canada, 226 p.

Bustin, A.M.M., Hyndman, R.D., Kao, H., and Cassidy, J.F., 2007, Evidence for underthrusting beneath the Queen Charlotte margin, from teleseismic receiver function analysis, Geophysical Journal International, v. 171, p. 1198-1211, doi:10.1111/j.1365-246X.2007.03583.x.

Calais, E., Béthoux, N., and Mercier de Lépinay, B., 1992, From transcurrent faulting to frontal subduction: a seismotectonic study of the northern Caribbean plate boundary from Cuba to Puerto Rico, Tectonics, v. 11, no. 1, p. 114-123, doi:10.1029/91TC02364.

Calais, E., Mazabraud, Y., Mercier de Lepinay, B., Mann, P., Mattioli, G., and Jansma, P., 2002, Strain partitioning and fault slip rates in the northeastern Caribbean from GPS measurements, Geophysical Research Letters, v. 106, p. 1–9, doi:10.1029/2002GL015397.

Calvert, A., Sandvol, E., Seber, D., Barazangi, M., Roecker, S., Mourabit, T., Vidal, F., Alguacil, G., and Jabour, N., 2000, Geodynamic evolution of the lithosphere and upper mantle beneath the Alboran region of the western Mediterranean: constraints from travel time tomography, Journal of Geophysical Research, v. 105, B5, p. 10871-10898, doi:10.1029/2000JB900024.

Campbell, D.C., and Saint-Ange, F., 2012, Hudson expedition 2010-023, northeast Newfoundland shelf and slope, June 18-July 3, 2010, Geological Survey of Canada, Open File 6930, 78 p, doi:10.4095/290238.

Carracedo, J.C., Day, S.J., Guillou, H., and Torrado, F.J.P., 1999, Giant Quaternary landslides in the evolution of La Palma and El Hierro Canary Islands, Journal of Volcanology and Geothermal Research, v. 94, no. 1-4, p. 169-190, doi:10.1016/S0377-0273(99)00102-X.

Cassidy, J.F., Ellis, R.M., Karavas, C., and Rogers, G.C., 1998, The northern limit of the subducted Juan de Fuca plate system, Journal of Geophysical Research, v. 103, B11, p. 26,949-26,961, doi:10.1029/98JB02140.

Cassidy, J.F., Rogers, G.C., and Waldhauser, F., 2000, Characterization of active faulting beneath the Strait of Georgia, Bulletin of the Seismological Society of America, v. 90, no.5, p. 1188-1199, doi:10.1785/0120000044.

Cauchon-Voyer, G., Locat, J., and St-Onge, G., 2008, Late-Quaternary morpho-sedimentology and submarine mass movements of the Betsiamites area, Lower St. Lawrence Estuary, Quebec, Canada, Marine Geology, v. 251, p. 233-252, doi:10.1016/j.margeo.2008.03.003.

Cauchon-Voyer, G., Locat, J., Leroueil, S., St-Onge, G., and Demers, D., 2011, Large-scale subaerial and submarine Holocene and recent mass movements in the Betsiamites area, Quebec, Canada, Engineering Geology, v. 121, p. 28-45, doi:10.1016/j.enggeo.2011.01.011.

Chassé, J., El-Sabh, M.I., and Murty, T.S., 1993, A numerical model for water level oscillations in the St. Lawrence Estuary, Canada, Part 2: Tsunamis, Marine Geodesy, v. 16, no. 2, p. 125-148, doi:10.1080/15210609309379684.

Chaytor, J.D., ten Brink, U.S., Solow, A.R., and Andrews, B.D., 2009, Size distribution of submarine landslides along the U.S. Atlantic margin, Marine Geology, v. 264, no. 1-2, p. 16-27, doi:10.1016/j.margeo.2008.08.007.

Cherniawsky, J.Y., Titov, V.V., Wang, K., and Li, J.-Y., 2007, Numerical simulations of tsunami waves and currents for southern Vancouver Island from a Cascadia megathrust earthquake, Pure and Applied Geophysics, v. 164, no. 2-3, p. 465-492, doi:10.1007/s00024-006-0169-0.

Christian, H.A., Mosher, D.C., Mulder, T., Barrie, J.V., and Courtney, R.C., 1997, Geomorphology and potential slope instability on Fraser River Delta foreslope, Vancouver, British Columbia, Canadian Geotechnical Journal, v. 34, no. 3, p. 432–446, doi:10.1139/t97-007.

Clague, J.J., Bobrowsky, P.T., and Hutchinson, I., 2000, A review of geological records of large tsunamis at Vancouver Island, British Columbia, and implications for hazard, Quaternary Science Reviews, v. 19, no. 9, p. 849-863, doi:10.1016/S0277-3791(99)00101-8.

Dash, R.K., Spence, G.D., Riedel, M., Hyndman, R.D., and Brocher, T.M., 2007, Upper-crustal structure beneath the Strait of Georgia, southwest British Columbia, Geophysical Journal International, v. 170, p. 800-812, doi:10.1111/j.1365-246X.2007.03455.x.

Davis, E.E., and Hyndman, R.D., 1989, Accretion and recent deformation of sediments along the northern Cascadia subduction zone, Geological Society of America Bulletin, v. 101, no. 11, p. 1465-1480, doi: 10.1130/0016-7606(1989)101<1465:AARDOS>2.3.CO;2.

Davis, E.E., and Riddihough, R.P., 1982, The Winona Basin: structure and tectonics, Canadian Journal of Earth Sciences, v. 19, no. 4, p. 767-788, doi:10.1139/e82-065.

Day, S., Kilburn, C., and McGuire, B., 2008, Tectonic threats in the Caribbean, Issues in Risk Science 8, Benfield UCL Hazard Research Centre, London, 32 p.

DeDontney, N., and Rice, J.R., 2011, Tsunami wave analysis and possibility of splay fault rupture during the 2004 Indian Ocean earthquake, Pure and Applied Geophysics, doi:10.1007/s00024-011-0438-4.

DeMets, C., Jansma, P.E., Mattioli, G.S., Dixon, T.H., Farina, F., Bilham, R., Calais, E., and Mann, P., 2000, GPS geodetic constraints on Caribbean–North America plate motion, Geophysical Research Letters, v. 27, p. 437–440, doi:10.1029/1999GL005436.

Dengler, L.A., and Magoon, O.T., 2006, Reassessing Crescent City, California's tsunami risk, Proceedings of the 8th U.S. National Conference on Earthquake Engineering, San Francisco, California, Paper 1451, 10 p.

Deptuck, M.E., Mosher, D.C., Campbell, D.C., Hughes-Clarke, J.E., and Noseworthy, D., 2007, Along slope variations in mass failures and relationships to major Plio-Pleistocene morphological elements, SW Labrador Sea, In: Lykousis, V., Sakellariou, D., and Locat, J. (eds.), Submarine Mass Movements and their Consequences, Advances in Natural and Technological Hazards Research, v. 27, Springer, the Netherlands, p. 37-46.

Dixon, T.H., Farina, F., DeMets, C., Jansma, P., Mann, P., and Calais, E., 1998, Relative motion between the Caribbean and North American plates and related boundary zone deformation from a decade of GPS observations, Journal of Geophysical Research, v. 103, B7, p. 15,157-15,182, doi:10.1029/97JB03575.

Dolan, J.F., and Wald, D.J., 1998, The 1943-1953 north-central Caribbean earthquakes: active tectonic setting, seismic hazards and implications for Caribbean-North America plate motions, In: Dolan, J.F., and Mann, P. (eds.), Active strike-slip and collisional tectonics of the northern Caribbean plate boundary zone, Geological Society of America Special Paper 326, p. 143-169.

Doser, D.I., Rodriguez, C.M., and Flores, C., 2005, Historical earthquakes of the Puerto Rico-Virgin Islands region (1915-1963), In: Mann, P. (ed.), Active tectonics and seismic hazards of Puerto Rico, the Virgin Islands, and offshore areas, Geological Society of America Special Paper 385, p. 103-114.

Dunbar, D.S., and Harper, J.R., 1993, Numerical simulation of tsunamigenic submarine slope failure in the Fraser River delta, British Columbia, Marine Geodesy, v. 16, no. 2, p. 101-108, doi:10.1080/15210609309379682.

Dunbar, D., LeBlond, P.H., and Murty, T.S., 1989, Maximum tsunami amplitudes and associated currents on the coast of British Columbia, Science of Tsunami Hazards, v. 7, no. 1, p. 3-44.

Dziak, R.P., 2006, Explorer deformation zone: evidence of a large shear zone and reorganization of the Pacific-Juan de Fuca-North American triple junction, Geology, v. 34, no. 3, p. 213-216, doi:10.1130/G22164.1.

Dziewonzki, A.M., and Anderson, D.L., 1981, Preliminary reference Earth model, Physics of the Earth and Planetary Interiors, v. 25, p. 297-356, doi:10.1016/0031-9201(81)90046-7.

Ebel, J.E., 2011, A new analysis of the magnitude of the February 1663 earthquake at Charlevoix, Quebec, Bulletin of the Seismological Society of America, v. 101, no. 3, p. 1024-1038, doi:10.1785/0120100190.

El-Sabh, M.I., Murty, T.S., and Dumais, J.-F., 1988, Tsunami hazards in the St. Lawrence Estuary, Canada, In: El-Sabh, M.I., and Murty, T.S. (eds.), Natural and Man-Made Hazards, D. Reidel Publishing, Dordrecht, the Netherlands, p. 201-213.

Evans, S.G., 2001, Landslides, In: Brooks, G.R. (ed.), A Synthesis of Geological Hazards in Canada, Geological Survey of Canada, Bulletin 548, p. 43-79.

Fernandes, R.M.S., Ambrosius, B.A.C., Noomen, R., Bastos, L., Wortel, M.J.R., Spakman, W., and Govers, R., 2003, The relative motion between Africa and Eurasia as derived from ITRF2000 and GPS data, Geophysical Research Letters, v. 30, no. 16, 1828, doi:10.1029/2003GL017089.

Fernandes, R.M.S., Miranda, J.M., Meijninger, B.M.L., Bos, M.S., Noomen, R., Bastos, L., Ambrosius, B.A.C., and Riva, R.E.M., 2007, Surface velocity field of the Ibero-Maghrebian segment of the Eurasia-Nubia plate boundary, Geophysical Journal International, v. 169, p. 315-324, doi:10.1111/j.1365-246X.2006.03252.x.

Fine, I.V., Rabinovich, A.B., Thomson, R.E., and Kulikov, E.A., 2003, Numerical modeling of tsunami generation by submarine and subaerial landslides, In: Yalçiner, A.C., Pelinovsky, E.N., Okal, E., and Synolakis, C.E. (eds.), Submarine Landslides and Tsunamis, Kluwer Academic Publishers, p. 69-88.

Fine, I.V., Rabinovich, A.B., Bornhold, B.D., Thomson, R.E., and Kulikov, E.A., 2005, The Grand Banks landslide-generated tsunami of November 18, 1929: preliminary analysis and numerical modeling, Marine Geology, v. 215, no. 1-2, p. 45-57, doi:10.1016/j.margeo.2004.11.007.

Fine, I.V., Cherniawsky, J.Y., Rabinovich, A.B., and Stephenson, F., 2009, Numerical modeling and observations of tsunami waves in Alberni Inlet and Barkley Sound, British Columbia, Pure and Applied Geophysics, v. 165, p. 2019-2044, doi:10.1007/s00024-008-0414-9.

Frankel, A.D., 2011, Summary of November 2010 meeting to evaluate turbidite data for constraining the recurrence parameters of great Cascadia earthquakes for the update of the national seismic hazard maps, U.S. Geological Survey Open-File Report 2011-1310, 13p.

Garcia-Orellana, J., Gràcia, E., Vizcaino, A., Masqué, P., Olid, C., Martínez-Ruiz, F., Piñero, E., Sanchez-Cabeza, J.-A., and Dañobeitia, J., 2006, Identifying instrumental and historical earthquake records in the SW Iberian margin using 210Pb turbidite chronology, Geophysical Research Letters, v. 33, L24601, doi:10.1029/2006GL028417.

Geist, E.L., 2002, Complex earthquake rupture and local tsunamis, Journal of Geophysical Research, v. 107, B5, doi:10.1029/2000JB000139.

Geist, E.L., 2005, Local tsunami hazards in the Pacific Northwest from Cascadia subduction zone earthquakes, U.S. Geological Survey Professional Paper 1661-B, 17 p.

Geist, E.L., and Bilek, S.L., 2001, Effect of depth-dependent shear modulus on tsunami generation along subduction zones, Geophysical Research Letters, v. 28, no. 7, p. 1315-1318, doi:10.1029/2000GL012385.

Geist, E.L., and Parsons, T., 2006, Probabilistic analysis of tsunami hazards, Natural Hazards, v. 37, p. 277-314, doi:10.1007/s11069-005-4646-z.

Geist, E.L., and Parsons, T., 2009, Assessment of source probabilities for potential tsunamis affecting the U.S. Atlantic coast, Marine Geology, v. 264, no. 1-2, p. 98-108, doi:10.1016/j.margeo.2008.08.005.

Geist, E.L., Titov, V.V., and Synolakis, C.E., 2006, Tsunami: wave of change, Scientific American, v. 294, p. 56-63, doi:10.1038/scientirficamerican0106-56.

Geist, E.L., Parsons, T., ten Brink, U.S., and Lee, H.J., 2009a, Chapter 4: Tsunami probability, In: Bernard, E.N., and Robinson, A.R. (eds.), The Sea, v. 15: Tsunamis, Harvard University Press, Cambridge, Massachusetts, p. 93-136.

Geist, E.L., Lynett, P.J., and Chaytor, J.D., 2009b, Hydrodynamic modeling of tsunamis from the Currituck landslide, Marine Geology, v. 264, no. 1-2, p. 41-52, doi:10.1016/j.margeo.2008.09.005.

Giles, M.K., Mosher, D.C., Piper, D.J.W., and Wach, G.D., 2010, Mass transport processes on the southwestern Newfoundland Slope, In: Mosher, D.C., Shipp, R.C., Moscardelli, L., Chaytor, J.D.,

Baxter, C.D.P., Lee, H.J., and Urgeles, R. (eds.), Submarine Mass Movements and their Consequences, Advances in Natural and Technological Hazards Research, v. 28, Springer, the Netherlands, p. 657-666.

Gisler, G., Weaver, R., and Gittings, M.L., 2006, SAGE calculations of the tsunami threat from La Palma, Science of Tsunami Hazards, v. 24, no. 4, p. 288-301.

Gisler, G., Weaver, R., and Gittings, M., 2011, Calculations of asteroid impacts into deep and shallow water, Pure and Applied Geophysics, v. 168, p. 1187-1198, doi:10.1007/s00024-010-0225-7.

Goldfinger, C., 2009, Paleoseismically derived probabilities for Cascadia great earthquakes, Geological Society of America Abstracts with Programs, v. 41, no. 7, p. 520.

Goldfinger, C., Kulm, L.D., McNeill, L.C., and Watts, P., 2000, Super-scale failure of the southern Oregon Cascadia margin, Pure and Applied Geophysics, v. 157, no. 6-8, p. 1189-1226, doi:10.1007/s000240050023.

Goldfinger, C., Nelson, C.H., Johnson, J.E., and the Shipboard Scientific Party, 2003, Holocene earthquake records from the Cascadia subduction zone and northern San Andreas Fault based on precise dating of offshore turbidites, Annual Reviews of Earth and Planetary Sciences, v. 31, p. 555-577, doi:10.1146/annurev.earth.31.100901.141246.

Goldfinger, C., Nelson, C.H., Morey, A.E., Johnson, J.E., Patton, J., Karabanov, E., Gutiérrez-Pastor, J., Eriksson, A.T., Gràcia, E., Dunhill, G., Enkin, R.J., Dallimore, A., and Vallier, T., 2012, Turbidite event history: methods and implications for Holocene paleoseismicity of the Cascadia subduction zone, U.S. Geological Survey Professional Paper 1661-F, 170 p.

Goto, K., Chagué-Goff, C., Fujino, S., Goff, J., Jaffe, B., Nishimura, Y., Richmond, B., Sugawara, D., Szczuciński, W., Tappin, D.R., Witter, R.C., and Yulianto, E., 2011, New insights of tsunami hazard from the 2011 Tohoku-oki event, Marine Geology, v. 290, no. 1-4, p. 46-50, doi:10.1016/j.margeo2011.10.004.

Gràcia, E., Dañobeitia, J., Vergés, J., and the PARSIFAL Team, 2003, Mapping active faults offshore Portugal (36°N-38°N): implications for seismic hazard assessment along the southwest Iberian margin, Geology, v. 31, no. 1, p. 83-86, doi:10.1130/0091-7613(2003)031<0083:MAFOPN>2.0.CO;2.

Gràcia, E., Vizcaino, A., Escutia, C., Asioli, A., Rodés, A., Garcia-Orellano, J., Lebreiro, S., and Goldfinger, C., 2010, Holocene earthquake record offshore Portugal (SW Iberia): testing turbidite paleoseismology in a slow-convergence margin, Quaternary Science Reviews, v. 29, p. 1156-1172, doi:10.1016/j.quascirev.2010.01.010.

Grantz, A., Phillips, R.L., Mullen, M.W., Starratt, S.W., Jones, G.A., Sathy Naidu, A., and Finney, B.P., 1996, Character, paleoenvironment, rate of accumulation, and evidence for seismic triggering of Holocene turbidites, Canada Abyssal Plain, Arctic Ocean, Marine Geology, v. 133, p. 51-73, doi:10.1016/0025-3227(96)00015-1.

Grilli, S.T., Taylor, O.-D.S., Baxter, C.D.P., and Maretzki, S., 2009, A probabilistic approach for determining submarine landslide tsunami hazard along the upper east coast of the United States, Marine Geology, v. 264, no. 1-2, p. 74-97, doi:10.1016/j.margeo.2009.02.010.

Gusiakov, V.K., 2009, Chapter 2: Tsunami history: recorded, In: Bernard, E.N., and Robinson, A.R. (eds.), The Sea, v. 15: Tsunamis, Harvard University Press, Cambridge, Massachusetts, p. 23-53.

Gutscher, M.-A., and Westbrook, G.K., 2009, Great earthquakes in slow-subduction, low-taper margins, In: Lallemand, S., and Funicello, F. (eds.), Subduction Zone Geodynamics, Springer-Verlag, Berlin Heidelberg, p. 119-133, doi:10.1007/978-3-540-87974-9.

Gutscher, M.-A., Malod, J., Rehault, J.-P., Contrucci, I., Klingelhoefer, F., Mendes-Victor, L., and Spakman, W., 2002, Evidence for active subduction beneath Gibraltar, Geology, v. 30, p. 1071-1074, doi:10.1130/0091-7613(2002)030<1071:EFASBG>2.0.CO;2.

Gutscher, M.-A., Baptista, M.A., and Miranda, J.M., 2006, The Gibraltar Arc seismogenic zone (part 2): constraints on a shallow east dipping fault plane source for the 1755 Lisbon earthquake provided by tsunami modeling and seismic intensity, Tectonophysics, v. 426, p. 153-166, doi:10.1016/j.tecto.2006.02.025.

Gutscher, M.-A., Baptista, M.A., Miranda, J.M., Omara, R., and Marcaillou, B., 2008, Long term hazard from Atlantic subduction zones (Antilles and Cadiz/Gibraltar) and the example of the great Lisbon earthquake and tsunami of 1755, Eos Transactions, American Geophysical Union, v. 89, no. 53, Abstract OS53B-1307.

Gutscher, M., Dominguez, S., Westbrook, G.K., and Leroy, P., 2009a, Deep structure, recent deformation and analog modeling of the Gulf of Cadiz accretionary wedge: implications for the 1755 Lisbon earthquake, Tectonophysics, v. 475, p. 85-97, doi:10.1016/j.tecto.2008.11.031.

Gutscher, M., Westbrook, G.K., Marcaillou, B., Graindorge, D., Gailler, A., Pichot, T., and Maury, R., 2009b, How wide is the seismogenic zone of the Lesser Antilles forearc?, Eos Transactions, American Geophysical Union, v. 90, no. 52, Abstract T11D-08.

Gutscher, M.-A., Westbrook, G.K., Marcaillou, B., Graindorge, D., Gailler, A., Pichot, T., and Maury, R.C., 2010, Along strike variations in the width of the seismogenic zone of the Lesser Antilles subduction predicted by thermal modeling, Geophysical Research Abstracts, v. 12, EGU2010, p. 10600.

Gutscher, M.-A., Dominguez, S., Westbrook, G.K., Le Roy, P., Rosas, F., Duarte, J.C., Terrinha, P., Miranda, J.M., Graindorge, D., Gailler, A., Sallares, V., and Bartolome, R., 2012, The Gibraltar subduction: a decade of new geophysical data, Tectonophysics, v. 574-575, p. 72-91, doi:10.1016/j.tecto.2012.08.038.

Haflidason, H., Sejrup, H.P., Nygård, A., Mienert, J., Bryn, P., Lien, R., Forsberg, C.F., Berg, K., and Masson, D., 2004, The Storegga Slide: architecture, geometry and slide development, Marine Geology, v. 213, p. 201–234, doi:10.1016/j.margeo.2004.10.007.

Halchuk, S., and Adams, J., 2008, Fourth generation seismic hazard maps of Canada: maps and grid values to be used with the 2005 National Building Code of Canada, 1 CD-ROM.

Hanks, T.C., and Kanamori, H., 1979, A moment magnitude scale, Journal of Geophysical Research, v. 84, B5, p. 2348-2350, doi:10.1029/JB084iB05p02348.

Harbitz, C.B., Løvholt, F., Pedersen, G., and Masson, D.G., 2006, Mechanisms of tsunami generation by submarine landslides: a short review, Norwegian Journal of Geology, v. 86, p. 255-264.

Harper, J.R., Henry, R.F., and Stewart, G.G., 1988, Maximum storm surge elevations in the Tuktoyaktuk region of the Canadian Beaufort Sea, Arctic, v. 41, no. 1, p. 48–52.

Hasegawa, H.S., Chou, C.W., and Basham, P.W., 1979, Seismotectonics of the Beaufort Sea, Canadian Journal of Earth Sciences, v. 16, no. 4, p. 816-830, doi:10.1139/e79-072.

Haugerud, R.A., Harding, D.J., Johnson, S.Y., Harless, J.L., Weaver, C.S., and Sherrod, B.L., 2003, High-resolution Lidar topography of the Puget Lowland, Washington – a bonanza for Earth Science, GSA Today, June 2003, p. 4-10.

Hayward, N., Nedimović, M.R., Cleary, M., and Calvert, A.J., 2006, Structural variation along the Devil's Mountain fault zone, northwestern Washington, Canadian Journal of Earth Sciences, v. 43, p. 433-446, doi:10.1139/E06-002.

Heezen, B.C., and Ewing, M., 1952, Turbidity currents and submarine slumps, and the 1929 Grand Banks earthquake, American Journal of Science, v. 250, no. 12, p. 849-873, doi:10.2475/ajs.250.12.849.

Henry, R.F., and Heaps, N.S., 1976, Storm surges in the southern Beaufort Sea, Journal of the Fisheries Research Board of Canada, v. 33, no. 10, p. 2362-2376, doi:10.1139/f76-283.

Henry, R.F., and Murty, T.S., 1995, Tsunami amplification due to resonance in Alberni Inlet: normal modes, In: Tsuchiya, Y., and Shuto, N. (eds.), Tsunami: progress in prediction, disaster prevention and warning, Advances in Technological Hazards Research, v. 4, Kluwer Academic Publishers, Dordrecht, the Netherlands, p. 117-128.

Heuret, A., Lallemand, S., Funiciello, F., Piromallo, C., and Faccenna, C., 2011, Physical characteristics of subduction interface type seismogenic zones revisited, Geochemistry Geophysics Geosystems, v. 12, no. 1, doi:10.1029/2010GC003230.

Hill, P.R., Moran, K.M., and Blasco, S.M., 1982, Creep deformation of slope sediments in the Canadian Beaufort Sea, Geo-Marine Letters, v. 2, no. 3-4, p. 163-170, doi:10.1007/BF02462758.

Hill, P.R., Lewis, C.P., Desmarais, S., Kauppaymuthoo, V., and Rais, H., 2001, The Mackenzie Delta: sedimentary processes and facies of a high-latitude, fine-grained delta, Sedimentology, v. 48, no. 5, p. 1047-1078, doi:10.1046/j.1365-3091.2001.00408x.

Hills, J.G., and Goda, M.P., 2001, The asteroid tsunami project at Los Alamos, Science of Tsunami Hazards, v. 19, no. 1, p. 55-65.

Hodgson, E.A., 1946, British Columbia earthquake, June 23, 1946, The Journal of the Royal Astronomical Society of Canada, v. 40, no. 8, p. 285-319.

Hornbach, M.J., Lavier, L.L., and Ruppel, C.D., 2007, Triggering mechanism and tsunamigenic potential of the Cape Fear Slide complex, U.S. Atlantic margin, Geochemistry Geophysics Geosystems, v. 8, Q12008, doi:10.1029/2007GC001722.

Houseknecht, D.W., and Bird, K.J., 2011, Chapter 34: Geology and petroleum potential of the rifted margins of the Canada Basin, In: Spencer, A.M., Embry, A.F., Gautier, D.L., Stoupakova, A.V., and Sørensen, K. (eds.), Arctic Petroleum Geology, Geological Society, London, Memoirs, v. 35, p. 509-526, doi:10.1144/M35.34.

Huppertz, T.J., and Piper, D.J.W., 2009, The influence of shelf-crossing glaciation on continental slope sedimentation, Flemish Pass, eastern Canadian continental margin, Marine Geology, v. 265, p. 67-85, doi:10.1016/j.margeo.2009.06.017.

Hutchinson, I., and McMillan, A.D., 1997, Archaeological evidence for village abandonment associated with late Holocene earthquakes at the northern Cascadia subduction zone, Quaternary Research, v. 48, no. 1, p. 79-87, doi:10.1006/qres.1997.1890.

Hyndman, R.D., 2007, The seismogenic zone of subduction thrust faults: what we know and don't know, In: Dixon, T.H., and Moore, S.C. (eds.), The seismogenic zone of subduction thrust faults, Columbia Univ. Press, p. 15-40.

Hyndman, R.D., and Ellis, R.M., 1981, Queen Charlotte fault zone: microearthquakes from a temporary array of land stations and ocean bottom seismographs, Canadian Journal of Earth Sciences, v. 18, no. 4, p. 776-788, doi:10.1139/e81-071.

Hyndman, R.D., and Hamilton, T.S., 1993, Queen Charlotte area Cenozoic tectonics and volcanism and their association with relative plate motions along the northeastern Pacific margin, Journal of Geophysical Research, v. 98, B8, p. 14,257-14,277, doi:10.1029/93JB00506.

Hyndman, R.D., and Wang, K., 1995, The rupture zone of Cascadia great earthquakes from current deformation and the thermal regime, Journal of Geophysical Research, v. 100, no., B11, p. 22,133-22,154, doi:10.1029/95JB01970.

Hyndman, R.D., Mazzotti, S., Weichert, D., and Rogers, G.C., 2003, Frequency of large crustal earthquakes in Puget Sound – southern Georgia Strait predicted from geodetic and geological deformation rates, Journal of Geophysical Research, v. 108, B1, 2033, doi:10.1029/2001JB001710.

Hyndman, R.D., Cassidy, J.F., Adams, J., Rogers, G.C., and Mazzotti, S., 2005, Earthquakes and seismic hazard in the Yukon-Beaufort-Mackenzie, Canadian Society of Exploration Geophysicists Recorder, May 2005, p. 32-66.

Imamura, F., 2009, Chapter 10: Tsunami modeling: calculating inundation and hazard maps, In: Bernard, E.N., and Robinson, A.R. (eds.), The Sea, v. 15: Tsunamis, Harvard University Press, Cambridge, Massachusetts, p. 321-332.

Jacoby, G.C., Williams, P.L., and Buckley, B.M., 1992, Tree ring correlation between prehistoric landslides and abrupt tectonic events in Seattle, Washington, Science, v. 258, no. 5088, p. 1621-1623, doi:10.1126/science.258.5088.1621.

Jansma, P.E., Mattioli, G.S., Lopez, A., DeMets, C., Dixon, T.H., Mann, P., and Calais, E., 2000, Neotectonics of Puerto Rico and the Virgin Islands, northeastern Caribbean, from GPS geodesy, Tectonics, v. 19, no. 6, p. 1021-1037, doi:10.1029/1999TC001170.

Jenner, K.A., and Hill, P.R., 1998, Recent, arctic deltaic sedimentation: Olivier Islands, Mackenzie Delta, North-west Territories, Canada, Sedimentology, v. 45, no. 6, p. 987-1004, doi:10.1046/j.1365-3091.1998.00193.x.

Jibson, R.W., Harp, E.L., Michael, J.A., 2000, A method for producing digital probabilistic seismic landslide hazard maps, Engineering Geology, v. 58, no. 3-4, p. 271-289, doi:10.1016/S0013-7952(00)00039-9.

Johnson, S.Y., Potter, C.J., Armentrout, J.M., Miller, J.J., Finn, C., and Weaver, C.S., 1996, The southern Whidbey Island fault: an active structure in the Puget Lowland, Washington, Geological Society of America Bulletin, v. 108, no. 3, p. 334-354, doi:10.1130/0016-7606(1996)108<0334:TSWIFA>2.3.CO;2.

Johnson, S.Y., Dadisman, S.V., Mosher, D.C., Blakely, R.J., and Childs, J.R., 2001, Active tectonics of the Devils Mountain fault and related structures, northern Puget Lowland and eastern Strait of Juan de Fuca region, Pacific Northwest, U.S. Geological Survey Professional Paper 1643, 65 p. text, 2 tables, 38 figs., 2 plates.

Johnson, S.Y., Nelson, A.R., Personius, S.F., Wells, R.E., Kelsey, H.M., Sherrod, B.L., Okumura, K., Koehler, R., III, Witter, R.C., Bradley, L.-A., and Harding, D.J., 2004, Evidence for late Holocene earthquakes on the Utsalady Point fault, northern Puget Lowland, Washington, Bulletin of the Seismological Society of America, v. 94, no. 6, p. 2299-2316, doi:10.1785/0120040050.

Johnston, A.C., 1996, Seismic moment assessment of earthquakes in stable continental regions-III. New Madrid 1811-1812, Charleston 1886 and Lisbon 1755, Geophysical Journal International, v. 126, no. 2, p. 314-344, doi:10.1111/j.1365-246X.1996.tb05294.x.

Jolly, W.T., Lidiak, E.G., and Dickin, A.P., 2008, Bimodal volcanism in northeast Puerto Rico and the Virgin Islands (Greater Antilles Island Arc): genetic links with Cretaceous subduction of the mid-Atlantic ridge Caribbean spur, Lithos, v. 103, p. 393-414, doi:10.1016/j.lithos.2007.10.008.

Kao, H., Shan, S.-J., Dragert, H., and Rogers, G., 2009, Northern Cascadia Episodic Tremor and Slip: A decade of tremor observations from 1997 to 2007, Journal of Geophysical Research, v. 114, B00A12, doi:10.1029/2008JB006046.

Karlin, R.E., Holmes, M., Abella, S.E.B., and Sylwester, R., 2004, Holocene landslides and a 3500-year record of Pacific Northwest earthquakes from sediments in Lake Washington, Geological Society of America Bulletin, v. 116, no. 1/2, p. 94-108, doi:10.1130/B25158.1.

Kayen, R.E., and Lee, H.J., 1991, Pleistocene slope instability of gas hydrate-laden sediment on the Beaufort sea margin, Marine Georesources and Geotechnology, v. 10, no. 1-2, p. 125-141, doi:10.1080/10641199109379886.

Kelsey, H.M., Sherrod, B., Johnson, S.Y., and Dadisman, S.V., 2004, Land-level changes from a late Holocene earthquake in the northern Puget Lowland, Washington, Geology, v. 32, no. 6, p. 469-472, doi:10.1130/G20361.1.

Kelsey, H.M., Sherrod, B.L., Blakely, R.J., and Haugerud, R.A., 2012, Holocene faulting in the Bellingham forearc basin: upper-plate deformation at the northern end of the Cascadia subduction zone, Journal of Geophysical Research, v. 117, B03409, doi:10.1029/2011JB008816.

Knight, B., 2006, Model prediction of Gulf and southern Atlantic coast tsunami impacts from a distribution of sources, Science of Tsunami Hazards, v. 24, no. 5, p. 304-312.

Korup, O., and Clague, J.J., 2009, Natural hazards, extreme events, and mountain topography, Quaternary Science Reviews, v. 28, no. 11-12, p. 977-990, doi:10.1016/j.quascirev.2009.02.021.

Koshimura, S., Mofjeld, H.O., González, F.I., and Moore, A.L., 2002, Modeling the 1100 bp paleotsunami in Puget Sound, Washington, Geophysical Research Letters, v. 29, no. 20, 1948, doi:10.1029/2002GL015170.

Kreemer, C., Govers, R., Furlong, K.P., and Holt, W.E., 1998, Plate boundary deformation between the Pacific and North America in the Explorer region, Tectonophysics, v. 293, no. 3-4, p. 225-238, doi:10.1016/S0040-1951(98)00089-4.

Kulikov, E.A., Rabinovich, A.B., Thomson, R.E., and Bornhold, B.D., 1996, The landslide tsunami of November 3, 1994, Skagway Harbor, Alaska, Journal of Geophysical Research, v. 101, C3, p. 6609-6615, doi:10.1029/95JC03562.

LaForge, R.C., and McCann, W.R., 2005, A seismic source model for Puerto Rico, for use in probabilistic ground motion hazard analyses, In: Mann, P. (ed.), Active tectonics and seismic hazards of Puerto

Rico, the Virgin Islands, and offshore areas, Geological Society of America Special Paper 385, p. 223-248.
Lamontagne, M., 2009, Possible earthquake triggers of submarine landslides in the estuary of the St. Lawrence River: insights from the earthquake catalogue, Geological Survey of Canada, Open File 6007, 1 CD-ROM, 61 p.
Lander, J., 1995, Nonseismic event in Skagway, Alaska, Tsunami Newsletter, v. 27, no. 1, p. 8-9.
Lander, J.F., Whiteside, L.S., and Lockridge, P.A., 2002, A brief history of tsunamis in the Caribbean Sea, Science of Tsunami Hazards, v. 20, no. 2, p. 57-94.
Lane, L., 2002, Tectonic evolution of the Canadian Beaufort Sea – Mackenzie Delta region" a brief review, Canadian Society of Exploration Geophysicists Recorder, February 2002, p. 49-56.
Lee, H.J., 2009, Timing of occurrence of large submarine landslides on the Atlantic Ocean margin, Marine Geology, v. 264, no. 1-2, p. 53-64, doi:10.1016/j.margeo.2008.09.009.
Leonard, L.J., Hyndman, R.D., and Mazzotti, S., 2004, Coseismic subsidence in the 1700 great Cascadia earthquake: Coastal estimates versus elastic dislocation models, Geological Society of America Bulletin, v. 116, p. 655-670, doi:10.1130/B25369.1.
Leonard, L.J., Hyndman, R.D., Mazzotti, S., Nykolaishen, L., Schmidt, M., and Hippchen, S., 2007, Current deformation in the northern Canadian Cordillera inferred from GPS measurements, Journal of Geophysical Research, v. 112, B11401, doi:10.1029/2007JB005061.
Leonard, L.J., Rogers, G.C., and Hyndman, R.D., 2010a, Annotated bibliography of references relevant to tsunami hazard in Canada, Geological Survey of Canada, Open File 6552, 269 p.
Leonard, L.J., Currie, C.A., Mazzotti, S., and Hyndman, R.D., 2010b, Rupture area and displacement of past Cascadia great earthquakes from coastal coseismic subsidence, Geological Society of America Bulletin, v. 122, p. 2079-2096, doi:10.1130/B30108.1.
Lewis, T., Francus, P., and Bradley, R.S., 2007, Limnology, Sedimentology, and hydrology of a jökulhlaup into a meromictic High Arctic lake, Canadian Journal of Earth Sciences, v. 44, p. 791-806, doi:10.1139/E06-125.
Li, G., Piper, D.J.W., and Campbell, D.C., 2010, The Quaternary Lancaster Sound trough-mouth fan, NW Baffin Bay, In: Atlantic Geoscience Society Abstracts, Atlantic Geology, v. 46, p. 59.
Lintern, D.G., and Hill, P.R., 2010, An underwater laboratory at the Fraser River delta, Eos Transactions, American Geophysical Union, v. 91, no. 38, p. 333-334, doi:10.1029/2010EO380001.
Liu, P.L.-F., 2009, Chapter 9: Tsunami modeling: propagation, In: Bernard, E.N., and Robinson, A.R. (eds.), The Sea, v. 15: Tsunamis, Harvard University Press, Cambridge, Massachusetts, p. 295-319.
Liu, Y., and Rice, J.R., 2007, Spontaneous and triggered aseismic deformation transients in a subduction fault model, Journal of Geophysical Research, v. 112, B09404, doi:10.1029/2007JB004930.
Locat, J., Martin, F., Levesque, C., Locat, P., Leroueil, S., Konrad, J.M., Urgeles, R., Canals, M., and Duchesne, M.J., 2003, Submarine mass movements in the upper Saguenay Fjord, (Québec, Canada), triggered by the 1663 earthquake, In: Locat, J., and Mienert, J. (eds.), Submarine Mass Movements and their Consequences, Advances in Natural and Technological Hazards Research, v. 19, Kluwer Academic Publishers, Dordrecht, the Netherlands, p. 509-519.
López, C., Spence, G., Hyndman, R., and Kelley, D., 2010, Frontal ridge slope failure at the northern Cascadia margin: margin-normal fault and gas hydrate control, Geology, v. 38, no. 11, p. 967-970, doi:10.1130/G31136.1.
Ludwin, R.S., Dennis, R., Carver, D., McMillan, A.D., Losey, R., Clague, J., Jonientz-Trisler, C., Bowechop, J., Wray, J., and James, K., 2005, Dating the 1700 Cascadia earthquake: great coastal earthquakes in Native stories, Seismological Research Letters, v. 76, no. 2, p. 140-148, doi:10.1785/gssrl.76.2.140.
Luque, L., Lario, J., Civis, J., Silva, P.G., Zazo, C., Goy, J.L., and Dabrio, C.J., 2002, Sedimentary record of a tsunami during Roman times, Bay of Cadiz, Spain, Journal of Quaternary Science, v. 17, no. 5-6, p. 623-631, doi:10.1002/jqs.711.
Macayeal, D.R., Abbot, D.S., and Sergienko, O.V., 2011, Iceberg-capsize tsunamigenesis, Annals of Glaciology, v. 52, no. 58, p. 51-56.

MacLean, B., Vilks, G., Hardy, I., Deonarine, B., Jennings, A.E., and Manley, W.F., 2001, Quaternary sediments in Hudson Strait and Ungava Bay, In: MacLean, B. (ed.), Marine Geology of Hudson Strait and Ungava Bay, Eastern Arctic Canada: Late Quaternary Sediments, Depositional Environments, and Late Glacial-Deglacial History Derived from Marine and Terrestrial Studies, Geological Survey of Canada, Bulletin 566, p. 71-125.

Mader, C., 2001, Modeling the La Palma landslide tsunami, Science of Tsunami Hazards, v. 19, no. 3, p. 150-170.

Manaker, D.M., Calais, E., Freed, A.M., Ali, S.T., Przybylski, P., Mattioli, G., Jansma, P., Prépetit, C., and de Chabalier, J.B., 2008, Interseismic plate coupling and strain partitioning in the northeastern Caribbean, Geophysical Journal International, v. 174, p. 889-903, doi:10.1111/j.1365-246X.2008.03819.x.

Mann, P., Calais, E., Ruegg, J.-C., DeMets, C., Jansma, P.E., and Mattioli, G.S., 2002, Oblique collision in the northeastern Caribbean from GPS measurements and geological observations, Tectonics, v. 21, no. 6., 1057, doi:10.1029/2001TC001304.

Masson, D.G., Watts, A.B., Gee, M.J.R., Urgeles, R., Mitchell, N.C., Le Bas, T.P., and Canals, M., 2002, Slope failures on the flanks of the western Canary Islands, Earth-Science Reviews, v. 57, no. 1-2, p. 1-35, doi:10.1016/S0012-8252(01)00069-1.

Mathewes, R.W., and Clague, J.J., 1994, Detection of large prehistoric earthquakes in the Pacific Northwest by microfossil analysis, Science, v. 264, no. 5159, p. 688-691, doi:10.1126/science.264.5159.688.

Mazzotti, S., and Adams, J., 2004, Variability of near-term probability for the next great earthquake on the Cascadia subduction zone, Bulletin of the Seismological Society of America, v. 94, no. 5, p. 1954-1959, doi:10.1785/012004032.

Mazzotti, S., and Adams, J., 2005, Rates and uncertainties on seismic moment and deformation in eastern Canada, Journal of Geophysical Research, v. 110, B09301, doi:10.1029/2004JB003510.

Mazzotti, S., Hyndman, R.D., Flück, P., Smith, A.J., and Schmidt, M., 2003a, Distribution of the Pacific/North America motion in the Queen Charlotte Islands-S. Alaska plate boundary zone, Geophysical Research Letters, v. 30, no. 14, 1762, doi:10.1029/2003GL017586.

Mazzotti, S., Dragert, H., Henton, J., Schmidt, M., Hyndman, R., James, T., Lu, Y., and Craymer, M., 2003b, Current tectonics of northern Cascadia from a decade of GPS measurements, Journal of Geophysical Research, v. 108, B12, 2554, doi:10.1029/2003JB002653.

Mazzotti, S., James, T.S., Henton, J., and Adams, J., 2005, GPS crustal strain, postglacial rebound, and seismic hazard in eastern North America: the Saint Lawrence valley example, Journal of Geophysical Research, v. 110, B11301, doi:10.1029/2004JB003590.

Mazzotti, S., Leonard, L.J., Hyndman, R.D., and Cassidy, J.F., 2008, Tectonics, dynamics and seismic hazard in the Canada-Alaska Cordillera, In: Freymueller, J.T., Haeussler, P.J., Wesson, R.L., and Ekström, G. (eds.), Active tectonics and seismic potential of Alaska, AGU Monograph, p. 297-319.

McAdoo, B.G., and Watts, P., 2004, Tsunami hazard from submarine landslides on the Oregon continental slope, Marine Geology, v. 203, no. 3-4, p. 235-245, doi:10.1016/S0025-3227(03)00307-4.

McCaffrey, R., Long, M.D., Goldfinger, C., Zwick, P.C., Nabelek, J.L., Johnson, C.K., and Smith, C., 2000, Rotation and plate locking at the southern Cascadia subduction zone, Geophysical Research Letters, v. 27, no. 19, p. 3117-3120, doi:10.1029/2000GL011768.

McCann, W.R., 1985, On the earthquake hazards of Puerto Rico and the Virgin Islands, Bulletin of the Seismological Society of America, v. 75, no. 1, p. 251-262.

McMurtry, G.M., Fryer, G.J., Tappin, D.R., Wilkinson, I.P., Williams, M., Fietzke, J., Garbe-Schoenberg, D., and Watts, P., 2004a, Megatsunami deposits on Kohala volcano, Hawaii, from flank collapse of Mauna Loa, Geology, v. 32, p. 741–744, doi:10.1130/G20642.1.

McMurtry, G.M., Watts, P., Fryer, G.J., Smith, J.R., and Imamura, F., 2004b, Giant landslides, mega-tsunamis, and paleo-sea level in the Hawaiian Islands, Marine Geology, v. 203, p. 219–233, doi:10.1016/S0025-3227(03)00306-2.

Mercado, A., and McCann, W., 1998, Numerical simulation of the 1918 Puerto Rico tsunami, Natural Hazards, v. 18, no. 1, p. 57-76, doi:10.1023/A:1008091910209.

Miller, D.J., 1960, Giant waves in Lituya Bay, Alaska, U.S. Geological Survey Professional Paper 354-C, p. 51-86.

Monserrat, S., Vilibić, I., and Rabinovich, A.B., 2006, Meteotsunamis: atmospherically induced destructive ocean waves in the tsunami frequency band, Natural Hazards and Earth System Sciences, v. 6, no. 6, p. 1035-1051, doi:10.5194/nhess-6-1035-2006.

Moore, G.W., and Moore, J.G., 1984, Deposit from a giant wave on the island of Lanai, Hawaii, Science, v. 226, no. 4680, p. 1312–1315, doi:10.1126/science.226.4680.1312.

Moore, J.G., Normark, W.R., and Holcomb, R.T., 1994a, Giant Hawaiian landslides, Annual Review of Earth and Planetary Sciences, v. 22, p. 119-144, doi:10.1146/annurev.ea.22.050194.001003.

Moore, J.G., Bryan, W.B., and Ludwig, K.R., 1994b, Chaotic deposition by a giant wave, Molokai, Hawaii, Geological Society of America Bulletin, v. 106, no. 7, p. 962–967, doi:10.1130/0016-7606(1994)106<0962:CDBAGW>2.3.CO;2.

Morales, J.A., Borrego, J., San Miguel, E.G., López-González, N., and Carro, B., 2008, Sedimentary record of recent tsunamis in the Huelva Estuary (southwestern Spain), Quaternary Science Reviews, v. 27, p. 734-746, doi:10.1016/j.quascirev.2007.12.002.

Mosher, D.C., 2009, Submarine landslides and consequent tsunamis in Canada, Geoscience Canada, v. 36, no. 4, p. 179-190.

Mosher, D.C., and Piper, D.J.W., 2007, Analysis of multibeam seafloor imagery of the Laurentian Fan and the 1929 Grand Banks landslide area, In: Lykousis, V., Sakellariou, D., and Locat, J. (eds.), Submarine Mass Movements and their Consequences, Advances in Natural and Technological Hazards Research, v. 27, Springer, the Netherlands, p. 77-88.

Mosher, D.C., Moran, K.M., and Hiscott, R.N., 1994, Late Quaternary sediment, sediment mass flow processes and slope instability on the Scotian Slope, Sedimentology, v. 41, no. 5, p. 1039-1061, doi:10.1111/j.1365-3091.1994.tb01439.x.

Mosher, D.C, Hunter, J.A., Christian, H.A., and Luternauer, J.L., 1997, Onshore/offshore geohazards in the Vancouver region of western Canada: field, modelling and mapping techniques and results, In: Marinos, P.G., Koukis, G.C., Tsiambaos, G.C., and Stournaras, G.C. (eds.), Engineering Geology and the Environment, Balkema Publishers, Rotterdam, p. 875-883.

Mosher, D.C. Cassidy, J.F., Lowe, C., Mi, Y., Hyndman, R.D., Rogers, G.C., and Fisher, M., 2000, Neotectonics in the Strait of Georgia: first tentative correlation of seismicity with shallow geological structure in southwestern British Columbia, In: Current Research, Geological Survey of Canada, paper 2000-A22, 9 p.

Mosher, D.C., Monahan, P.A., Barrie, J.V., and Courtney, R.C., 2004, Coastal submarine failures in the Strait of Georgia, British Columbia: Landslides of the 1946 Vancouver Island earthquake, Journal of Coastal Research, v. 20, no. 1, p. 277-291, doi:10.2112/1551-5036(2004)20[277:CSFITS]2.0.CO;2.

Mosher, D.C., Xu, Z., and Shimeld, J., 2010, The Pliocene Shelburne mass-movement and consequent tsunami, western Scotian Slope, In: Mosher, D.C., Shipp, R.C., Moscardelli, L., Chaytor, J.D., Baxter, C.D.P., Lee, H.J., and Urgeles, R. (eds.), Submarine Mass Movements and their Consequences, Advances in Natural and Technological Hazards Research, v. 28, Springer, the Netherlands, p. 765-775.

Mosher, D.C., Shimeld, J., Hutchinson, D., Lebedeva-Ivanova, N., and Chapman, C.B., 2012, Submarine landslides in Arctic sedimentation: Canada Basin, In: Yamada, Y., Kawamura, K., Ikehara, K., Ogawa, Y., Urgeles, R., Mosher, D., Chaytor, J., and Strasser, M. (eds.), Submarine Mass Movements and their Consequences, Advances in Natural and Technological Hazards Research, v. 31, Springer, the Netherlands, p. 147-157, doi:10.1007/978-94-007-2162-3_13.

Muir-Wood, R., and Mignan, A., 2009, A phenomenological reconstruction of the Mw 9 November 1st 1755 earthquake source, In: Mendes-Victor, L.A. et al. (eds.), The 1755 Lisbon earthquake: revisited, Geotechnical, Geological, and Earthquake Engineering 7, Springer, p. 121-146, doi:10.1007/978-1-4020-8609-0_8.

Murty, T.S., 1977, Seismic sea waves – tsunamis, Fisheries Research Board of Canada Bulletin 198, Ottawa, Ontario, 337 p.

Murty, T.S., 1979, Submarine slide-generated water waves in Kitimat Inlet, British Columbia, Journal of Geophysical Research, v. 84, C12, p. 7777-7779, doi:10.1029/JC084iC12p07777.

Murty, T.S., 1983, Tsunamis and storm surges in the Canadian Arctic and implications for offshore work in the Beaufort Sea, Eos Transactions, American Geophysical Union, v. 64, no. 9, p. 89.

National Geophysical Data Center / World Data Center (NGDC/WDC) Historical Tsunami Database, Boulder, CO, USA (available at http://www.ngdc.noaa.gov/hazard/tsu_db.shtml; accessed 2011).

Negredo, A.M., Bird, P., Sanz de Galdeano, C., and Buforn, E., 2002, Neotectonic modeling of the Ibero-Maghrebian region, Journal of Geophysical Research, v. 107, B11, 2292, doi:10.1029/2001JB000743.

Ng, M.K.-F., LeBlond, P.H., and Murty, T.S., 1992, Tsunami threat to the Pacific coast of Canada due to local earthquakes, Natural Hazards, v. 5, no. 2, p. 205-210, doi:10.1007/BF00127007.

Nixon, M.F., and Grozic, J.L.H., 2007, Submarine slope failure due to gas hydrate dissociation: a preliminary quantification, Canadian Geotechnical Journal, v. 44, p. 314-325, doi:10.1139/T06-121.

NOAA West Coast/Alaska Tsunami Warning Center, 2009a, Amplitudes for the September 29, 2009 Samoa tsunami, http://wcatwc.arh.noaa.gov/previous.events/09-29-09-Samoa/09-29-09.htm.

NOAA West Coast/Alaska Tsunami Warning Center, 2009b, Amplitudes for the October 7, 2009 Torres Islands, Vanuatu tsunami, http://wcatwc.arh.noaa.gov/previous.events/10-07-09/10-07-09.htm.

O'Loughlin, K.F., and Lander, J.F., 2003, Caribbean tsunamis: a 500-year history from 1498-1998, Advances in Natural and Technological Hazards Research, v. 20, Kluwer Academic Publishers, Dordrecht, the Netherlands, 263 p.

Pararas-Carayannis, G., 2002, Evaluation of the threat of mega tsunami generation from postulated massive slope failures of island stratovolcanoes on La Palma, Canary Islands, and on the island of Hawaii, Science of Tsunami Hazards, v. 20, no. 5, p. 251-277.

Paull, C., Dallimore, S., Hughes-Clarke, J., Blasco, S., Lundsten, E., Ussler, W., Graves, D., Sherman, A., Conway, K., Melling, M., Vagle, S., and Collett, T., 2011, Tracking the decomposition of submarine permafrost and gas hydrate under the shelf and slope of the Beaufort Sea, Proceedings of the 7th International Conference on Gas Hydrates, Edinburgh, Scotland, UK, July 17-21, 12 p.

Peters, R., Jaffe, B., Gelfenbaum, G., and Peterson, C., 2003, Cascadia tsunami deposit database, U.S. Geological Survey Open-File Report 03-13, 24 p.

Pilkey, O.H., 1988, Basin plains; giant sedimentation events, Geological Society of America Special Paper 229, p. 93-99.

Piper, D.J.W., 2005, Late Cenozoic evolution of the continental margin of eastern Canada, Norwegian Journal of Geology, v. 85, p. 305-318.

Piper, D.J.W., 2007, Labrador geological framework report to C-Core, unpublished report, 9 p.

Piper, D.J.W., and Campbell, D.C., 2005, Quaternary geology of Flemish Pass and is application to geohazard evaluation for hydrocarbon development, Petroleum Resources and Reservoirs, Special Paper 43, p. 29-43.

Piper, D.J.W., and Gould, K., 2004, Late Quaternary geological history of the continental slope, South Whale Subbasin, and implications for hydrocarbon development, southwestern Grand Banks of Newfoundland, In: Current Research 2004-D1, Geological Survey of Canada, 13 p.

Piper, D.J.W., and Ingram, S., 2003, Major Quaternary failures on the East Scotian Rise, In: Current Research 2003-D1, Geological Survey of Canada, 7 p.

Piper, D.J.W., and McCall, C., 2003, A synthesis of the distribution of submarine mass movements on the eastern Canadian margin, In: Locat, J., and Mienert, J. (eds.), Submarine Mass Movements and their Consequences, Advances in Natural and Technological Hazards Research, v. 19, Kluwer Academic Publishers, Dordrecht, the Netherlands, p. 291-298.

Piper, D.J.W., and Normark, W.R., 2009, Processes that initiate turbidity currents and their influence on turbidites: a marine geology perspective, Journal of Sedimentary Research, v. 79, p. 347-362, doi:10.2110/jsr.2009.046.

Piper, D.J.W., Mosher, D.C., Gauley, B.-J., Jenner, K., and Campbell, D.C., 2003, The chronology and recurrence of submarine mass movements on the continental slope off southeastern Canada, In: Locat, J., and Mienert, J. (eds.), Submarine Mass Movements and their Consequences, Advances in Natural and Technological Hazards Research, v. 19, Kluwer Academic Publishers, Dordrecht, the Netherlands, p. 299-306.

Piper, D.J.W., Tripsanas, E., Mosher, D.C., and MacKillop, K., 2011, Paleoseismicity of the continental margin of eastern Canada: rare regional failures and associated turbidites in Orphan Basin, unpublished manuscript, 38 p., 2 tables, 17 figures.

Pisaric, M.F.J., Thienpont, J.R., Kokelj, S.V., Nesbitt, H., Lantz, T.C., Solomon, S., and Smol, J.P., 2011, Impacts of a recent storm surge on an Arctic delta ecosystem examined in the context of the last millennium, Proceedings of the National Academy of Sciences of the United States of America, v. 108, no. 22, p. 8960-8965, doi:10.1073/pnas.1018527108.

Plafker, G., 1967, Surface faults on Montague Island associated with the 1964 Alaska earthquake, U.S. Geological Survey Professional Paper 548-G, 42 p., 2 plates.

Pohlman, J.W., Riedel, M., Waite, W., Rose, K., Lapham, L., Hamilton, T.S., Enkin, R., Spence, G.D., Hyndman, R., and Haacke, R., 2008, Geochemical investigation of slope failure on the northern Cascadia margin frontal ridge, Eos Transactions, American Geophysical Union, v. 89, no. 53, Abstract OS32A-08.

Poncet, R., Campbell, C., Dias, F., Locat, J., and Mosher, D., 2010, A study of the tsunami effects of two landslides in the St. Lawrence estuary, In: Mosher, D.C., Shipp, R.C., Moscardelli, L., Chaytor, J.D., Baxter, C.D.P., Lee, H.J., and Urgeles, R. (eds.), Submarine Mass Movements and their Consequences, Advances in Natural and Technological Hazards Research, v. 28, Springer, the Netherlands, p. 755-764.

Priest, G.R., Goldfinger, C., Wang, K., Witter, R.C., Zhang, Y., and Baptista, A.M., 2009, Confidence limits for tsunami-inundation limits in northern Oregon inferred from a 10,000-year history of great earthquakes at the Cascadia subduction zone, Natural Hazards, 47 p., doi:10.1007/s11069-009-9453-5.

Prior, D.B., Wiseman, W.J., and Gilbert, R., 1981, Submarine processes on a fan delta, Howe Sound, British Columbia, Geo-Marine Letters, v. 1, no. 2, p. 85-90, doi:10.1007/BF02463323.

Prior, D.B., Bornhold, B.D., Coleman, J.M., and Bryant, W.R., 1982, Morphology of a submarine slide, Kitimat Arm, British Columbia, Geology, v. 10, no. 11, p. 588-592, doi:10.1130/0091-7613(1982)10<588:MOASSK>2.0.CO;2.

Rabinovich, A.B., Thomson, R.E., Bornhold, B.D., Fine, I.V. and Kulikov, E.A., 2003, Numerical modelling of tsunamis generated by hypothetical landslides in the Strait of Georgia, British Columbia, Pure and Applied Geophysics, v. 160, no. 7, p. 1273–1313, doi:10.1007/s000240300006.

Rabinovich, A.B., Thomson, R.E., and Stephenson, F.E., 2006, The Sumatra tsunami of 26 December 2004 as observed in the North Pacific and North Atlantic oceans, Surveys in Geophysics, v. 27, no. 6, p. 647-677, doi:10.1007/s10712-006-9000-9.

Rabinovich, A.B., Thomson, R.E., Titov, V.V., Stephenson, F.E., and Rogers, G.C., 2008, Locally generated tsunamis recorded on the coast of British Columbia, Atmosphere-Ocean, v. 46, no. 3, p. 343-360, doi:10.3137/ao.460304.

Reid, H.F., and Taber, S., 1919, The Porto Rico earthquakes of October-November, 1918, Bulletin of the Seismological Society of America, v. 9, no. 4, p. 95-127.

Reimnitz, E. and Maurer, D. K., 1978, Storm surges in the Alaskan Beaufort Sea, U.S. Geological Survey Open-File Report 78-593, 26 p.

Riddihough, R., 1984, Recent movements of the Juan de Fuca plate system, Journal of Geophysical Research, v. 89, B8, p. 6980-6994, doi:10.1029/JB089iB08p06980.

Ristau, J.P., 2004, Seismotectonics of western Canada from regional moment tensor analysis, Ph.D. thesis, University of Victoria, Victoria, Canada, 209 p.

Ristau, J., Rogers, G.C., and Cassidy, J.F., 2007, Stress in western Canada from regional moment tensor analysis, Canadian Journal of Earth Sciences, v. 44, p. 127-148, doi:10.1139/E06-057.

Roger, J., Baptista, M.A., Mosher, D., Hébert, H., and Sahal, A., 2010a, Tsunami impact on Newfoundland, Canada, due to far-field generated tsunamis: implications on hazard assessment, Proceedings of the 9th U.S. National and 10th Canadian Conference on Earthquake Engineering, Toronto, July 25-29, Paper 1837, 6 p.

Roger, J., Allgeyer, S., Hébert, H., Baptista, M.A., Loevenbruck, A., and Schindelé, F., 2010b, The 1755 Lisbon tsunami in Guadeloupe archipelago: source sensitivity and investigation of resonance effects, The Open Oceanography Journal, v. 4, p. 58-70.

Roger, J., Baptista, M.A., Sahal, A., Accary, F., Allgeyer, S., and Hébert, H., 2011, The transoceanic 1755 Lisbon tsunami in Martinique, Pure and Applied Geophysics, v. 168, no. 6-7, p. 1015-1031, doi:10.1007/s00024-010-0216-8.

Rogers, G.C., 1980, A documentation of soil failure during the British Columbia earthquake of 23 June, 1946, Canadian Geotechnical Journal, v. 17, no. 1, p. 122-127, doi:10.1139/t80-011.

Rogers, G.C., and Hasegawa, H.S., 1978, A second look at the British Columbia earthquake of June 23, 1946, Bulletin of the Seismological Society of America, v. 68, no. 3, p. 653-675.

Rohr, K.M.M., and Furlong, K.P., 1995, Ephemeral plate tectonics at the Queen Charlotte triple junction, Geology, v. 23, no. 11, p. 1035-1038, doi:10.1130/0091-7613(1995)023<1035:EPTATQ>2.3.CO;2.

Rohr, K.M.M., and Tryon, A.J., 2010, Pacific-North America plate boundary reorganization in response to a change in relative plate motion: offshore Canada, Geochemistry Geophysics Geosystems, v. 11, no. 6, Q06007, doi:10.1029/2009GC003019.

Rohr, K.M.M., Scheidhauer, M., and Trehu, A.M., 2000, Transpression between two warm mafic plates: the Queen Charlotte fault revisited, Journal of Geophysical Research, v. 105, B4, p. 8147-8172, doi:10.1029/1999JB900403.

Rubin, K.H., Fletcher, C.H., III, and Sherman, C., 2000, Fossiliferous Lana'i deposits formed by multiple events rather than a single giant tsunami, Nature, v. 408, p. 675-681, doi:10.1038/35047008.

Ruffman, A., 1994, The November 18, 1929 "Tidal Wave": Canada's most tragic earthquake, abstract, Spring Meeting, Geological Association of Canada: Newfoundland Section, Atlantic Geology, v. 30, no. 2, p. 157-158.

Ruffman, A., 2001, Potential for large-scale submarine slope failure and tsunami generation along the U.S. mid-Atlantic coast, Comment, Geology, v. 29, no. 10, p. 967, doi:10.1130/0091-7613(2001)029<0967:PFLSSS>2.0.CO;2.

Ruffman, A., 2006, Documentation of the farfield parameters of the November 1, 1755 "Lisbon" tsunami along the shores of the western Atlantic Ocean, Program and Abstracts, International Tsunami Society Third Tsunami Symposium, Honolulu, HI, May 23-25.

Ruffman, A., and Hann, V., 2006, The Newfoundland tsunami of November 18, 1929: an examination of the twenty-eight deaths of the "south coast disaster", Newfoundland and Labrador Studies, v. 21, no. 1, p. 97-148.

Ruffman, A., and Murty, T., 2006, Tsunami hazards in the Arctic regions of North America, Greenland and the Norwegian Sea, Program and Abstracts, International Tsunami Society Third Tsunami Symposium, Honolulu, HI, May 23-25.

Satake, K., Shimazaki, K., Tsuji, Y., and Ueda, K., 1996, Time and size of a giant earthquake in Cascadia inferred from Japanese tsunami records of January 1700, Nature, v. 379, p. 246-249, doi:10.1038/379246a0.

Satake, K., Wang, K., and Atwater, B.F., 2003, Fault slip and seismic moment of the 1700 Cascadia earthquake inferred from Japanese tsunami descriptions, Journal of Geophysical Research, v. 108, B11, 2535, doi:10.1029/2003JB002521.

Scheffers, A., and Kelletat, D., 2005, Tsunami relics on the coastal landscape west of Lisbon, Portugal, Science of Tsunami Hazards, v. 23, no. 1, p. 3-16.

Scheffers, A., Scheffers, S., and Kelletat, D., 2005, Paleo-tsunami relics on the southern and central Antillean Island arc, Journal of Coastal Research, v. 21, no. 2, p. 263-273. doi:10.2112/03-0144.1.

Scholz, N., Riedel, M., Spence, G., Dugan, B., Daigle, H., Hyndman, R.D., James, T.S., and Naegeli, K., 2010, Slope failure of continental frontal ridges offshore Vancouver Island, British Columbia, Eos Transactions, American Geophysical Union, v. 91, no. 52, Abstract OS13E-1291.

Schuster, R.L., Logan, R.L., and Pringle, P.T., 1992, Prehistoric rock avalanches in the Olympic Mountains, Washington, Science, v. 258, no. 5088, p. 1620-1621, doi:10.1126/science.258.5088.1620.

Serpelloni, E., Vannucci, G., Pondrelli, S., Argnani, A., Casula, G., Anzidei, M., Baldi, P., and Gasperini, P., 2007, Kinematics of the western Africa-Eurasia plate boundary from focal mechanisms and GPS data, Geophysical Journal International, v. 169, p. 1180-1200, doi:10.1111/j.1365-246X.2007.03367.x.

Shennan, I., Bruhn, R., and Plafker, G., 2009, Multi-segment earthquakes and tsunami potential of the Aleutian megathrust, Quaternary Science Reviews, v. 28, no. 1-2, p. 7-13, doi:10.1016/j.quascirev.2008.09.016.

Sherrod, B.L., Bucknam, R.C., and Leopold, E.B., 2000, Holocene relative sea level changes along the Seattle fault at Restoration Point, Washington, Quaternary Research, v. 54, p. 384-393, doi:10.1006/qres.2000.2180.

Sherrod, B.L., Mazzotti, S., and Haugerud, R., 2008, Comparison of geodetic and paleoseismic rates of deformation in the Puget Sound-Georgia Basin, Pacific Northwest, Eos Transactions, American Geophysical Union, v. 89, no. 53, Fall Meeting Supplement, Abstract T21B-1953.

Skvortsov, A., and Bornhold, B., 2007, Numerical simulation of the landslide-generated tsunami in Kitimat Arm, British Columbia, Canada, 27 April 1975, Journal of Geophysical Research, v. 112, F02028, doi:10.1029/2006JF000499.

Smith, A.J., Hyndman, R.D., Cassidy, J.F., and Wang, K., 2003, Structure, seismicity, and thermal regime of the Queen Charlotte transform margin, Journal of Geophysical Research, v. 108, B11, 2539, doi:10.1029/2002JB002247.

Solares, J.M.M., and Arroyo, A.L., 2004, The great historical 1755 earthquake: effects and damage in Spain, Journal of Seismology, v. 8, no. 2, p. 275-294, doi:10.1023/B:JOSE.0000021365.94606.03.

Solheim, A., Berg, K., Forsberg, C.F., and Bryn, P., 2005, The Storegga Slide complex: repetitive large scale sliding with similar cause and development, Marine and Petroleum Geology, v. 22, p. 97-107, doi:10.1016/j.marpetgeo.2004.10.013.

Somerville, P.G., Sato, T., Ishii, T., Collins, N.F., Dan, K., and Fujiwara, H., 2002, Characterizing heterogeneous slip models for large subduction earthquakes for strong ground motion prediction, In: Proceedings of the 11th Japan Earthquake Engineering Symposium, Architectural Institute of Japan, p. 163-166.

Sørensen, M.B., Spada, M., Babeyko, A., Wiemer, S., and Grünthal, G., 2012, Probabilistic tsunami hazard in the Mediterranean Sea, Journal of Geophysical Research, v. 117, B01305, doi:10.1029/2010JB008169.

Spaeth, M.G., and Berkman, S.C., 1967, The tsunami of March 28, 1964, as recorded at tide stations, Coast and Geodetic Survey Technical Bulletin, no. 33, US Department of Commerce, 86p.

Stephenson, F.E., and Rabinovich, A.B., 2009, Tsunamis on the Pacific coast of Canada recorded in 1994-2007, Pure and Applied Geophysics, v. 166, no. 1-2, p. 177-210, doi:10.1007/s00024-008-0440-7.

Stephenson, F., Rabinovich, A.B., Solovieva, O.N., Kulikov, E.A., and Yakovenko, O.I., 2007, Catalogue of tsunamis, British Columbia, Canada: 1700-2007, Preprint, P.P. Shirshov Institute of Oceanology, Moscow, Russia, 133 p.

Stephenson, F.E., Solovieva, O.N., Rabinovich, A.B., Yakovenko, O.I., and Kulikov, E.A., 2012, Tsunamis on the Pacific coast of Canada: From Prehistoric Time to the Present, Advances in Natural and Technological Hazards Research, v. 24, Springer, 225 p., in press (for publication in 2013).

Stich, D., Serpelloni, E., Mancilla, F., and Morales, J., 2006, Kinematics of the Iberia-Maghreb plate contact from seismic moment tensors and GPS observations, Tectonophysics, v. 426, p. 295-317, doi:10.1016/j.tecto.2006.08.004.

Stich, D., Mancilla, F., Pondrelli, S., and Morales, J., 2007, Source analysis of the February 12th 2007, Mw 6.0 Horseshoe earthquake: implications for the 1755 Lisbon earthquake, Geophysical Research Letters, v. 34, L12308, doi:10.1029/2007GL030012.

Strasser, F.O., Arango, M.C., and Bommer, J.J., 2010, Scaling of the source dimension of interface and intraslab subduction-zone earthquakes with moment magnitude, Seismological Research Letters, v. 81, no. 6, p. 941-950, doi:10.1785/gssrl.81.6.941.

Suleimani, E., Nicolsky, D.J., Haeussler, P.J., and Hansen, R., 2011, Combined effects of tectonic and landslide-generated tsunami runup at Seward, Alaska during the M_w 9.2 1964 earthquake, Pure and Applied Geophysics, v. 168, p. 1053-1074, doi:10.1007/s00024-010-0228-4.

Syvitski, J.P.M., Burrell, D.C., and Skei, J.M., 1987, Chapter 5: Subaqueous slope failure, In: Fjords: Processes and Products, Springer-Verlag, New York, p. 175-209.

Szczuciński, W., 2012, The post-depositional changes of the onshore 2004 tsunami deposits on the Andaman Sea coast of Thailand, Natural Hazards, v. 60, no. 1, p. 115-133, doi:10.1007/s11069-011-9956-8.

Taggart, B.E., Lundberg, J., Carew, J.L., and Mylroie, J.E., 1993, Holocene reef-rock boulders on Isla de Mona, Puerto Rico transported by a hurricane or seismic sea wave, Geological Society of America Abstracts with Programs, v. 25, no. 6, A-61.

Tappin, D.R., McNeil, L.C., Henstock, T., and Mosher, D., 2007, Mass wasting processes – offshore Sumatra, In: Lykousis, V., Sakellariou, D., and Locat, J. (eds.), Submarine Mass Movements and their Consequences, Advances in Natural and Technological Hazards Research, v. 27, Springer, the Netherlands, p. 327-336.

ten Brink, U., and Lin, J., 2004, Stress interaction between subduction earthquakes and forearc strike-slip faults: modeling and application to the northern Caribbean plate boundary, Journal of Geophysical Research, v. 109, B12310, doi:10.1029/2004JB003031.

ten Brink, U.S., and López-Venegas, A.M., 2012, Plate interaction in the NE Caribbean subduction zone from continuous GPS observations, Geophysical Research Letters, v. 39, L10304, doi:10.1029/2012GL051485.

ten Brink, U.S., Lee, H.J., Geist, E.L., and Twichell, D., 2009a, Assessment of tsunami hazard to the U.S. east coast using relationships between submarine landslides and earthquakes, Marine Geology, v. 264, no. 1-2, p. 65-73, doi:10.1016/j.margeo.2008.05.011.

ten Brink, U.S., Marshak, S., and Granja Bruña, J.-L., 2009b, Bivergent thrust wedges surrounding oceanic island arcs: insight from observations and sandbox models of the northeastern Caribbean plate, Geological Society of America Bulletin, v. 121, no. 11/12, p. 1522-1536, doi:10.1130/B26512.1.

Terzaghi, K., 1956, Varieties of submarine slope failures, Proceedings of the 8th Texas Conference on Soil Mechanics and Foundation Engineering, 41 p.

Thiebot, E., and Gutscher, M.-A., 2006, The Gibraltar Arc seismogenic zone (part 1): constraints on a shallow east dipping fault plane source for the 1755 Lisbon earthquake provided by seismic data, gravity and thermal modeling, Tectonophysics, v. 426, p. 135-152, doi:10.1016/j.tecto.2006.02.024.

Thio, H.K., Somerville, P., and Polet, J., 2010, Probabilistic tsunami hazard in California, Pacific Earthquake Engineering Research Center Report 2010/108, 331 p.

Thomson, R.E., Rabinovich, A.B., and Krassovski, M.V., 2007, Double jeopardy: concurrent arrival of the 2004 Sumatra tsunami and storm-generated waves on the Atlantic coast of the United States and Canada, Geophysical Research Letters, v. 34, L15607, doi:10.1029/2007GL030685.

Tocque, P., 1846, Wandering thoughts, or solitary hours, Thomas Richardson and Son, London, 387 p.

Trifunac, M.D., and Todorovska, M.I., 2003, Tsunami source parameters of submarine earthquakes and slides, In: Locat, J., and Mienert, J. (eds.), Submarine Mass Movements and their Consequences, Advances in Natural and Technological Hazards Research, v. 19, Kluwer Academic Publishers, Dordrecht, the Netherlands, p. 121-128.

Tripsanas, E.K., and Piper, D.J.W., 2008, Glaciogenic debris-flow deposits of Orphan Basin, offshore eastern Canada: sedimentological and rheological properties, origin, and relationship to meltwater discharge, Journal of Sedimentary Research, v. 78, no. 11, p. 724-744, doi:12.2110/jsr.2008.082.

Turcotte, D.L., and Schubert, G., 2002, Geodynamics, 2nd edition, Cambridge University Press, Cambridge, UK, 456 p.

Tuttle, M.P., and Atkinson, G.M., 2010, Localization of large earthquakes in the Charlevoix seismic zone, Quebec, Canada, during the past 10,000 years, Seismological Research Letters, v. 81, no. 1, p. 140-147, doi:10.1785/gssrl.81.1.140.

Twichell, D.C., Chaytor, J.D., ten Brink, U.S., and Buczkowski, B., 2009, Morphology of late Quaternary submarine landslides along the U.S. Atlantic continental margin, Marine Geology, v. 264, no. 1-2, p. 4-15, doi:10.1016/j.margeo.2009.01.009.

van Zeyl, D.P., 2009, Evaluation of subaerial landslide hazards in Knight Inlet and Howe Sound, British Columbia, M.Sc. thesis, Simon Fraser University, Vancouver, Canada, 199 p.

Vernant, P., Fadil, A., Mourabit, T., Ouazar, D., Koulali, A., Davila, J.M., Garate, J., McClusky, S., and Reilinger, R., 2010, Geodetic constraints on active tectonics of the Western Mediterranean: implications for the kinematics and dynamics of the Nubia-Eurasia plate boundary zone, Journal of Geodynamics, v. 49, p. 123-129, doi:10.1016/j.jog.2009.10.007.

Wang, K., Wells, R., Mazzotti, S., Hyndman, R.D., and Sagiya, T., 2003, A revised dislocation model of interseismic deformation of the Cascadia subduction zone, Journal of Geophysical Research, v. 108, no. B1, 2026, doi:10.1029/201JB001227.

Ward, S.N., 2001, Landslide tsunami, Journal of Geophysical Research, v. 106, no. 6, p. 11,201-11,215.

Ward, S.N., and Asphaug, E., 2000, Asteroid impact tsunami: a probabilistic hazard assessment, Icarus, v. 145, no. 1, p. 64-78, doi:10.1006/icar.1999.6336.

Ward, S.N., and Day, S., 2001, Cumbre Vieja Volcano – potential collapse and tsunami at La Palma, Canary Islands, Geophysical Research Letters, v. 28, no. 17, p. 3397-3400, doi:10.1029/2001GL013110.

Ward, S.N., and Day, S., 2005, Tsunami thoughts, CSEG Recorder, December 2005, p. 38-44.

Watt, S., Buckley, M., and Jaffe, B., 2011, Inland fields of dispersed cobbles and boulders as evidence for a tsunami on Anegada, British Virgin Islands, Natural Hazards, doi:10.1007/s11069-011-9848-y.

Watts, P., 2003, Probabilistic analyses of landslide tsunami hazards, In: Locat, J., and Mienert, J. (eds.), Submarine Mass Movements and their Consequences, Advances in Natural and Technological Hazards Research, v. 19, Kluwer Academic Publishers, Dordrecht, the Netherlands, p. 163-170.

Watts, P., 2004, Probabilistic predictions of landslides tsunamis off southern California, Marine Geology, v. 203, no. 3-4, p. 281-301, doi:10.1016/S0025-3227(03)00311-6.

Waythomas, C.F., Watts, P., Shi, F., and Kirby, J.T., 2009, Pacific Basin tsunami hazards associated with mass flows in the Aleutian arc of Alaska, Quaternary Science Reviews, v. 28, no. 11-12, p. 1006-1019, doi:10.1016/j.quascirev.2009.02.019.

Webster, J.M., Clague, D.A., and Braga, J.C., 2007, Support for the giant wave hypothesis: evidence from submerged terraces off Lanai, Hawaii, International Journal of Earth Sciences, v. 96, p. 517-524, doi:10.1007/s00531-006-0107-5.

Wells, D.L., and Coppersmith, K.J., 1994, New empirical relationships among magnitude, rupture length, rupture width, rupture area, and surface displacement, Bulletin of the Seismological Society of America, v. 84, no. 4, p. 974-1002.

Wessel, P., and Smith, W.H.F., 1995, New version of the Generic Mapping Tools released, Eos Transactions, American Geophysical Union, v. 76, no. 33, p. 329, doi:10.1029/95EO00198.

Whitmore, P.M., 1993, Expected tsunami amplitudes and currents along the North American coast for Cascadia subduction zone earthquakes, Natural Hazards, v. 8, p. 59-73.

Whitmore, P., Benz, H., Bolton, M., Crawford, G., Dengler, L., Fryer, L., Goltz, J., Hansen, R., Kryzanowski, K., Malone, S., Oppenheimer, D., Petty, E., Rogers, G., and Wilson, J., 2008, NOAA/West Coast and Alaska Tsunami Warning Center Pacific Ocean response criteria, Science of Tsunami Hazards, v. 27, no. 1, p. 1-21.

Whitmore, P., ten Brink, U., Caropolo, M., Huerfano-Moreno, V., Knight, W., Sammler, W., and Sandrik, A., 2009, NOAA/West Coast/Alaska Tsunami Warning Center Atlantic Ocean response criteria, Science of Tsunami Hazards, v. 28, no. 2, p. 86-107.

Wigen, S.O., 1960, Tsunami of May 22, 1960, west coast of Canada, Technical Report, Marine Sciences Branch, 6 p.

Wigen, S.O., 1983, Historical study of tsunamis at Tofino, Canada, In: Iida, K., and Iwasaki, T. (eds.), Tsunamis – Their Science and Engineering, Terra Scientific Publishing, Tokyo, p. 105-119.

Wigen, S.O., and White, W.R.H., 1964, Tsunami of March 27-29, 1964, west coast of Canada, Department of Mines and Technical Surveys, Ottawa, Ontario, 12 p.

Williams, H., and Hutchinson, I., 2000, Stratigraphic and microfossil evidence for late Holocene tsunamis at Swantown marsh, Whidbey Island, Washington, Quaternary Research, v. 54, p. 218-227, doi:10.1006/qres.2000.2162.

Williams, H.F.L., Hutchinson, I., and Nelson, A.R., 2005, Multiple sources for late-Holocene tsunamis at Discovery Bay, Washington State, USA, The Holocene, v. 15, no. 1, p. 60-73, doi:10.1191/0956683605hl784rp.

Willoughby, E.C., and Hyndman, R.D., 2005, Earthquake rate, slip rate, and the effective seismic thickness for oceanic transform faults of the Juan de Fuca plate system, Geophysical Journal International, v. 160, p. 855-868, doi:10.1111/j.1365-246X.2005.02523.x.

Wynn, R.B., and Masson, D.G., 2003, Canary Islands landslides and tsunami generation: can we use turbidite deposits to interpret landslide processes, In: Locat, J., and Mienert, J. (eds.), Submarine Mass Movements and their Consequences, Advances in Natural and Technological Hazards Research, v. 19, Kluwer Academic Publishers, Dordrecht, the Netherlands, p. 325-332.

Xu, Z., 2007, The all-source Green's function and its application to tsunami problems, Science of Tsunami Hazards, v. 26, no. 1, p. 59-69.

Yuan, T., Spence, G.D., and Hyndman, R.D., 1992, Structure beneath Queen Charlotte Sound from seismic-refraction and gravity interpretations, Canadian Journal of Earth Sciences, v. 29, no. 7, p. 1509-1529, doi:10.1139/e92-120.

Zahibo, N., Pelinovsky, E., Yalciner, A.C., Kurkin, A., Koselkov, A., and Zaitsev, A., 2003, The 1867 Virgin Island tsunami, Natural Hazards and Earth System Sciences, v. 3, no. 5, p. 367-376, doi:10.5194/nhess-3-367-2003.

Zitellini, N., Mendes, L.A., Cordoba, D., Danobeitia, J., Nicolich, R., Pellis, G., Ribeiro, A., Sartori, R., Torelli, L., Bartolome, R., Bortoluzzi, G., Calafato, A., Carrilho, F., Casoni, L., Chierici, F., Corela, C., Correggiari, A., Della Vedova, B., Gracia, E., Plomet, P., Landuzzi, M., Ligi, M., Magagnoli, A., Marozzi, G., Matias, L., Penitenti, D., Rodriguez, P., Rovere, M., Terrinha, P., Vigliotti, L., and Zahinos Ruiz, A., 2001, Source of 1755 Lisbon earthquake and tsunami investigated, Eos Transactions, v. 82, no. 26, p. 285, 290-291, doi:10.1029/EO082i026p00285-01.

Zitellini, N., Gràcia, E., Matias, L., Terrinha, P., Abreu, M.A., DeAlteriis, G., Henriet, J.P., Dañobeitia, Masson, D.G., Mulder, T., Ramella, R., Somoza, L., and Diez, S., 2009, The quest for the Africa-Eurasia plate boundary west of the Strait of Gibraltar, Earth and Planetary Science Letters, v. 280, p. 13-50, doi:10.1016/j.epsl.2008.12.005.

Table 1. Damaging coastal tsunamis (from geological sources) documented in Canada

Date	Source Location	Impact Location (Canada)	Tsunami Source	Earthquake Magnitude	Wave Amplitude (m)	Runup (m)	Damage	References
WIDESPREAD IMPACT								
Jan 26 1700	Cascadia subduction zone, N. CA - S. BC	W. coast, esp. W. Vancouver Is. and inlets	Local megathrust earthquake	*M*~9.0	~5-8; up to 16*	min. 3†	Widespread fatalities; destruction of villages	e.g., Satake et al. 1996; Hutchinson & McMillan 1997; Cherniawsky et al. 2007
May 22 1960	Southern Chile	W. Vancouver Is. and Queen Charlotte Is. (QCI)	Far-field megathrust earthquake	M_w 9.5	1.3# (Tofino)	0.1-2.1	Flooding	Wigen 1960; Stephenson et al. 2007 (& references therein)
Mar 27 1964	Prince William Sound, Alaska	W. Vancouver Is., esp. Port Alberni, and QCI	Far-field megathrust earthquake	M_w 9.2	2.4# (Tofino); ≥ 5.2# (Pt. Alberni)	0.1-8.0	~$10m damage (1964)	Wigen & White 1964; Stephenson et al. 2007 (& references therein)
Nov 18 1929	Grand Banks, off Newfoundland	Burin Peninsula, Newfoundland	Earthquake-triggered landslide	M_s 7.2	3-8	13	28 fatalities; $400k damage (1929)	e.g., Ruffman 2001; Fine et al. 2005
LOCAL IMPACT								
~16th century	Knight Inlet, BC	Same as source	Rock avalanche	n/a	~2-6§	?	Many fatalities; destruction of village	Bornhold et al. 2007
Jun 23 1946	Deep Bay, Strait of Georgia, BC	Same as source	Earthquake-triggered submarine landslide	M_s 7.3	1-2	?	1 fatality; local flooding and damage	Hodgson 1946; Murty 1977
Apr 27 1975	Kitimat Arm, BC	Same as source	Construction-induced submarine landslide	n/a	6-11§	8.2	Substantial local damage	Murty 1979; Skvortsov & Bornhold 2007
Nov 03 1994**	Skagway, AK	Same as source	Construction-induced submarine landslide	n/a	5-6	9-11	1 fatality; $16-21 million damage to harbour/docks	Lander 1995; Kulikov et al. 1996

* Modelled values for release of 500 years of accumulated strain.

† Runup from tsunami deposits likely lower than actual runup.

Wave amplitude measured peak-to-trough; other values are wave height above state of tide (zero-to-peak amplitude).

§ Modelled values, not observed.

** Not in Canada; included because fjord environment is similar to much of BC coast, and facilities were Canadian-owned.

Table 2. Tsunami runup relative to M_W predicted from the empirical relations of Abe (1995)

M_w	D_L* (km)	Limiting mean runup H_L† (m)	Limiting max runup $2H_L$# (m)	Distance where Hr=3m§ (km)	Distance where Hr=1.5m§ (km)	Distance where $2Hr$=1.5m** (km)
9.2	224	20.0	39.9	1490	2980	5950
9.1	200	17.8	35.6	1180	2360	4720
9.0	178	15.8	31.7	938	1875	3750
8.9	158	14.1	28.3	745	1490	2980
8.8	141	12.6	25.2	590	1180	2360
8.7	126	11.2	22.4	470	940	1880
8.6	112	10.0	20.0	375	750	1500
8.5	100	8.9	17.8	300	600	1200
8.4	89	7.9	15.9	235	470	940
8.3	79	7.1	14.2	187	375	750
8.2	71	6.3	12.6	150	300	600
8.1	63	5.6	11.2	118	236	472
8.0	56	5.0	10.0	94	190	375
7.9	50	4.5	8.9	75	150	300
7.8	45	4.0	8.0	59	118	236
7.7	40	3.5	7.1	47	94	188
7.6	35	3.2	6.3	37	75	150
7.5	32	2.8	5.6	-	60	120
7.4	28	2.5	5.0	-	47	94
7.3	25	2.2	4.5	-	37	75
7.2	22	2.0	4.0	-	30	60
7.1	20	1.8	3.6	-	24	47
7.0	18	1.6	3.2	-	19	38
6.9	16	1.4	2.8	-	-	30
6.8	14	1.3	2.5	-	-	24
6.7	13	1.1	2.2	-	-	19
6.6	11	1.0	2.0	-	-	15
6.5	10	0.9	1.8	-	-	12
6.4	9	0.8	1.6	-	-	10
6.3	8	0.7	1.4	-	-	-

* Maximum distance D_L from the source at which limiting near-source mean runup (H_L) and maximum local runup ($2H_L$) may occur, where $\log D_L = 0.5M_w - 2.25$.

† Limiting near-source mean local runup H_L, where $\log H_L = 0.5M_w - 3.3$. Possible as far as distance D_L from the source.

Limiting near-source maximum local runup $2H_L$, possible as far as distance D_L from the source.

§ Local mean runup Hr at distance D from source, where $\log Hr = M_w - \log D - 5.55$.

** Local maximum runup $2Hr$ possible at distance D from source.

Table 3. Probabilities of exceedance of potentially damaging tsunami runup from far-field tsunamis at locations in coastal British Columbia

Affected Regions*	Frequency (*Hr*≥1.5 m, /y)			Frequency (*Hr*≥3 m, /y)			P(*Hr*≥1.5 m, 50 y)			P(*Hr*≥3 m, 50 y)		
	min	best	max	min	best	max	min	best	max	min	best	max
WHG-N, WHG-S, NMC&EHG-N, CMC&EHG-S, WVI-N, WVI-S[†]	0.0050	0.0114	0.0224	0.0000	0.0000	0.0030	0.2212	0.4345	0.6737	0.0000	0.0000	0.1393
JDF-W, JDF-E&GI, QCS[#]	0.0000	0.0016	0.0055	0.0000	0.0000	0.0000	0.0000	0.0769	0.2404	0.0000	0.0000	0.0000

* Zones defined in Appendix C.

[†] Frequency based on recurrence relation of tide gauge peak-to-trough tsunami wave amplitude data at Tofino (Fig. 3). Peak-to-trough measurements are approximately equivalent to local mean runup *Hr* (Abe, 1995). Probability is only strictly applicable for location of Tofino tide gauge; extrapolation to other areas is an approximation.

[#] Frequency based on empirical scaling factor of 0.6 for peak-to-trough wave amplitudes at Victoria tide gauge relative to Tofino (Fig. 3). Probability is only strictly applicable for location of Victoria tide gauge.

Table 4. Tide gauge amplitude measurements and ratios of some larger tsunamis at Tofino and Victoria, British Columbia

	Tsunami Event (source location and year)						
	Aleutians 1946	Kamchatka 1952	Chile 1960	Alaska 1964	Samoa 2009	Chile 2010	Japan 2011
Tofino max peak-to-trough amplitude (m)	0.57	0.60	1.26	2.40	0.13	0.37	1.25
Victoria max peak-to-trough amplitude (m)	0.21	0.36	0.73	1.44	0.08	0.23	0.52
Amplitude ratio: Victoria relative to Tofino	0.37	0.60	0.58	0.60	0.58	0.63	0.42

Table 5. Probabilities of exceedance of potentially damaging runup from tsunamis generated by megathrust earthquakes on the Cascadia subduction zone (M~9.0 long ruptures and $M \geq 8$ southern ruptures)

Affected Regions*	M_w	Estimated frequency (/y)			$Hr \geq 1.5$ m?†	$2Hr \geq 1.5$ m?†	$Hr \geq 3$ m?†	$2Hr \geq 3$ m?†	P($Hr \geq 1.5$ m, 50 y)#			P($Hr \geq 3$ m, 50 y)#		
		min	best	max					min	best	max	min	best	max
WHG-N, WHG-S, NMC&EHG-N, CMC&EHG-S, QCS, WVI-N, JDF-W, JDF-E&GI														
	~9	0.0013	0.0019	0.0037	Yes	Yes	Yes	Yes	0.0613	0.0900	0.1690	0.0613	0.0900	0.1690
	≥ 8	0.0008	0.0010	0.0013	No	Yes	No	No	0.0196	0.0244	0.0322	0.0000	0.0000	0.0000
WVI-S														
	~9	0.0013	0.0019	0.0037	Yes	Yes	Yes	Yes	0.0613	0.0900	0.1690	0.0613	0.0900	0.1690
	≥ 8	0.0008	0.0010	0.0013	Yes	Yes	No	Yes	0.0392	0.0488	0.0645	0.0196	0.0244	0.0322
GS§														
	~9	0.0013	0.0019	0.0037	Yes	Yes	No	Yes	0.0613	0.0900	0.1690	0.0000	0.0000	0.0423
	≥ 8	0.0008	0.0010	0.0013	No	Yes	No	No	0.0000	0.0122	0.0161	0.0000	0.0000	0.0000

* Zones defined in Appendix C.

† Local mean runup Hr and local max runup $2Hr$ estimated at various distances using a combination of tsunami modelling by Cherniawsky et al. (2007) and the empirical relations of Abe (1995), as in Equations 12-14 and Table 2.

Probability of tsunami runup is based on probability of earthquake occurrence where local mean runup $Hr \geq 1.5$ or 3 m is expected. Probability reduced by 50% where only local runup maxima $2Hr \geq 1.5$ or 3 m are expected.

§ Tsunami impact poorly constrained in Georgia Strait. For southern events, we assume that local runup maxima $2Hr \geq 1.5$ m are improbable but cannot be ruled out (probability reduced to 25% of earthquake probability, with a minimum of 0). For long ruptures, localized maxima ≥ 3 m are modelled in only a few isolated locations. Thus for the vast majority of this zone, runup is not expected to exceed 3 m. We assign a min and best probability of 0 for runup ≥ 3 m, and for a max estimate reduce the probability to 25% of the max earthquake probability.

Table 6. Estimation of earthquake magnitude and recurrence on the Explorer megathrust

Rupture	Length (km)	Width# (km)	Area (km^2)	M_w§			Seismic moment M_o (Nm)**			Slip (m)††			Slip rate (mm/y)##			Recurrence (y)§§		
				min	best	max	min	best	max	min	best	max	min	best	max	min	best	max
EXP,WIN*	85,175	37.5,18.75	6469	7.38	7.66	7.95	1.3E+20	3.5E+20	9.4E+20	2.01	5.39	14.47	14.4	16.2	18.0	112	**333**	**1005**
EXP†	85	37.5	3188	7.12	7.40	7.69	5.3E+19	1.4E+20	3.8E+20	1.66	4.46	11.97	20.0	22.5	25.0	**66**	198	598

* Assumed full rupture on Explorer section, locking and rupture decreasing to zero northward through the Winona block section as far as the Dellwood Knolls.

† Rupture only on Explorer section; Winona block excluded.

Width of effective full-rupture zone for Explorer section equivalent to the width of the locked zone (25 km) and half the coseismic transition zone (12.5 km) from Mazzotti et al. (2003b). Winona section width is an average, assuming linear northward decrease to zero from Explorer section values.

§ Moment magnitude estimated from rupture area (Equation 6).

** Seismic moment corresponding to earthquakes of listed M_w (Equation 7).

†† Mean fault slip calculated from Equation 8 using listed M_o and rupture area values, and an effective shear modulus of 1×10^{10} N/m^2.

Convergence rate averaged over the assumed rupture area (equal to the EXP/NA rate on the Explorer section, tapering to zero through the Winona section).

§§ Earthquake recurrence corresponding to listed M_w calculated from earthquake slip and convergence rate values (Equation 9). Values in bold are those used in the tsunami analysis for corresponding min (7.1), best (7.7) and max (8.0) M_w.

Table 7. Probabilities of exceedance of potentially damaging runup from tsunamis generated by earthquakes on the Explorer megathrust

Affected Regions*	M_w	Estimated frequency (/y)	P(50 y)	$Hr \geq 1.5$ m?†	$2Hr \geq 1.5$ m?†	$Hr \geq 3$ m?†	$2Hr \geq 3$ m?†	P($Hr \geq 1.5$ m, 50 y)#			P($Hr \geq 3$ m, 50 y)#		
								min	best	max	min	best	max
WHG-N								0.0000	0.0000	0.0243	0.0000	0.0000	0.0000
	7.1	0.0152	0.5312	No	No	No	No						
	7.4	0.0089	0.3601	No	No	No	No						
	7.7	0.0030	0.1394	No	No	No	No						
	8	0.0010	0.0485	No	Yes	No	No						
WHG-S, NMC&EHG-N, CMC&EHG-S, QCS, WVI-S								0.0000	0.0697	0.0697	0.0000	0.0000	0.0243
	7.1	0.0152	0.5312	No	No	No	No						
	7.4	0.0089	0.3601	No	No	No	No						
	7.7	0.0030	0.1394	No	Yes	No	No						
	8	0.0010	0.0485	Yes	Yes	No	Yes						
WVI-N								0.0485	0.1394	0.5312	0.0485	0.1394	0.2656
	7.1	0.0152	0.5312	Yes	Yes	No	Yes						
	7.4	0.0089	0.3601	Yes	Yes	No	Yes						
	7.7	0.0030	0.1394	Yes	Yes	Yes	Yes						
	8	0.0010	0.0485	Yes	Yes	Yes	Yes						

***** Zones defined in Appendix C.

† Local mean runup *Hr* and local max runup 2*Hr* estimated at various distances using the empirical relations of Abe (1995), as in Equations 12-14 and Table 2.

Probability of tsunami runup is based on probability of earthquake occurrence where local mean runup $Hr \geq 1.5$ or 3 m is expected. Probability reduced by 50% where only local runup maxima $2Hr \geq 1.5$ or 3 m are expected.

Table 8. Estimation of earthquake magnitude and recurrence on the Queen Charlotte megathrust

Rupture length (km)	Rupture width (km)	Area (km^2)	M_w*			Seismic moment M_o (Nm)†			Slip (m)#			Slip rate§	Recurrence (y)**		
			min	best	max	min	best	max	min	best	max	(mm/y)	min	best	max
250	32	8000	7.46	7.74	8.03	1.7E+20	4.6E+20	1.2E+21	2.13	5.71	15.33	8.0	**266**	713	1916
400	32	12800	7.63	7.92	8.20	3.1E+20	8.3E+20	2.2E+21	2.41	6.48	17.39	8.0	301	810	**2174**

***** Moment magnitude estimated from rupture area (Equation 6).

† Seismic moment corresponding to earthquakes of listed M_w (Equation 7).

Mean fault slip calculated from Equation 8 using listed M_o and rupture area values, and an effective shear modulus of 1×10^{10} N/m^2.

§ Mean convergence rate applied to the assumed rupture area.

** Earthquake recurrence corresponding to listed M_w calculated from earthquake slip and convergence rate values (Equation 9). Values in bold are those used in the tsunami analysis for corresponding min and max M_w. We use the mean of the two "best" values in the tsunami analysis.

Table 9. Probabilities of exceedance of potentially damaging runup from tsunamis generated by earthquakes on the Queen Charlotte megathrust

Affected Regions*	M_w	Estimated frequency (/y)	P(50 y)	$Hr \geq 1.5$ m?†	$2Hr \geq 1.5$ m?†	$Hr \geq 3$ m?†	$2Hr \geq 3$ m?†	P($Hr \geq 1.5$ m, 50 y)#			P($Hr \geq 3$ m, 50 y)#		
								min	best	max	min	best	max
WHG-N, WHG-S								0.0227	0.0636	0.1714	0.0227	0.0636	0.0857
	7.5	0.0038	0.1714	Yes	Yes	No	Yes						
	7.8	0.0013	0.0636	Yes	Yes	Yes	Yes						
	8.2	0.0005	0.0227	Yes	Yes	Yes	Yes						
NMC&EHG-N, CMC&EHG-S, QCS, WVI-N								0.0000	0.0318	0.0318	0.0000	0.0000	0.0114
	7.5	0.0038	0.1714	No	No	No	No						
	7.8	0.0013	0.0636	No	Yes	No	No						
	8.2	0.0005	0.0227	Yes	Yes	No	Yes						
WVI-S								0.0000	0.0000	0.0114	0.0000	0.0000	0.0000
	7.5	0.0038	0.1714	No	No	No	No						
	7.8	0.0013	0.0636	No	No	No	No						
	8.2	0.0005	0.0227	No	Yes	No	No						

* Zones defined in Appendix C.

† Local mean runup Hr and local max runup $2Hr$ estimated at various distances using the empirical relations of Abe (1995), as in Equations 12-14 and Table 2.

Probability of tsunami runup is based on probability of earthquake occurrence where local mean runup $Hr \geq 1.5$ or 3 m is expected. Probability reduced by 50% where only local runup maxima $2Hr \geq 1.5$ or 3 m are expected.

Table 10. Probabilities of exceedance of potentially damaging runup at coastal sites in Juan de Fuca Strait and Georgia Strait from tsunamis generated by earthquakes on local crustal faults

Affected Regions*	M_w	Frequency† (/y over 6300 km²)	P(50 y)	A(*Hr*≥1.5 m)# (km²)	A(2*Hr*≥1.5 m)# (km²)	A(2*Hr*≥3 m)# (km²)	P(*Hr*≥1.5 m, 50 y)§ min	best	max	P(*Hr*≥3 m, 50 y)§ min	best	max
JDF-E&GI												
	7.5	0.0001	0.0051	5655	22619	5655	0.0046			0.0023		
	7.5	0.0004	0.0175	5655	22619	5655		0.0157			0.0079	
	7.5	0.0011	0.0554	5655	22619	5655			0.0497			0.0249
JDF-W, GS**												
	7.5						0.0023			0.0011		
	7.5							0.0079			0.0039	
	7.5								0.0249			0.0124

* Zones defined in Appendix C.

† Frequency from seismicity recurrence relation estimated over a 6300 km² region in E. Juan de Fuca Strait, 48.1-48.8°N, 236.4-237.5°E.

Area from which sources could produce, at a coastal point of interest, local mean runup $Hr \geq 1.5$ m, local max runup $2Hr \geq 1.5$ m or 3 m. Estimated from relations of Abe (1995; Equations 12-14; Table 2). Area of half a circle, $0.5\pi r^2$, where r is max distance to source, and point of interest is at centre, with circle assumed to lie half on land, half underwater. Note: areas outside of 60-km radius lie either under land or outside seismicity area; thus probability of *2Hr* from distances > 60 km is excluded.

§ Probability of tsunami runup is based on probability of earthquake occurrence where local mean runup $Hr \geq 1.5$ m is expected, averaged over relevant area. Probability reduced by 50% where only local runup maxima $2Hr \geq 3$ m are expected.

** These areas are poorly constrained but assumed to have a relatively low tsunami hazard from crustal faults. Arbitrary probabilities are assigned that are half those of JDF-E&GI.

Table 11. Probabilities of exceedance of potentially damaging runup at coastal sites in Hecate Strait from tsunamis generated by earthquakes on local crustal faults

Affected Regions*	M_w†	Frequency (/y over 19300 km²)	P(50 y)	A(*Hr*≥1.5 m)** (km²)	A(2*Hr*≥1.5 m)** (km²)	A(2*Hr*≥3 m)** (km²)	P(*Hr*≥1.5 m, 50 y)†† min	best	max	P(*Hr*≥3 m, 50 y)†† min	best	max
NMC&EHG-N, CMC&EHG-S												
	6.8	0.0037#	0.1685	-	905	-	0.0040			**0.0000**		
	7.1	0.0014#	0.0664	905	3470	905		**0.0075**			**0.0016**	
	7.4	0.0005#	0.0253	3470	13880	3470			**0.0114**			**0.0023**
	7.4	0.0001§	0.0050	3470	13880	3470	**0.0027**			0.0004		

* Zones defined in Appendix C.

† M_w based on Equation 6 with 1500 km² maximum fault area (Bustin, 2006).

Frequency in Hecate Strait estimated using Equations 7-9, with a rupture area of 1500 km², effective shear modulus of $1x10^{10}$ N/m², and 5 mm/y convergence from GPS data (Mazzotti et al., 2003a).

§ Estimated frequency in Hecate Strait based on seismicity recurrence relation (Bustin, 2006).

** Area from which sources could produce, at a coastal point of interest, local mean runup $Hr \geq 1.5$ m, local max runup $2Hr \geq 1.5$ m or 3 m. Estimated from relations of Abe (1995; Equations 12-14; Table 2). Area of half a circle, $0.5\pi r^2$, where r is max distance to source, and point of interest is at centre, with circle assumed to lie half on land, half under water.

†† Probability of tsunami runup is based on probability of earthquake occurrence where local mean runup $Hr \geq 1.5$ m is expected, averaged over relevant area. Probability reduced by 50% where only local runup maxima $2Hr \geq 1.5$ or 3 m are expected. Preferred values for min, best, and max are in bold.

Table 12. Probabilities of exceedance of potentially damaging runup at Pacific coastal sites from tsunamis generated by large landslides offshore the Hawaiian Islands

Affected Regions*	Estimated frequency (/y)†	P(50 y)	*Hr*≥1.5 m?#	2*Hr*≥1.5 m?#	*Hr*≥3 m?#	2*Hr*≥3 m?#	P(*Hr*≥1.5 m, 50 y)§			P(*Hr*≥3 m, 50 y)§		
							min	best	max	min	best	max
WHG-N, WHG-S, NMC&EHG-N, CMC&EHG-S, QCS, WVI-N, WVI-S, JDF-W, JDF-E&GI												
	0.000004	0.0002	Yes	Yes	Yes	Yes	**0.0002**			0.0002		
	0.000007	0.0004	Yes	Yes	No	Yes		**0.0004**	**0.0004**		**0.0002**	**0.0002**
	0.000011	0.0005	No	Yes	No	No		0.0003		**0.0000**		

* Zones defined in Appendix C.

† Frequency calculated from the average recurrence of giant Hawaiian submarine landslides (see text).

Runup based on the assumptions that large volcanic flank collapses could result in local mean runup $Hr \geq 1.5$ m and that NE flank collapses could produce $Hr \geq 3$ m.

§ Probability of tsunami runup is based on probability of tsunamigenic slide occurrence where local mean runup $Hr \geq 1.5$ or 3 m is expected. Probability reduced by 50% where only local runup maxima $2Hr \geq 1.5$ or 3 m are expected. Preferred values for min, best, and max are in bold.

Table 13. Probabilities of exceedance of potentially damaging runup at Pacific coastal sites from tsunamis generated by large landslides offshore the Aleutian Islands

Affected Regions*	Estimated frequency (/y)†			*Hr*≥1.5 m?#	2*Hr*≥1.5 m?#	*Hr*≥3 m?#	2*Hr*≥3 m?#	P(*Hr*≥1.5 m, 50 y)§			P(*Hr*≥3 m, 50 y)§		
	min	best	max					min	best	max	min	best	max
WHG-N, WHG-S, NMC&EHG-N, CMC&EHG-S, QCS, WVI-N, WVI-S, JDF-W, JDF-E&GI													
	0.00020	0.00033	0.00040	Yes	Yes	No	Yes	**0.0100**	**0.0165**	**0.0198**	0.0050	0.0083	0.0099
	0.00013	0.00025	0.00029	Yes	Yes	Yes	Yes	0.0062	0.0124	0.0142	**0.0062**	**0.0124**	**0.0142**

* Zones defined in Appendix C.

† Approximate frequency of tsunamigenic slides based on the modelling of Waythomas et al. (2009; see text). Upper: slides ≥ 400 km^3; lower: slides ≥ 500-800 km^3.

Runup based on the assumptions that slides ≥ 400 km^3 could result in local mean runup $Hr \geq 1.5$ m and that slides ≥ 500-800 km^3 could produce $Hr \geq 3$ m.

§ Probability of tsunami runup is based on probability of tsunamigenic slide occurrence where local mean runup $Hr \geq 1.5$ or 3 m is expected. Probability reduced by 50% where only local runup maxima $2Hr \geq 1.5$ or 3 m are expected. Preferred values for min, best, and max are in bold.

Table 14. Estimation of Gibraltar-Cadiz M_w~8.5 earthquake recurrence from potential fault sources and paleoseismic data

Fault Source*	**Length (km)**	**Width (km)**	**Thickness (km)**	**Area (km^2)**	**Dip (°)**	**μ ($x10^{10}$ N/m^2)**	**Slip†**	**Convergence#**	**Conv. rate§**	**Recurrence**	**Reference**
							(m)	**(m)**	**(mm/y)**	**(y)**	
Marques de Pombal-Guadalquivir				11000	24-45	3	20	14-18	4-5	2800-4500	Baptista et al. (2003)
Horseshoe plain	175-350		50		55	6	10	5.75	4-5	1150-1450	Stich et al. (2007)
Gibraltar-Cadiz	180	210				3	5	5	2.5-5	1000-2000	Thiebot & Gutscher (2006)
Paleoseismic source(s)										**1951 (868-2790)**	Gràcia et al. (2010)

***** Potential fault sources of "Lisbon-type" M_w 8.5 earthquakes. Paleoseismic source refers to paleoseismic evidence for such events over the past ~9000 years (turbidite and tsunami deposits).
† Slip required to produce an M_w 8.5 earthquake on a fault source with properties listed in previous columns, estimated using Equations 7 and 8.
# Horizontal convergence equivalent to slip on the dipping fault source.
§ Tectonic convergence rate applied to the assumed rupture area to estimate recurrence.
****** Earthquake recurrence corresponding to M_w 8.5 and convergence rate values (Equation 9). Values in bold are those used in the tsunami analysis (calculated from the combined turbidite-tsunami deposit paleoseismic record of past Lisbon-type events).

Table 15. Probabilities of exceedance of potentially damaging runup from tsunamis generated by Gibraltar-Cadiz M_w~8.5 earthquakes

Affected Regions*	**Estimated frequency (/y)†**			***Hr*≥1.5 m?#**	**2*Hr*≥1.5 m?#**	***Hr*≥3 m?#**	**2*Hr*≥3 m?#**	**P(*Hr*≥1.5 m, 50 y)§**			**P(*Hr*≥3 m, 50 y)§**		
	min	**best**	**max**					**min**	**best**	**max**	**min**	**best**	**max**
ATL-OUT-N, ATL-OUT-S, SE-NFLD	0.0004	0.0005	0.0012	Yes	Yes	No	Yes	0.0178	0.0253	0.0560	0.0089	0.0127	0.0280
ATL-INN, HS	0.0004	0.0005	0.0012	No	Yes	No	No	0.0089	0.0127	0.0280	0.0000	0.0000	0.0000

***** Zones defined in Appendix C.
† Frequency of M_w~8.5 earthquakes from paleoseismic data (Table 14).
# Local mean runup *Hr* and local max runup 2*Hr* approximated based on the modelling of Roger et al. (2010a) and Barkan et al. (2009).
§ Probability of tsunami runup is based on probability of earthquake occurrence where local mean runup $Hr \geq 1.5$ or 3 m is expected. Probability reduced by 50% where only local runup maxima $2Hr \geq 1.5$ or 3 m are expected.

Table 16. Probabilities of exceedance of potentially damaging runup from tsunamis generated by earthquakes on the Puerto Rico trench

Affected Regions*	Estimated frequency (/y)†			*Hr*≥1.5 m?#	2*Hr*≥1.5 m?#	*Hr*≥3 m?#	2*Hr*≥3 m?#	P(*Hr*≥1.5 m, 50 y)§			P(*Hr*≥3 m, 50 y)§		
	min	best	max					min	best	max	min	best	max
ATL-OUT-S, SE-NFLD, ATL-INN	0.0001	0.0003	0.0010	Yes	Yes	No	Yes	0.0071	0.0124	0.0488	0.0036	0.0062	0.0244
ATL-OUT-N, HS	0.0001	0.0003	0.0010	No	Yes	No	No	0.0036	0.0062	0.0244	0.0000	0.0000	0.0000

* Zones defined in Appendix C.

† Estimated frequency of M_w~8.5-9 earthquakes from Geist and Parsons (2009).

Local mean runup *Hr* and local max runup 2*Hr* approximated based on far-field tsunami runup from global events (see text).

§ Probability of tsunami runup is based on probability of earthquake occurrence where local mean runup $Hr \geq 1.5$ or 3 m is expected. Probability reduced by 50% where only local runup maxima $2Hr \geq 1.5$ or 3 m are expected.

Table 17. Probabilities of exceedance of potentially damaging runup from tsunamis generated by earthquakes on the Lesser Antilles subduction zone

Affected Regions*	Estimated frequency (/y)†			*Hr*≥1.5 m?#	2*Hr*≥1.5 m?#	*Hr*≥3 m?#	2*Hr*≥3 m?#	P(*Hr*≥1.5 m, 50 y)§			P(*Hr*≥3 m, 50 y)§		
	min	best	max					min	best	max	min	best	max
ATL-OUT-S	0.0006	0.0009	0.0019	Yes	Yes	No	Yes	0.0312	0.0461	0.0884	0.0156	0.0230	0.0442
SE-NFLD, ATL-INN	0.0006	0.0009	0.0019	No	Yes	No	No	0.0156	0.0230	0.0442	0.0000	0.0000	0.0000

* Zones defined in Appendix C.

† Frequency of M_w~9 earthquakes is estimated as half the frequency of *M*~9 earthquakes on the Cascadia subduction zone, based on a convergence rate that is approximately half.

Local mean runup *Hr* and local max runup 2*Hr* approximated based on far-field tsunami runup from global events and the potential for topographic steering from the Mid-Atlantic Ridge (see text).

§ Probability of tsunami runup is based on probability of earthquake occurrence where local mean runup $Hr \geq 1.5$ or 3 m is expected. Probability reduced by 50% where only local runup maxima $2Hr \geq 1.5$ or 3 m are expected.

Table 18. Probabilities of exceedance of potentially damaging runup at coastal sites from tsunamis generated by Atlantic continental slope landslides

Affected Regions*	Slide† (km)	Estimated frequency (/y)# min	best	max	*Hr*≥1.5 m?§	2*Hr*≥1.5 m?§	*Hr*≥3 m?§	2*Hr*≥3 m?§	P(*Hr*≥1.5 m, 50 y)** min	best	max	P(*Hr*≥3 m, 50 y)** min	best	max
ATL-OUT-N, ATL-OUT-S	50	0.00006	0.00010	0.00015	Yes	Yes	No	Yes	**0.0029**	**0.0051**	**0.0077**	0.0015	0.0025	0.0039
	70	0.00005	0.00009	0.00014	Yes	Yes	Yes	Yes	0.0024	0.0044	0.0068	**0.0024**	**0.0044**	**0.0068**
SE-NFLD	50	0.00015	0.00025	0.00038	Yes	Yes	No	Yes	**0.0074**	**0.0125**	**0.0186**	0.0037	0.0062	0.0093
	70	0.00011	0.00020	0.00031	Yes	Yes	Yes	Yes	0.0055	0.0099	0.0155	**0.0055**	**0.0099**	**0.0155**
ATL-INN, HS	50	0.00006	0.00010	0.00015	No	Yes	No	No	0.0015	0.0025	0.0039	0.0000	0.0000	0.0000
	70	0.00005	0.00009	0.00014	Yes	Yes	No	Yes	**0.0024**	**0.0044**	**0.0068**	**0.0012**	**0.0022**	**0.0034**

***** Zones defined in Appendix C.

† Along-slope extent of landslide for which the estimated frequencies are given.

Approximate frequency of tsunamigenic slides based on the cumulative size-frequency relations (Fig. 13) of past failures in Orphan Basin (extrapolated to the whole Atlantic margin) and Flemish Pass (only applicable to SE-NFLD, which we consider susceptible to 3 source areas, see text).

§ Runup based on the assumptions that slides ≥ 50 km in along-slope extent could result in local mean runup $Hr \geq 1.5$ m along the outer coast and slides ≥ 70 km could produce $Hr \geq 3$ m.

****** Probability of tsunami runup is based on probability of tsunamigenic slide occurrence where local mean runup $Hr \geq 1.5$ or 3 m is expected. Probability reduced by 50% where only local runup maxima $2Hr \geq 1.5$ or 3 m are expected. Preferred values for min, best, and max are in bold.

Table 19. Probabilities of exceedance of potentially damaging runup at Atlantic coastal sites from tsunamis generated by large landslides offshore the Canary Islands

Affected Regions*	Estimated frequency (/y)†	P(50 y)	*Hr*≥1.5 m?#	2*Hr*≥1.5 m?#	*Hr*≥3 m?#	2*Hr*≥3 m?#	P(*Hr*≥1.5 m, 50 y)§ min	best	max	P(*Hr*≥3 m, 50 y)§ min	best	max
ATL-OUT-S, ATL-INN, ATL-OUT-N, SE-NFLD,HS												
	0.000003	0.0002	Yes	Yes	Yes	Yes	**0.0002**			0.0002		
	0.000006	0.0003	Yes	Yes	No	Yes		**0.0003**			**0.0002**	**0.0002**
	0.000010	0.0005	No	Yes	No	No			**0.0003**	**0.0000**		

***** Zones defined in Appendix C.

† Frequency of potentially tsunamigenic slides (estimated as ≥ 150 km^3) calculated from the cumulative volume-frequency relationship of slide deposits (Masson et al., 2002; Fig. 14).

Runup based on the simplified assumptions that local mean runup $Hr \geq 1.5$ m could result from 150 km^3 slides, that events with a shorter recurrence interval could produce only local maxima ≥ 1.5 m and those with a longer recurrence interval could produce Hr ≥ 3 m.

§ Probability of tsunami runup is based on probability of tsunamigenic slide occurrence where local mean runup $Hr \geq 1.5$ or 3 m is expected. Probability reduced by 50% where only local runup maxima $2Hr \geq 1.5$ or 3 m are expected. Preferred values for min, best, and max are in bold.

Table 20. Estimation of earthquake magnitude and recurrence on the Mackenzie thrust*

Rupture length (km)	Rupture width (km)	Area (km^2)	M_w† min	M_w† best	M_w† max	Seismic moment M_o (Nm)# min	Seismic moment M_o (Nm)# best	Seismic moment M_o (Nm)# max	Slip (m)§ min	Slip (m)§ best	Slip (m)§ max	Slip rate** (mm/y)	Recurrence (y)†† min	Recurrence (y)†† best	Recurrence (y)†† max
200	30	6000	**7.35**	7.64	7.92	1.2E+20	3.2E+20	8.5E+20	1.97	5.28	14.18	2.0	**984**	2641	7092
250	55	13750	7.66	**7.94**	8.23	3.4E+20	9.1E+20	2.4E+21	2.46	6.60	17.73	2.0	1229	**3301**	8865
300	80	24000	7.86	8.15	**8.43**	6.9E+20	1.8E+21	4.9E+21	2.86	7.67	20.60	2.0	1428	3835	**10298**

* This potential tsunami source is not included in the final cumulative tsunami hazard, due to poor constraints.

† Moment magnitude estimated from rupture area (Equation 6).

Seismic moment corresponding to earthquakes of listed M_w (Equation 7).

§ Mean fault slip calculated from Equation 8 using listed M_o and rupture area values, and an effective shear modulus of $1x10^{10}$ N/m^2.

** Mean convergence rate applied to the assumed rupture area.

†† Earthquake recurrence corresponding to listed M_w calculated from earthquake slip and convergence rate values (Equation 9). Values in bold are those used in the tsunami analysis for corresponding min, best and max M_w.

Table 21. Probabilities of exceedance of potentially damaging runup from tsunamis generated by potential earthquakes on the Mackenzie thrust*

Affected Regions†	M_w	Estimated frequency (/y)	P(50 y)	*Hr*≥1.5 m?#	2*Hr*≥1.5 m?#	*Hr*≥3 m?#	2*Hr*≥3 m?#	P(*Hr*≥1.5 m, 50 y)§ min	P(*Hr*≥1.5 m, 50 y)§ best	P(*Hr*≥1.5 m, 50 y)§ max	P(*Hr*≥3 m, 50 y)§ min	P(*Hr*≥3 m, 50 y)§ best	P(*Hr*≥3 m, 50 y)§ max
N. Yukon and NW NWT								0.0000**	0.0150	0.0248	0.0000	0.0075	0.0075
	7.4	0.0010	0.0495	No	Yes	No	No						
	7.9	0.0003	0.0150	Yes	Yes	No	Yes						
	8.4	0.0001	0.0048	Yes	Yes	Yes	Yes						
S. Banks Is.								0.0000	0.0000	0.0048	0.0000	0.0000	0.0024
	7.4	0.0010	0.0495	No	No	No	No						
	7.9	0.0003	0.0150	No	No	No	No						
	8.4	0.0001	0.0048	Yes	Yes	No	Yes						
W. and S. Banks Is., W. Victoria Is., NE NWT, and NW Nunavut								0.0000	0.0000	0.0024	0.0000	0.0000	0.0000
	7.4	0.0010	0.0495	No	No	No	No						
	7.9	0.0003	0.0150	No	No	No	No						
	8.4	0.0001	0.0048	No	Yes	No	No						

* This potential tsunami source is not included in the final cumulative tsunami hazard, due to poor constraints.

† Zones not defined in Appendix C (because this source is not included in the final hazard calculation). See Figure 1 for locations.

Local mean runup *Hr* and local max runup 2*Hr* estimated at various distances using the empirical relations of Abe (1995), as in Equations 12-14 and Table 2.

§ Probability of tsunami runup is based on probability of earthquake occurrence where local mean runup $Hr \geq 1.5$ or 3 m is expected. Probability reduced by 50% where only local runup maxima $2Hr \geq 1.5$ or 3 m are expected.

** Minimum reduced to 0 to allow for the possibility that tectonic motion is aseismic and non-tsunamigenic.

Table 22. Cumulative probabilities of exceedance (in 50 y) of potentially damaging runup on the Pacific coast from multiple tsunami sources

Coastline At Risk*	Tsunami Source	P (*Hr*≥1.5 m)† (% in 50 y)			Equiv. recurrence(*Hr*≥1.5 m) (y)			P (*Hr*≥3 m)† (% in 50 y)			Equiv. recurrence(*Hr*≥3 m) (y)		
		min	best	max	min	best	max	min	best	max	min	best	max
WHG-N	Cascadia subduction zone (full)	6.13	9.00	16.90	790	530	270	6.13	9.00	16.90	790	530	270
	S. Cascadia subduction zone	1.96	2.44	3.22	2525	2025	1525	0.00	0.00	0.00	-	-	-
	Queen Charlotte subduction	2.27	6.36	17.14	2178	761	266	2.27	6.36	8.57	2178	761	558
	Explorer subduction	0.00	0.00	2.43	-	-	2033	0.00	0.00	0.00	-	-	-
	Far-field subduction zones	22.12	43.45	67.37	200	88	45	0.00	0.00	13.93	-	-	333
	Hawaiian Islands landslides	0.02	0.04	0.04	272000	136000	136000	0.00	0.02	0.02	-	272000	272000
	Aleutian Islands landslides	1.00	1.65	1.98	5000	3000	2500	0.62	1.24	1.42	8000	4000	3500
	TOTAL:	**36.07**	**53.78**	**73.88**	**112**	**65**	**37**	**11.27**	**15.86**	**23.41**	**418**	**289**	**187**
WHG-S	Cascadia subduction zone (full)	6.13	9.00	16.90	790	530	270	6.13	9.00	16.90	790	530	270
	S. Cascadia subduction zone	1.96	2.44	3.22	2525	2025	1525	0.00	0.00	0.00	-	-	-
	Queen Charlotte subduction	2.27	6.36	17.14	2178	761	266	2.27	6.36	8.57	2178	761	558
	Explorer subduction	0.00	6.97	6.97	-	692	692	0.00	0.00	2.43	-	-	2033
	Far-field subduction zones	22.12	43.45	67.37	200	88	45	0.00	0.00	13.93	-	-	333
	Hawaiian Islands landslides	0.02	0.04	0.04	272000	136000	136000	0.00	0.02	0.02	-	272000	272000
	Aleutian Islands landslides	1.00	1.65	1.98	5000	3000	2500	0.62	1.24	1.42	8000	4000	3500
	TOTAL:	**40.52**	**57.00**	**75.70**	**96**	**59**	**35**	**11.27**	**15.86**	**23.41**	**418**	**289**	**187**
NMC&EHG-N, CMC&EHG-S	Cascadia subduction zone (full)	6.13	9.00	16.90	790	530	270	6.13	9.00	16.90	790	530	270
	S. Cascadia subduction zone	1.96	2.44	3.22	2525	2025	1525	0.00	0.00	0.00	-	-	-
	Queen Charlotte subduction	0.00	3.18	3.18	-	1547	1547	0.00	0.00	1.14	-	-	4361
	Explorer subduction	0.00	6.97	6.97	-	692	692	0.00	0.00	2.43	-	-	2033
	Local crustal faults	0.27	0.75	1.14	18494	6642	4361	0.00	0.16	0.23	-	31225	21714
	Far-field subduction zones	22.12	43.45	67.37	200	88	45	0.00	0.00	13.93	-	-	333
	Hawaiian Islands landslides	0.02	0.04	0.04	272000	136000	136000	0.00	0.02	0.02	-	272000	272000
	Aleutian Islands landslides	1.00	1.65	1.98	5000	3000	2500	0.62	1.24	1.42	8000	4000	3500
	TOTAL:	**39.13**	**55.88**	**74.73**	**101**	**61**	**36**	**7.41**	**10.29**	**18.09**	**650**	**460**	**251**
QCS	Cascadia subduction zone (full)	6.13	9.00	16.90	790	530	270	6.13	9.00	16.90	790	530	270
	S. Cascadia subduction zone	1.96	2.44	3.22	2525	2025	1525	0.00	0.00	0.00	-	-	-
	Queen Charlotte subduction	0.00	3.18	3.18	-	1547	1547	0.00	0.00	1.14	-	-	4361
	Explorer subduction	0.00	6.97	6.97	-	692	692	0.00	0.00	2.43	-	-	2033
	Far-field subduction zones	0.00	7.69	24.04	-	625	182	0.00	0.00	0.00	-	-	-
	Hawaiian Islands landslides	0.02	0.04	0.04	272000	136000	136000	0.00	0.02	0.02	-	272000	272000
	Aleutian Islands landslides	1.00	1.65	1.98	5000	3000	2500	0.62	1.24	1.42	8000	4000	3500
	TOTAL:	**25.06**	**27.43**	**41.49**	**173**	**156**	**93**	**7.26**	**10.15**	**17.95**	**664**	**467**	**253**

Table 22. (Continued)

WVI-N	Cascadia subduction zone (full)	6.13	9.00	16.90	790	530	270	6.13	9.00	16.90	790	530	270
	S. Cascadia subduction zone	1.96	2.44	3.22	2525	2025	1525	0.00	0.00	0.00	-	-	-
	Queen Charlotte subduction	0.00	3.18	3.18	-	1547	1547	0.00	0.00	1.14	-	-	4361
	Explorer subduction	4.85	13.94	53.12	1006	333	66	4.85	13.94	26.56	1006	333	162
	Far-field subduction zones	22.12	43.45	67.37	200	88	45	0.00	0.00	13.93	-	-	333
	Hawaiian Islands landslides	0.02	0.04	0.04	272000	136000	136000	0.00	0.02	0.02	-	272000	272000
	Aleutian Islands landslides	1.00	1.65	1.98	5000	3000	2500	0.62	1.24	1.42	8000	4000	3500
	TOTAL:	**42.40**	**58.87**	**81.97**	**91**	**56**	**29**	**14.09**	**22.67**	**35.59**	**329**	**194**	**114**
WVI-S	Cascadia subduction zone (full)	6.13	9.00	16.90	790	530	270	6.13	9.00	16.90	790	530	270
	S. Cascadia subduction zone	3.92	4.88	6.45	1250	1000	750	1.96	2.44	3.22	2525	2025	1525
	Queen Charlotte subduction	0.00	0.00	1.14	-	-	4361	0.00	0.00	0.00	-	-	-
	Explorer subduction	0.00	6.97	6.97	-	692	692	0.00	0.00	2.43	-	-	2033
	Far-field subduction zones	22.12	43.45	67.37	200	88	45	0.00	0.00	13.93	-	-	333
	Hawaiian Islands landslides	0.02	0.04	0.04	272000	136000	136000	0.00	0.02	0.02	-	272000	272000
	Aleutian Islands landslides	1.00	1.65	1.98	5000	3000	2500	0.62	1.24	1.42	8000	4000	3500
	TOTAL:	**38.24**	**55.23**	**74.37**	**104**	**62**	**37**	**9.49**	**12.34**	**19.98**	**502**	**380**	**224**
JDF-W	Cascadia subduction zone (full)	6.13	9.00	16.90	790	530	270	6.13	9.00	16.90	790	530	270
	S. Cascadia subduction zone	1.96	2.44	3.22	2525	2025	1525	0.00	0.00	0.00	-	-	-
	Local crustal faults	0.23	0.79	2.49	21714	6304	1983	0.11	0.39	1.24	45430	12795	4007
	Far-field subduction zones	0.00	7.69	24.04	-	625	182	0.00	0.00	0.00	-	-	-
	Hawaiian Islands landslides	0.02	0.04	0.04	272000	136000	136000	0.00	0.02	0.02	-	272000	272000
	Aleutian Islands landslides	1.00	1.65	1.98	5000	3000	2500	0.62	1.24	1.42	8000	4000	3500
	TOTAL:	**17.42**	**20.07**	**35.60**	**261**	**223**	**114**	**7.61**	**10.50**	**18.31**	**632**	**451**	**247**
JDF-E&GI	Cascadia subduction zone (full)	6.13	9.00	16.90	790	530	270	6.13	9.00	16.90	790	530	270
	S. Cascadia subduction zone	1.96	2.44	3.22	2525	2025	1525	0.00	0.00	0.00	-	-	-
	Local crustal faults	0.46	1.57	4.97	10845	3160	981	0.23	0.79	2.49	21714	6304	1983
	Far-field subduction zones	0.00	7.69	24.04	-	625	182	0.00	0.00	0.00	-	-	-
	Hawaiian Islands landslides	0.02	0.04	0.04	272000	136000	136000	0.00	0.02	0.02	-	272000	272000
	Aleutian Islands landslides	1.00	1.65	1.98	5000	3000	2500	0.62	1.24	1.42	8000	4000	3500
	TOTAL:	**17.95**	**20.70**	**36.24**	**253**	**216**	**111**	**7.95**	**10.86**	**18.73**	**604**	**435**	**241**
GS	Cascadia subduction zone (full)	6.13	9.00	16.90	790	530	270	0.00	0.00	4.23	-	-	1157
	S. Cascadia subduction zone	0.00	1.22	1.61	-	4076	3076	0.00	0.00	0.00	-	-	-
	Local crustal faults	0.23	0.79	2.49	21714	6304	1983	0.11	0.39	1.24	45430	12795	4007
	TOTAL:	**7.96**	**10.82**	**18.71**	**603**	**437**	**241**	**0.11**	**0.39**	**4.32**	**45430**	**12795**	**1133**

* Zones defined in Appendix C.

† Probability of exceeding given tsunami runup from individual sources. Total probability is the cumulative value calculated using Equations 2-5 for min, best, and max.

Table 23. Cumulative probabilities of exceedance (in 50 y) of potentially damaging runup on the Atlantic coast from multiple tsunami sources

Coastline At Risk*	Tsunami Source	P (*Hr*≥1.5 m)† (% in 50 y)			Equiv. recurrence(*Hr*≥1.5 m) (y)			P (*Hr*≥3 m)† (% in 50 y)			Equiv. recurrence(*Hr*≥3 m) (y)		
		min	best	max	min	best	max	min	best	max	min	best	max
ATL-OUT-S	Continental slope landslides	0.29	0.51	0.77	17040	9810	6460	0.24	0.44	0.68	20530	11390	7280
	Gibraltar-Cadiz	1.78	2.53	5.60	2785	1951	868	0.89	1.27	2.80	5593	3912	1761
	Puerto Rico trench	0.71	1.24	4.88	7000	4000	1000	0.36	0.62	2.44	13864	8039	2024
	Lesser Antilles subduction	3.12	4.61	8.84	1580	1060	540	1.56	2.30	4.42	3185	2145	1106
	Canary Islands landslides	0.02	0.03	0.03	313000	159000	159000	0.00	0.02	0.02	-	313000	313000
	TOTAL:	**6.99**	**8.67**	**14.60**	**690**	**551**	**317**	**3.70**	**4.58**	**7.65**	**1325**	**1067**	**628**
SE-NFLD	Continental slope landslides	0.74	1.25	1.86	6748	3976	2659	0.55	0.99	1.55	9066	5051	3203
	Gibraltar-Cadiz	1.78	2.53	5.60	2785	1951	868	0.89	1.27	2.80	5593	3912	1761
	Puerto Rico trench	0.71	1.24	4.88	7000	4000	1000	0.36	0.62	2.44	13864	8039	2024
	Lesser Antilles subduction	1.56	2.30	4.42	3185	2145	1106	0.00	0.00	0.00	-	-	-
	Canary Islands landslides	0.02	0.03	0.03	313000	159000	159000	0.00	0.02	0.02	-	313000	313000
	TOTAL:	**5.94**	**7.16**	**12.07**	**817**	**673**	**389**	**2.24**	**2.86**	**5.25**	**2205**	**1721**	**927**
ATL-OUT-N	Continental slope landslides	0.29	0.51	0.77	17040	9810	6460	0.24	0.44	0.68	20530	11390	7280
	Gibraltar-Cadiz	1.78	2.53	5.60	2785	1951	868	0.89	1.27	2.80	5593	3912	1761
	Puerto Rico trench	0.36	0.62	2.44	13864	8039	2024	0.00	0.00	0.00	-	-	-
	Canary Islands landslides	0.02	0.03	0.03	313000	159000	159000	0.00	0.02	0.02	-	313000	313000
	TOTAL:	**2.85**	**3.66**	**7.16**	**1732**	**1342**	**673**	**1.29**	**1.72**	**3.26**	**3840**	**2885**	**1509**
ATL-INN	Continental slope landslides	0.24	0.44	0.68	20530	11390	7280	0.12	0.22	0.34	41085	22804	14584
	Gibraltar-Cadiz	0.89	1.27	2.80	5595	3927	1761	0.00	0.00	0.00	-	-	-
	Puerto Rico trench	0.71	1.24	4.88	7000	4000	1000	0.36	0.62	2.44	13864	8039	2024
	Lesser Antilles subduction	1.56	2.30	4.42	3185	2145	1106	0.00	0.00	0.00	-	-	-
	Local crustal faults	0.00	0.00	1.50	-	-	3300	0.00	0.00	0.75	-	-	6600
	Canary Islands landslides	0.02	0.03	0.03	313000	159000	159000	0.00	0.02	0.02	-	313000	313000
	TOTAL:	**4.21**	**5.19**	**9.47**	**1163**	**939**	**503**	**0.58**	**0.85**	**2.67**	**8647**	**5833**	**1845**
HS	Continental slope landslides	0.24	0.44	0.68	20530	11390	7280	0.12	0.22	0.34	41085	22804	14584
	Gibraltar-Cadiz	0.89	1.27	2.80	5595	3927	1761	0.00	0.00	0.00	-	-	-
	Puerto Rico trench	0.36	0.62	2.44	13864	8039	2024	0.00	0.00	0.00	-	-	-
	Canary Islands landslides	0.02	0.03	0.03	313000	159000	159000	0.00	0.02	0.02	-	313000	313000
	TOTAL:	**1.85**	**2.34**	**4.69**	**2681**	**2114**	**1042**	**0.14**	**0.23**	**0.36**	**36318**	**21255**	**13935**

* Zones defined in Appendix C.

† Probability of exceeding given tsunami runup from individual sources. Total probability is the cumulative value calculated using Equations 2-5 for min, best, and max.

Table 24. Cumulative probabilities of exceedance (in 50 y) of potentially damaging runup on the Arctic coast*

Coastline At Risk	Tsunami Source	P (*Hr*≥1.5 m) (% in 50 y)			Equiv. recurrence(*Hr*≥1.5 m) (y)			P (*Hr*≥3 m) (% in 50 y)			Equiv. recurrence(*Hr*≥3 m) (y)		
		min	best	max	min	best	max	min	best	max	min	best	max
N. YT, N. NT, S. Banks Is., W. Banks Is., W. Victoria Is., NW coasts of Arctic archipelago, Baffin Bay coast	Continental slope landslides	0.29	0.51	0.77	17036	9814	6464	0.24	0.44	0.68	20534	11390	7278
	TOTAL:	**0.29**	**0.51**	**0.77**	**17036**	**9814**	**6464**	**0.24**	**0.44**	**0.68**	**20534**	**11390**	**7278**

* Potential Mackenzie thrust source (Tables 20-21) excluded from cumulative tsunami hazard due to extremely poor constraints.

Table 25. Probabilistic runup hazard on the Pacific coast for different time periods

Coastline At Risk*	Return period *T* (y)	Runup† (m)		
		<1.5	1.5-2.9	≥3.0
WHG-N	50	min,best	max	
	100	min	best,max	
	500			min,best,max
	1000			min,best,max
	2500			min,best,max
WHG-S	50	min,best	max	
	100		min,best,max	
	500			min,best,max
	1000			min,best,max
	2500			min,best,max
NMC&EHG-N, CMC&EHG-S	50	min,best	max	
	100	min	best,max	
	500		min	best,max
	1000			min,best,max
	2500			min,best,max
QCS	50	min,best,max		
	100	min,best	max	
	500		min	best,max
	1000			min,best,max
	2500			min,best,max
WVI-N	50	min,best	max	
	100		min,best,max	
	500			min,best,max
	1000			min,best,max
	2500			min,best,max
WVI-S	50	min,best	max	
	100	min	best,max	
	500		min	best,max
	1000			min,best,max
	2500			min,best,max
JDF-W	50	min,best,max		
	100	min,best,max		
	500		min	best,max
	1000			min,best,max
	2500			min,best,max
JDF-E&GI	50	min,best,max		
	100	min,best,max		
	500		min	best,max
	1000			min,best,max
	2500			min,best,max
GS	50	min,best,max		
	100	min,best,max		
	500	min	best,max	
	1000		min,best,max	
	2500		min,best	max

* Zones defined in Appendix C.

† Level of runup (min, best, and max) estimated for given return period. Also shown in Appendix D.

Table 26. Probabilistic runup hazard on the Atlantic coast for different time periods

Coastline At Risk*	Return period *T* (y)	Runup† (m)		
		<1.5	1.5-2.9	≥3.0
ATL-OUT-S	50	min,best,max		
	100	min,best,max		
	500	min,best	max	
	1000		min,best	max
	2500			min,best,max
SE-NFLD	50	min,best,max		
	100	min,best,max		
	500	min,best	max	
	1000		min,best	max
	2500			min,best,max
ATL-OUT-N	50	min,best,max		
	100	min,best,max		
	500	min,best,max		
	1000	min,best	max	
	2500		min,best	max
ATL-INN	50	min,best,max		
	100	min,best,max		
	500	min,best,max		
	1000	min	best,max	
	2500		min,best	max
HS	50	min,best,max		
	100	min,best,max		
	500	min,best,max		
	1000	min,best,max		
	2500	min	best,max	

* Zones defined in Appendix C.

† Level of runup (min, best, and max) estimated for given return period. Also shown in Appendix D.

Table 27. Probabilistic runup hazard on the Arctic coast for different time periods*

Coastline At Risk	Return period *T* (y)	Runup† (m)		
		<1.5	**1.5-2.9**	**≥3.0**
N. YT, N. NT, S. Banks Is., W. Banks Is., W. Victoria Is., NW coasts of Arctic archipelago, Baffin Bay coast	50	min,best,max		
	100	min,best,max		
	500	min,best,max		
	1000	min,best,max		
	2500	min,best,max		

* Potential Mackenzie thrust source (Tables 20-21) excluded from cumulative tsunami hazard due to extremely poor constraints.

† Level of runup (min, best, and max) estimated for given return period. Also shown in Appendix D.

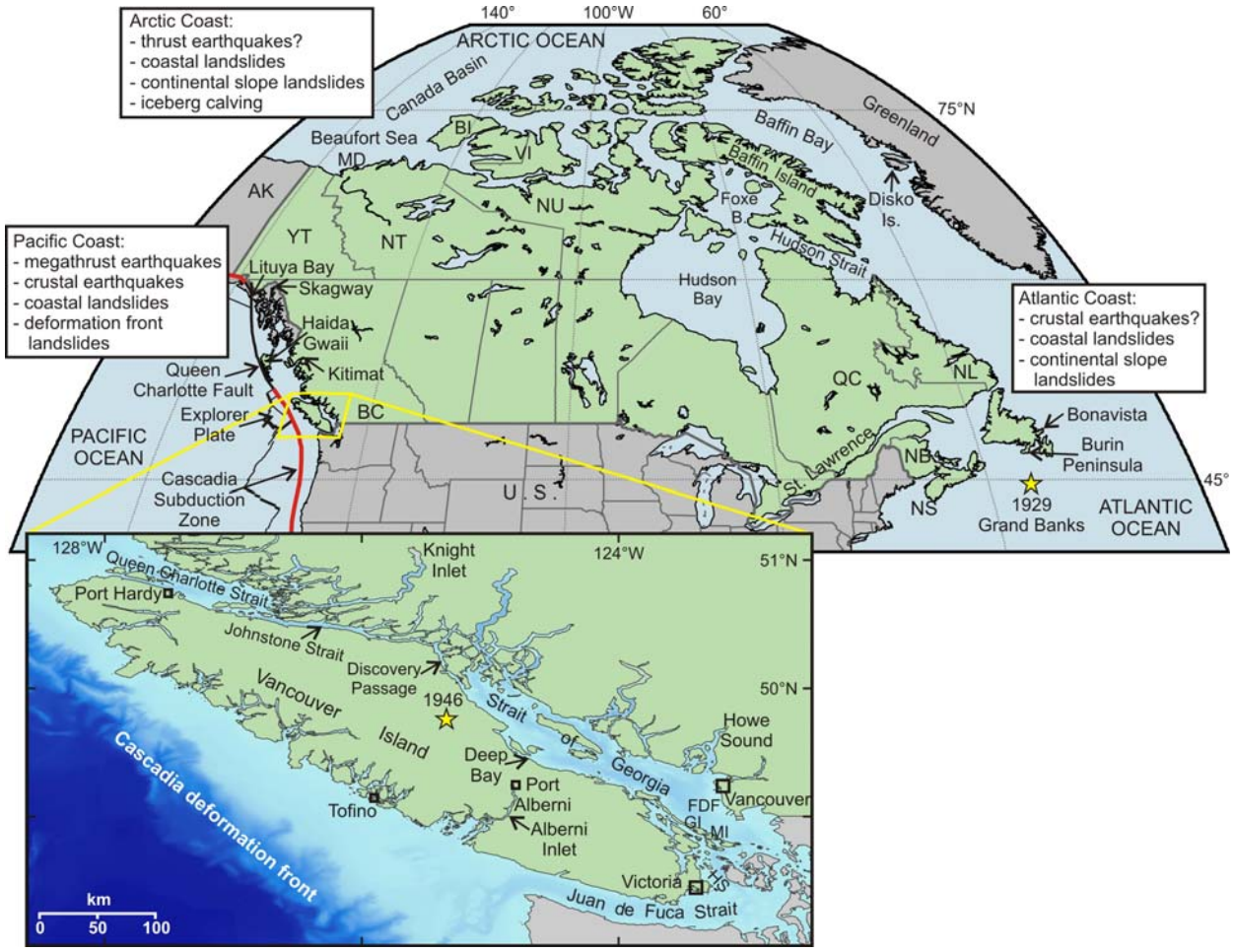

Figure 1. Location map with potential sources of local tsunamis on the Pacific, Arctic, and Atlantic coasts of Canada. Megathrust plate boundaries are shown in red (other boundaries in black). Yellow stars show the epicentres of the 1929 and 1946 earthquakes that triggered landslide tsunamis. BI: Banks Island; FDF: Fraser delta front; GI: Galiano Island; HS: Haro Strait; MD: Mackenzie delta; MI: Mayne Island; VI: Victoria Island.

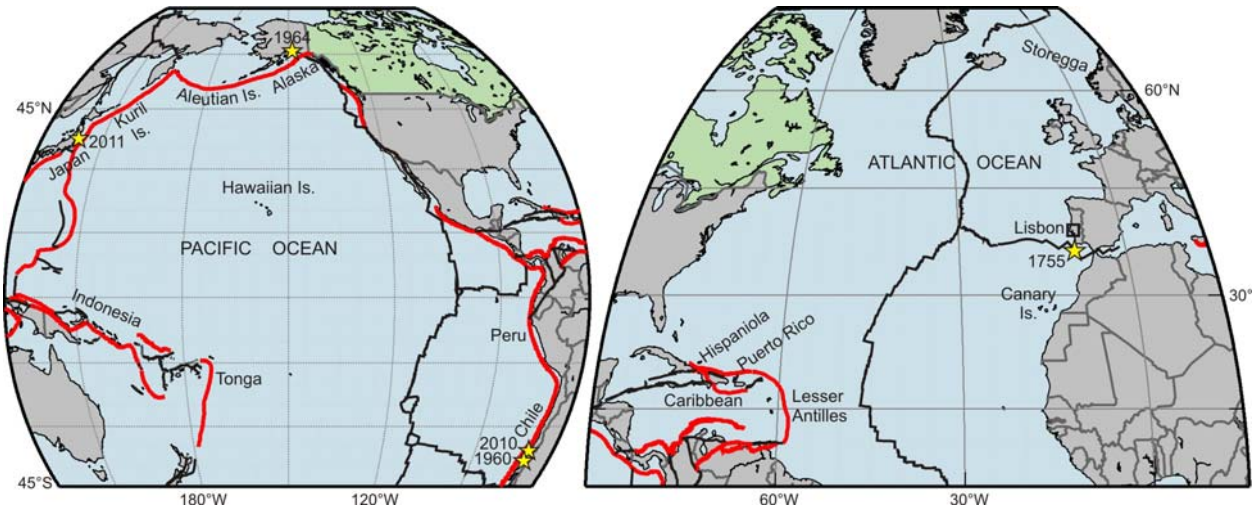

Figure 2. Potential sources of far-field tsunamis for the Pacific (left) and Atlantic (right) coasts of Canada. Plate boundaries as in Fig. 1. Yellow stars show the epicentres of earthquakes that spawned major historical far-field tsunamis.

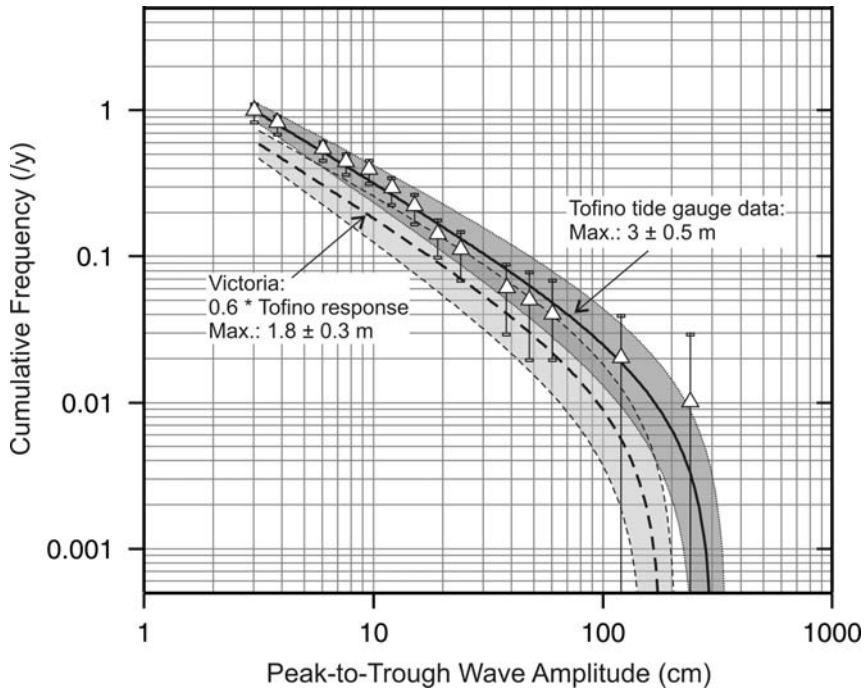

Figure 3. Cumulative frequency distribution of far-field tsunami peak-to-trough wave amplitudes at Tofino (white symbols; solid line; dark grey shading) and Victoria, BC (dashed line; light grey shading). The Tofino recurrence curve is based on tide gauge data (white symbols; error bars assume Poissonian statistics), and is tapered to the assigned maximum amplitude; the Victoria curve is based on a scaling relationship whereby amplitudes are assumed to be 0.6 of those measured at the Tofino tide gauge (Table 4). Empirical data suggest that peak-to-trough wave amplitudes are approximately equivalent to local mean runup *Hr* (Abe, 1995).

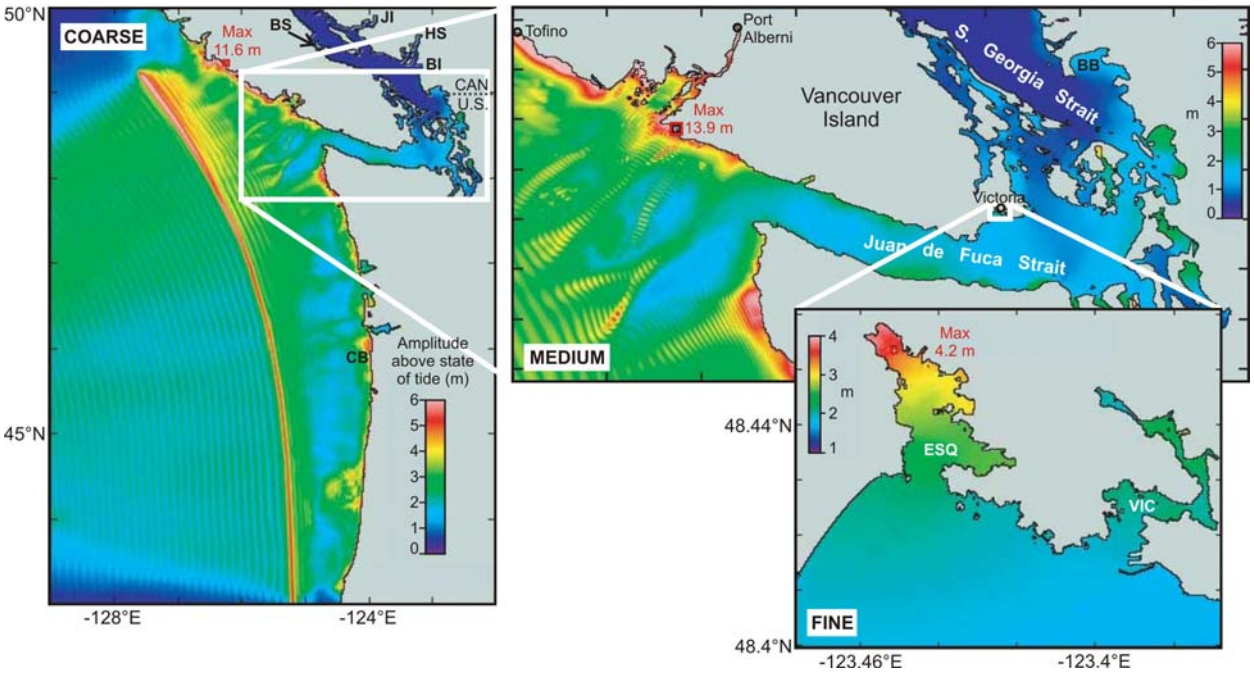

Figure 4. Maximum tsunami wave amplitudes (above state of tide) resulting from an M_w 9.0 Cascadia subduction zone earthquake modelled with a coarse-, medium-, and fine-resolution bathymetric grid (modified from Cherniawsky et al., 2007). BB: Boundary Bay; BS: Baynes Sound; JI: Jervis Inlet; HS: Howe Sound; BI: Burrard Inlet; CB: Cannon Beach, Oregon; ESQ: Esquimalt Harbour; VIC: Victoria Harbour.

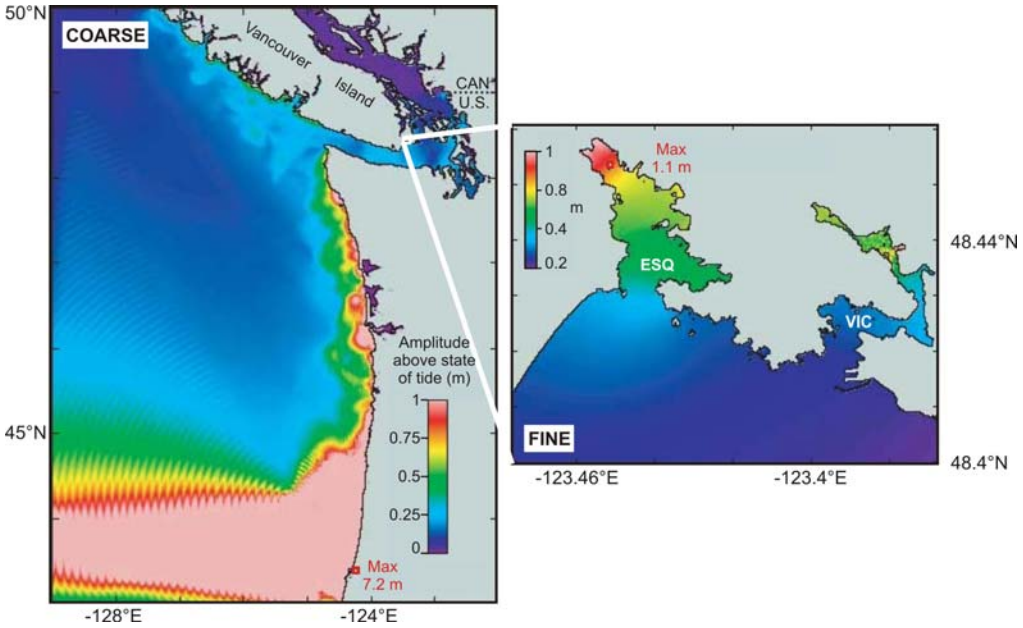

Figure 5. Maximum tsunami wave amplitudes (above state of tide) resulting from a southern Cascadia subduction zone earthquake modelled with a coarse- and fine-resolution bathymetric grid (modified from Cherniawsky et al., 2007). ESQ: Esquimalt Harbour; VIC: Victoria Harbour.

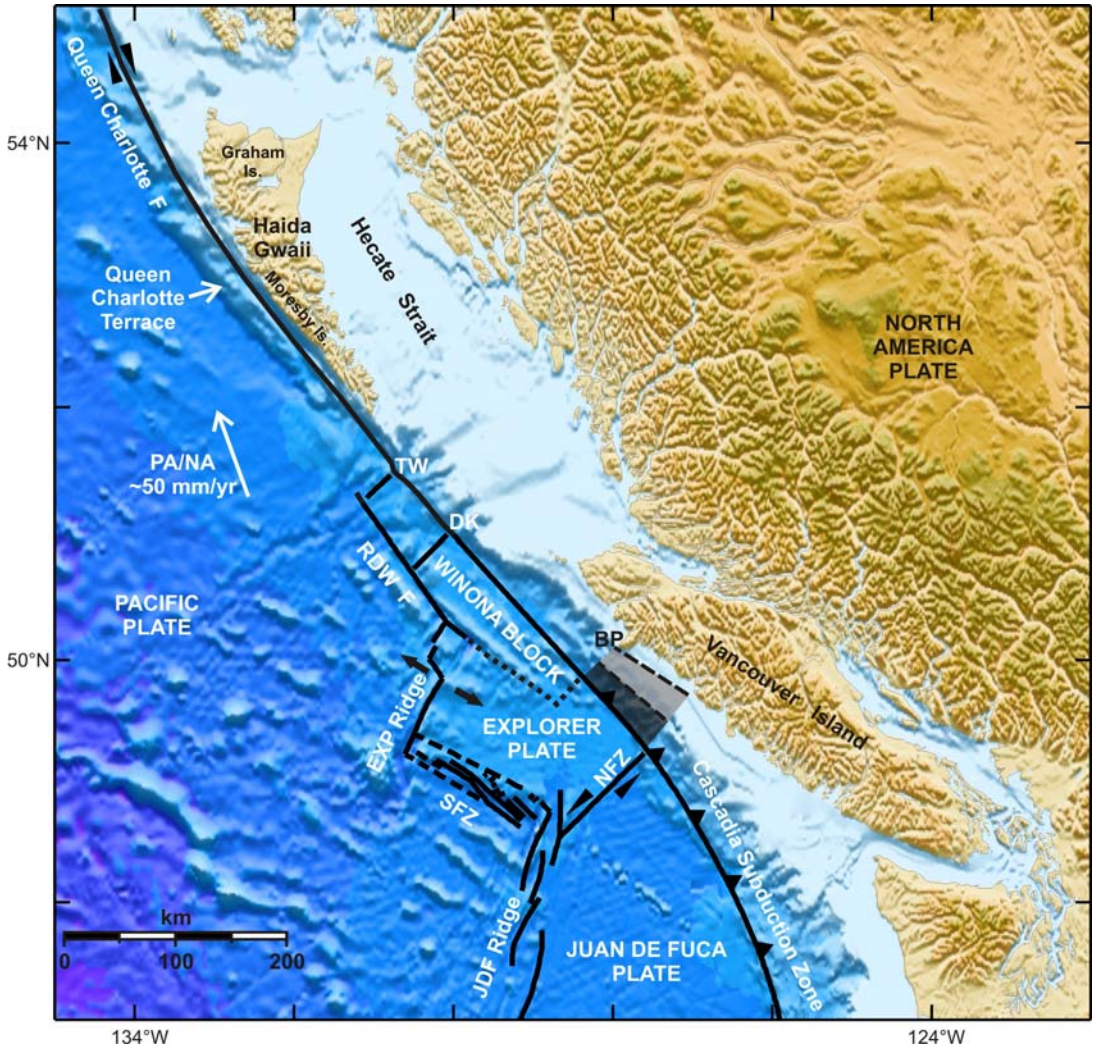

Figure 6. Tectonics of the Explorer and Queen Charlotte region. BP: Brooks Peninsula; DK: Dellwood Knolls; EXP: Explorer; JDF: Juan de Fuca; NFZ: Nootka fault zone; PA/NA: Pacific plate motion relative to North America; RDW F: Revere-Dellwood-Wilson fault; SFZ: Sovanco fault zone; TW: Tuzo Wilson seamounts. Dark and light grey shaded areas show the coseismic locked (seismogenic) and transition zones assumed for subduction of the Explorer plate (Mazzotti et al., 2003b; also see Table 6).

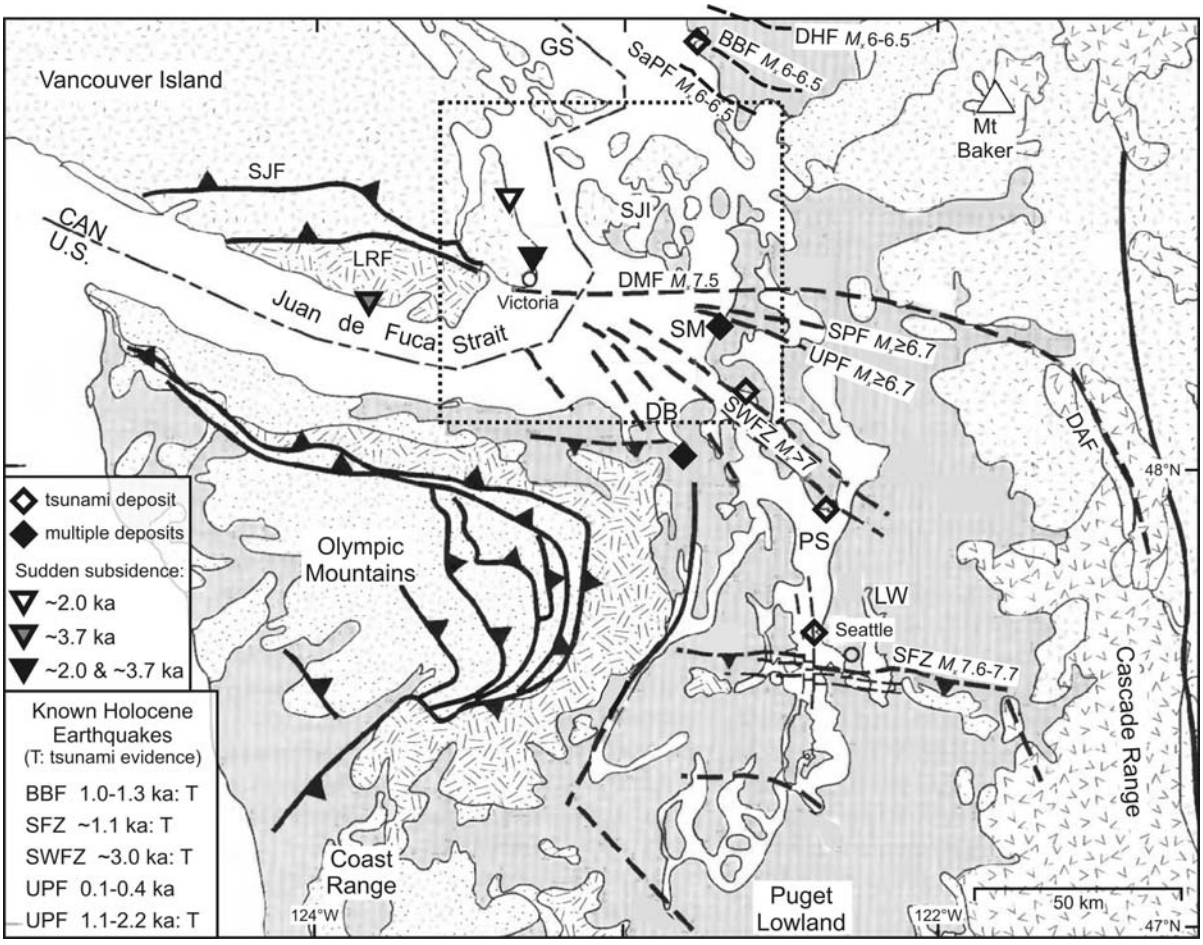

Figure 7. Crustal faults mapped in the region of Puget Sound-Juan de Fuca Strait (modified from Johnson et al., 2001, with additional faults from Kelsey et al., 2012). Box with dotted line outlines area of high seismicity used in the analysis. Data sources: BBF: Birch Bay fault, DHF: Drayton Harbor fault, SaPF: Sandy Point fault - Kelsey et al. (2012); DB: Discovery Bay - Williams et al. (2005); DMF: Devil's Mountain fault, SPF: Strawberry Point fault, UPF: Utsalady Point fault - Johnson et al. (2001;2004); SFZ: Seattle fault zone - Atwater and Moore (1992); Pratt et al. (1997); SM: Swantown Marsh - Williams and Hutchinson (2000); SWFZ: S. Whidbey Island fault zone - Johnson et al. (1996); Kelsey et al. (2004). S. Vancouver Is. subsidence data implies crustal earthquakes of unknown source; both also caused vertical motion at sites in Vancouver region, with possible tsunami evidence for ~3.7 ka event - Mathewes and Clague (1994). DAF: Darrington fault; GS: Georgia Strait; LRF: Leech River fault; LW: Lake Washington; PS: Puget Sound; SJF: San Juan fault; SJI: San Juan Islands.

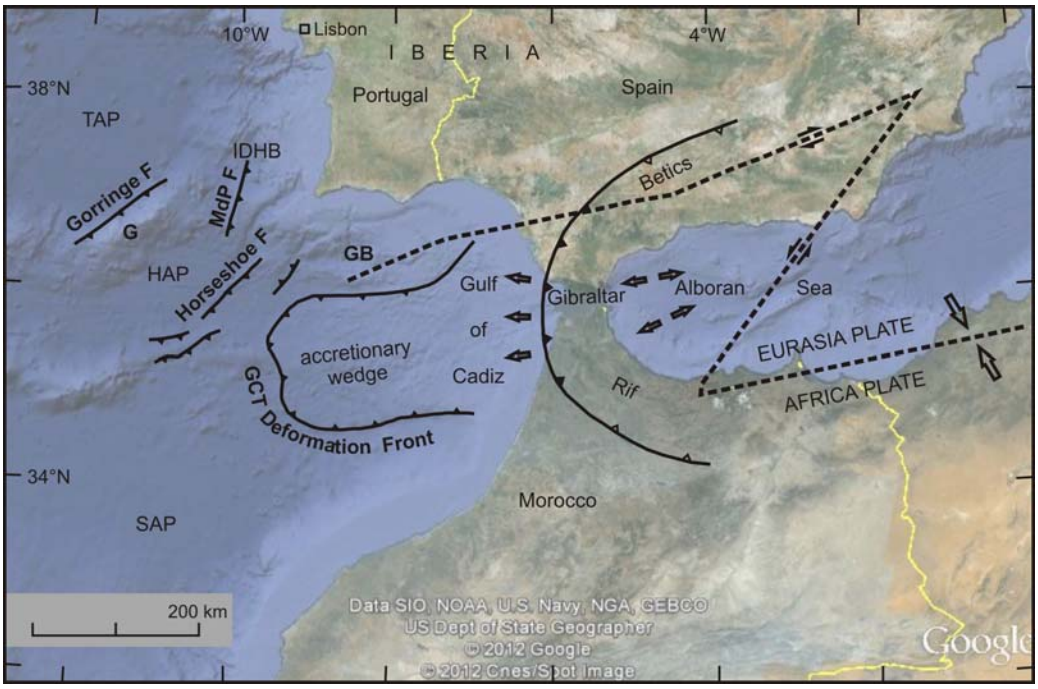

Figure 8. Tectonics of the Lisbon-Gulf of Cadiz region (faults and tectonics from Gutscher et al., 2009a; 2012). Dashed line represents likely position of Africa-Eurasia plate boundary. G: Gorringe Bank; GB: Guadalquivir Bank; GCT: Gibraltar Arc-Gulf of Cadiz Thrust subduction zone proposed by Gutscher et al. (2002). HAP: Horseshoe abyssal plain; IDHB: Infante Don Henrique Basin; MdP: Marques de Pombal; SAP: Seine abyssal plain; TAP: Tagus abyssal plain.

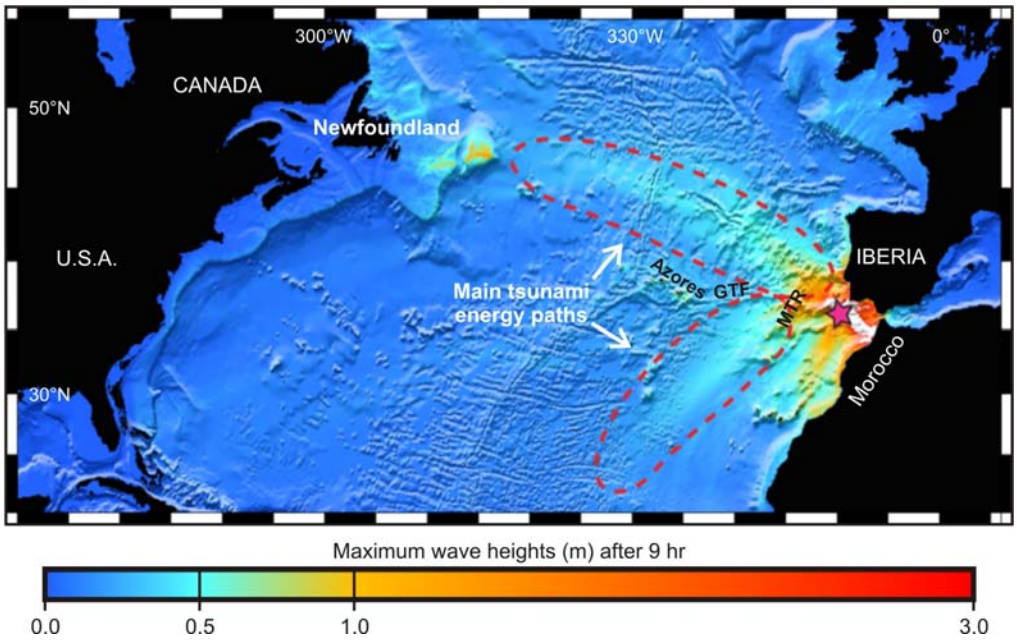

Figure 9. Far-field simulation of the 1755 Lisbon tsunami (after Roger et al., 2010a). Maximum modelled wave amplitudes (above state of tide) after 9 hours of tsunami propagation using the Marques de Pombal-Guadalquivir composite earthquake source of Baptista et al. (2003). GTF: Gloria Transform fault; MTR: Madeira-Tore Rise.

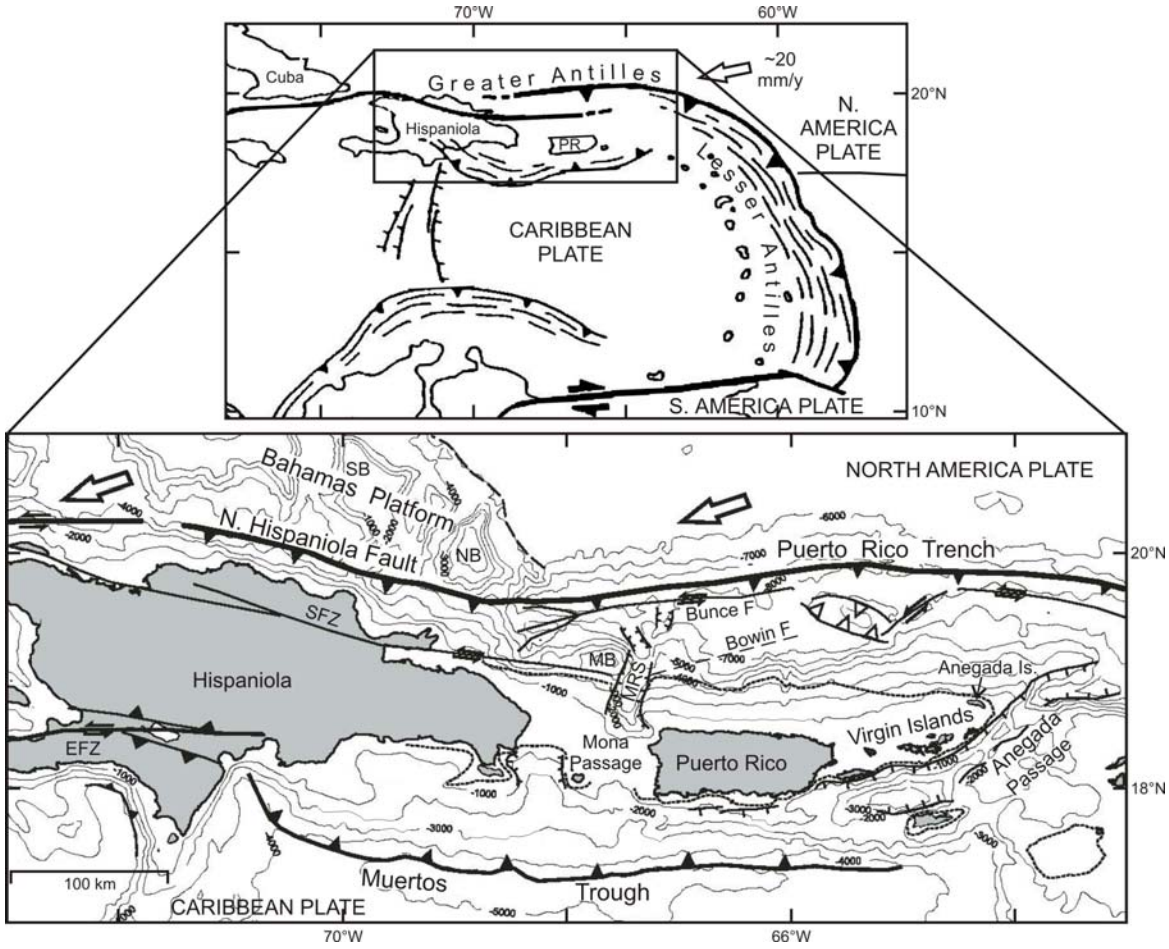

Figure 10. Tectonics of the NE Caribbean (modified from Calais et al., 1992 (upper) and ten Brink et al., 2009b (lower)). EFZ: Enriquillo fault zone; MB: Mona bank; MRS: Mona rift system; NB: Navidad bank; PR: Puerto Rico; SB: Silver bank; SFZ: Septentrional fault zone.

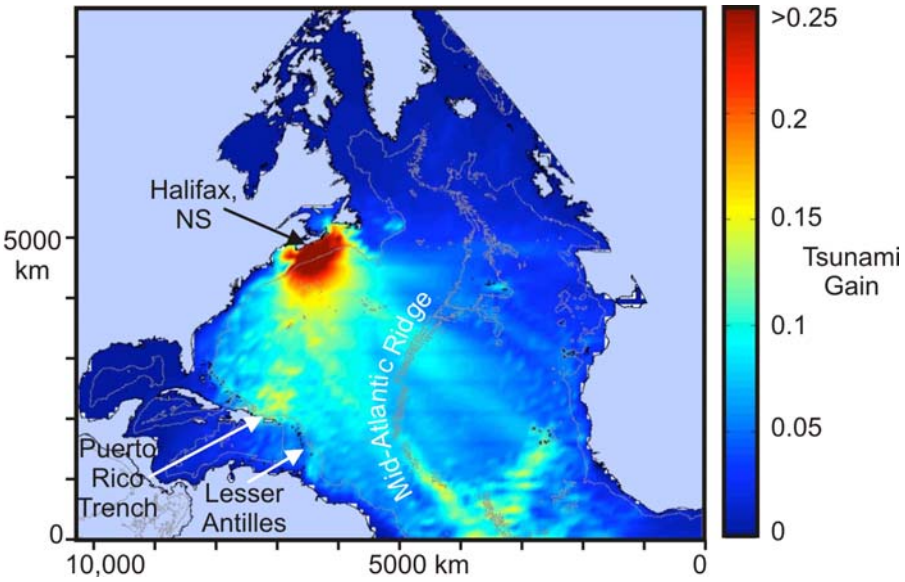

Figure 11. Tsunami gain map for Halifax, Nova Scotia (figure modified from Xu, 2007). Model produced using the All-Source Green's Function developed by Xu (2007). The colours show the wave amplitude expected at Halifax relative to one unit of vertical displacement at Atlantic Ocean sources with dimensions of 100 km x 100 km. For example, a 1000 km^2 source at the Puerto Rico trench with an initial sea surface displacement of 10 m would theoretically result in ~1.5 m wave amplitudes at Halifax. The model involves ocean propagation only; relative wave amplitudes would differ if source and runup effects were also considered.

Figure 12. Map of the southeastern Canadian continental margin. White star shows the 1929 M 7.2 earthquake epicentre; associated white line shows the along-slope failure extent of the Grand Banks landslide (thicker line for the section with the greatest failure volume, e.g., Mosher and Piper, 2007). White line along the coast of the Burin Peninsula (BP) shows the extent of the most severe tsunami damage in 1929. Other abbreviations: AP, Avalon Peninsula; CGFZ, Charlie Gibbs Fracture Zone; MTD, mass-transport deposit.

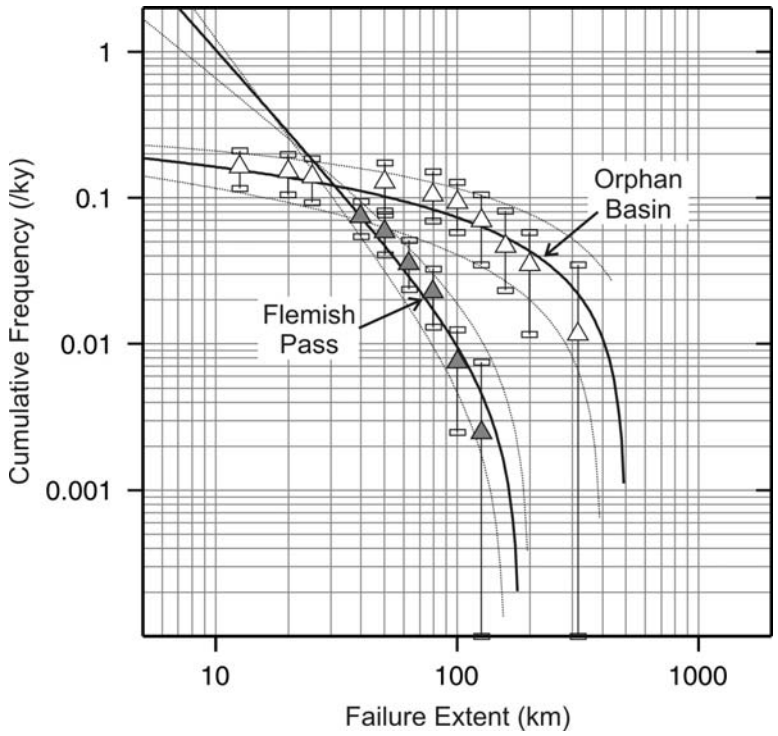

Figure 13. Cumulative frequency distribution of continental slope failures in two regions offshore eastern Newfoundland over the last 400 ky (Flemish Pass) and 85 ky (Orphan Basin). Data for Flemish Pass are from Piper and Campbell (2005) and Huppertz and Piper (2009); the recurrence relation and uncertainties assume maximum failure extent within Flemish Pass of 160-200 km. Data for Orphan Basin are from Piper et al. (2011); maximum failure extent within Orphan Basin is assumed to be 400-600 km.

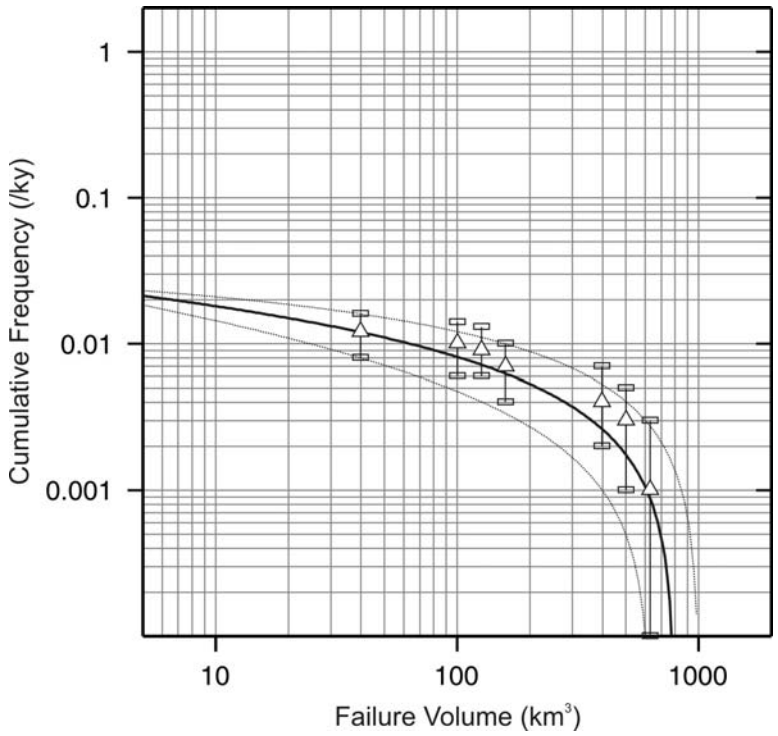

Figure 14. Cumulative frequency distribution of large volcanic flank failures in the western Canary Islands of La Palma, El Hierro, and Tenerife over the last million years (data from Masson et al., 2002); the recurrence relation and uncertainties assume maximum failure size from 650 km^3 (maximum observed) to 1000 km^3.

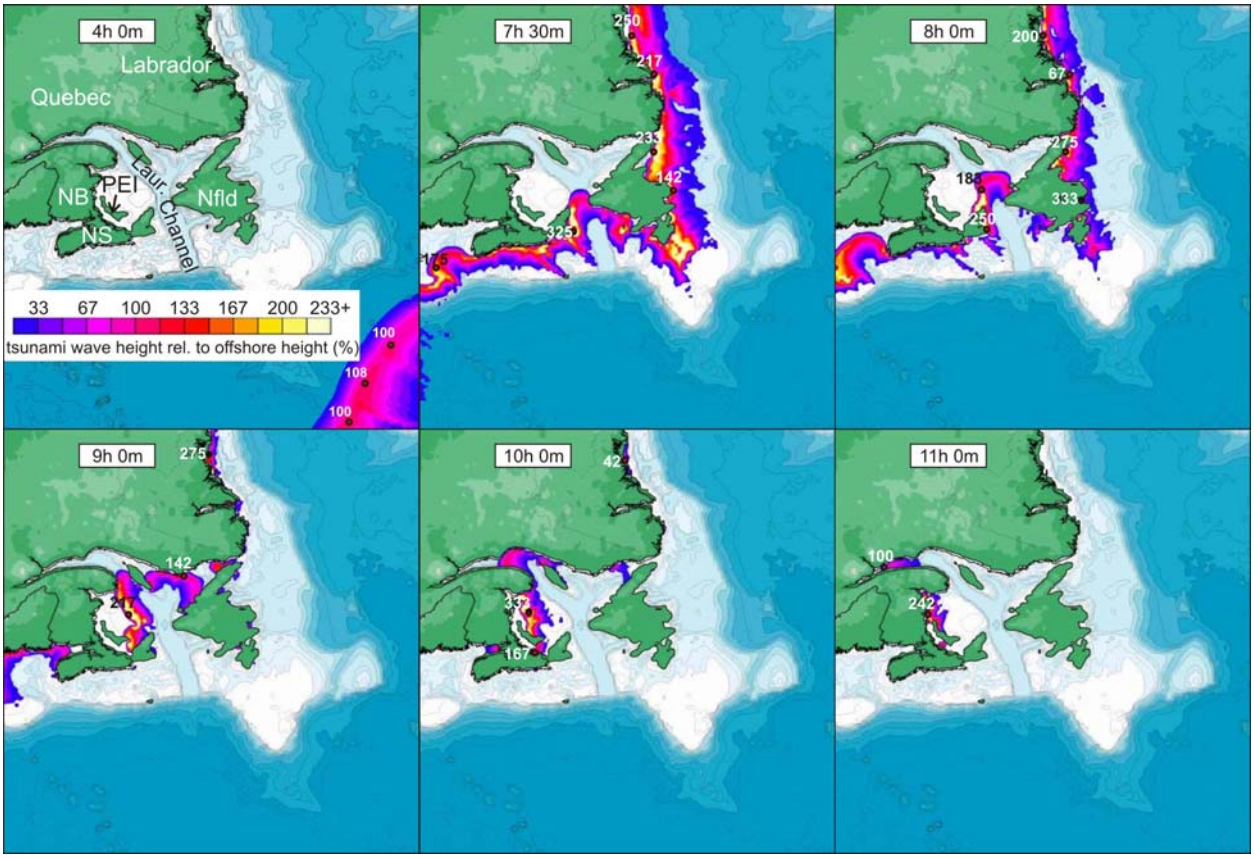

Figure 15. Modelled tsunami wave envelope arriving in eastern Canada at given time intervals after a 500 km^3 tsunamigenic collapse of La Palma volcano, Canary Islands (after Ward and Day, 2005: Quicktime movie links given in their Table 1). Note: numbers have been modified from the original publication to show the coastal/near-coastal wave amplitudes as percentages relative to the wave amplitude offshore. NB: New Brunswick; NS: Nova Scotia; Nfld: Newfoundland; PEI: Prince Edward Island; Laur. Channel: Laurentian Channel.

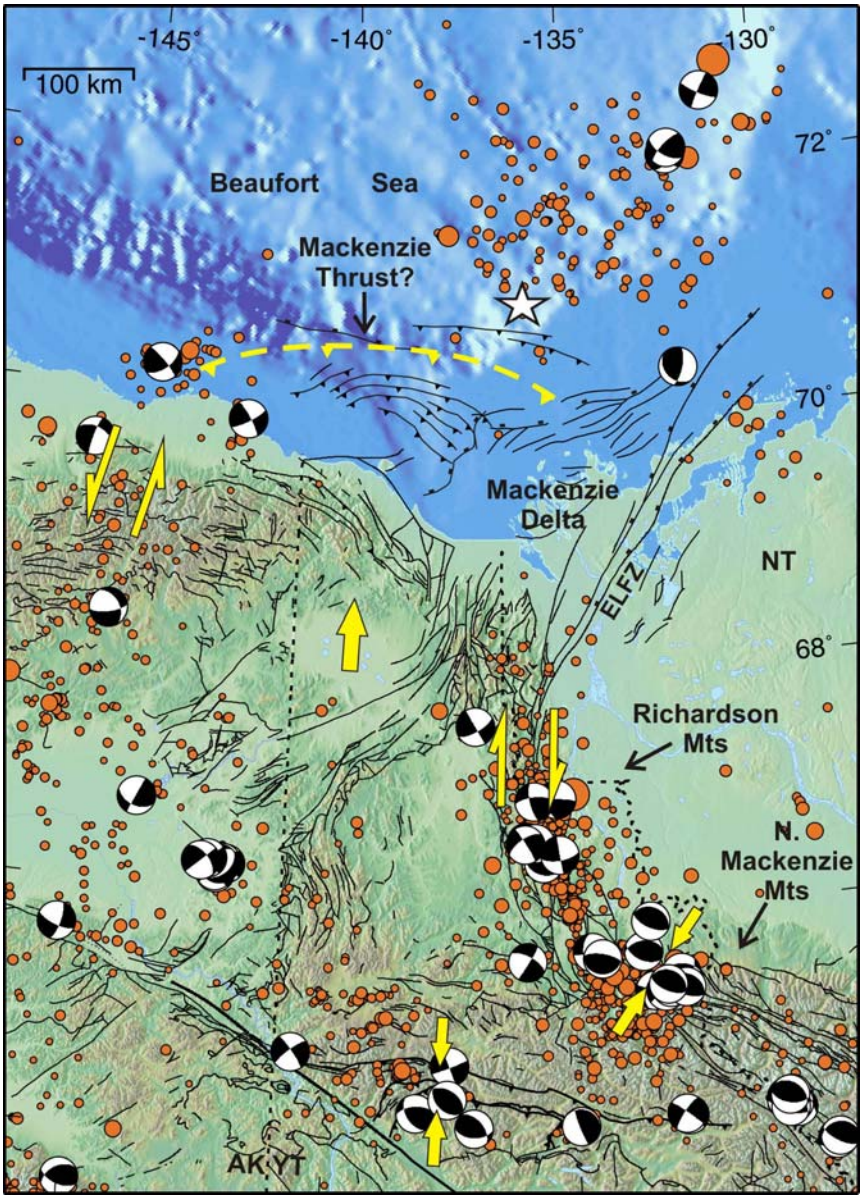

Figure 16. Tectonics of the northern Canada-Alaska Cordillera, and the setting of the potential Mackenzie thrust (dashed yellow line). Mapped faults are shown by black lines, seismicity by orange circles and earthquake mechanisms. Paired yellow arrows indicate styles of current deformation; single thicker arrow indicates northward residual motion. White star shows the location of a large submarine landslide scar (Hill et al., 1982). AK: Alaska; ELFZ: Eskimo Lakes fault zone; NT: Northwest Territories; YT: Yukon Territory.

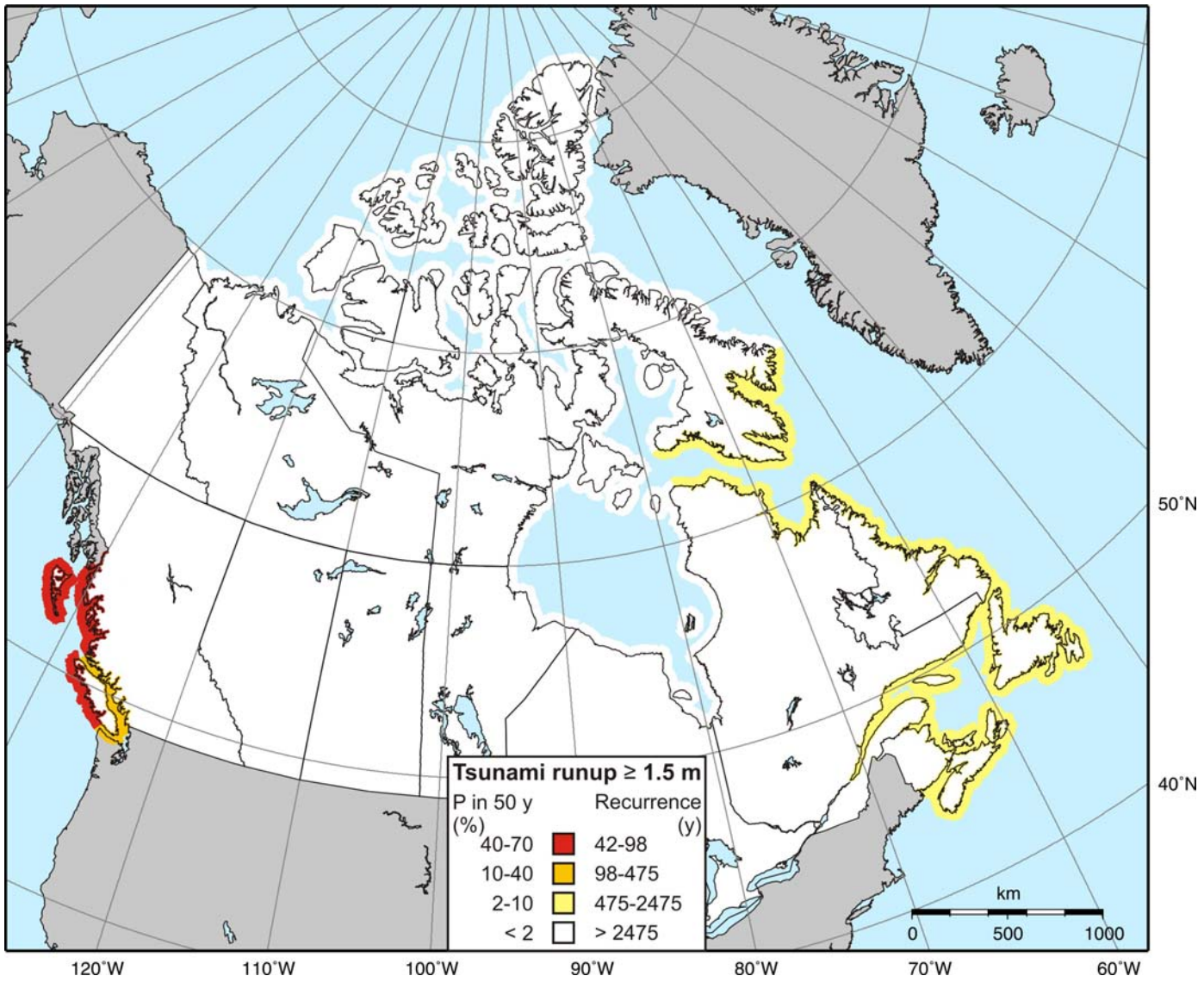

Figure 17. Probabilistic tsunami hazard map for Canada (runup exceeding 1.5 m in 50 y); colours correspond to the probability of exceedance of a potentially damaging (≥ 1.5 m) tsunami runup in a 50-year period (best estimate values from Tables 22-24).

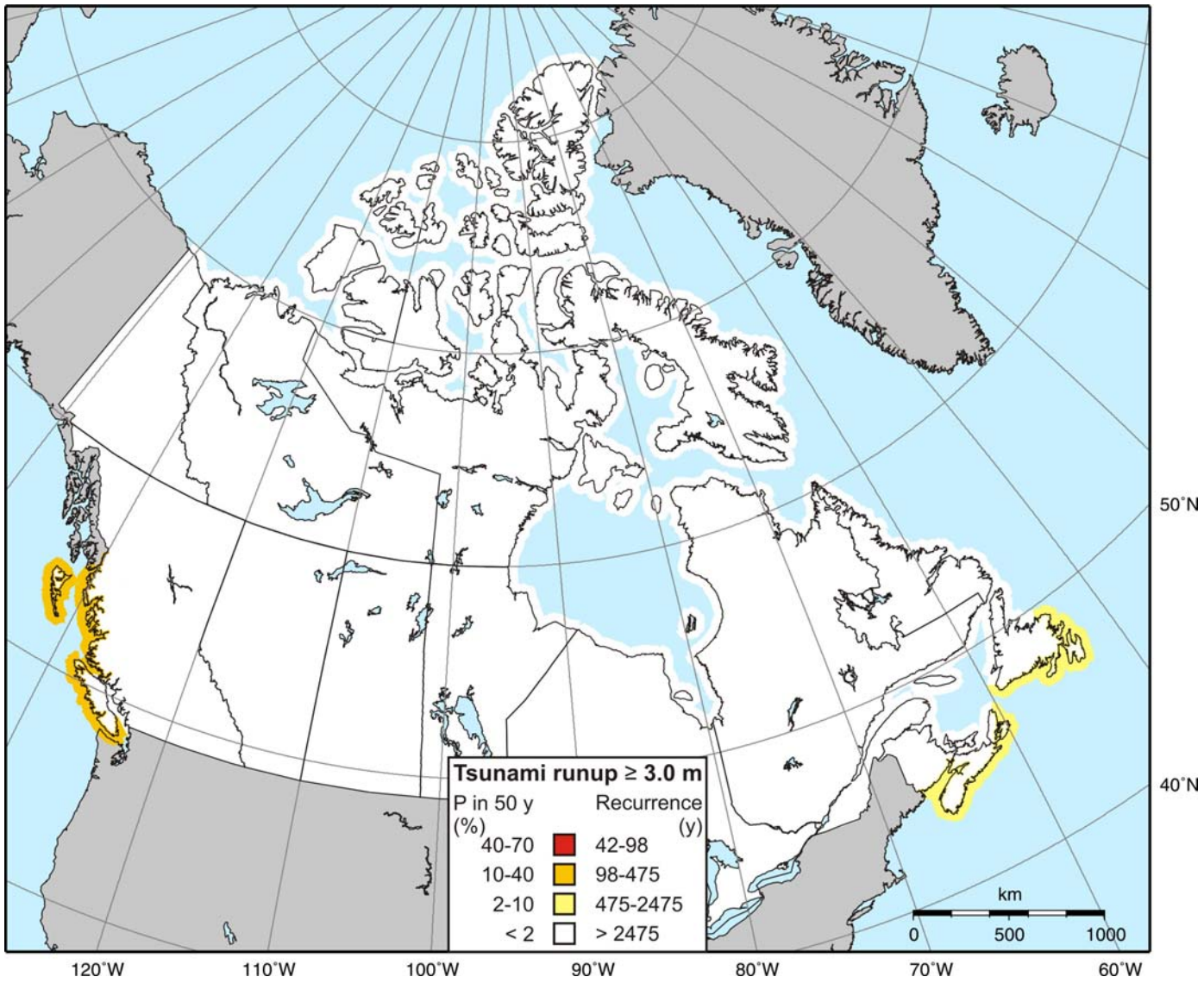

Figure 18. Probabilistic tsunami hazard map for Canada (runup exceeding 3 m in 50 y); colours correspond to the probability of exceedance of a significant (≥ 3 m) tsunami runup in a 50-year period (best estimate values from Tables 22-24).

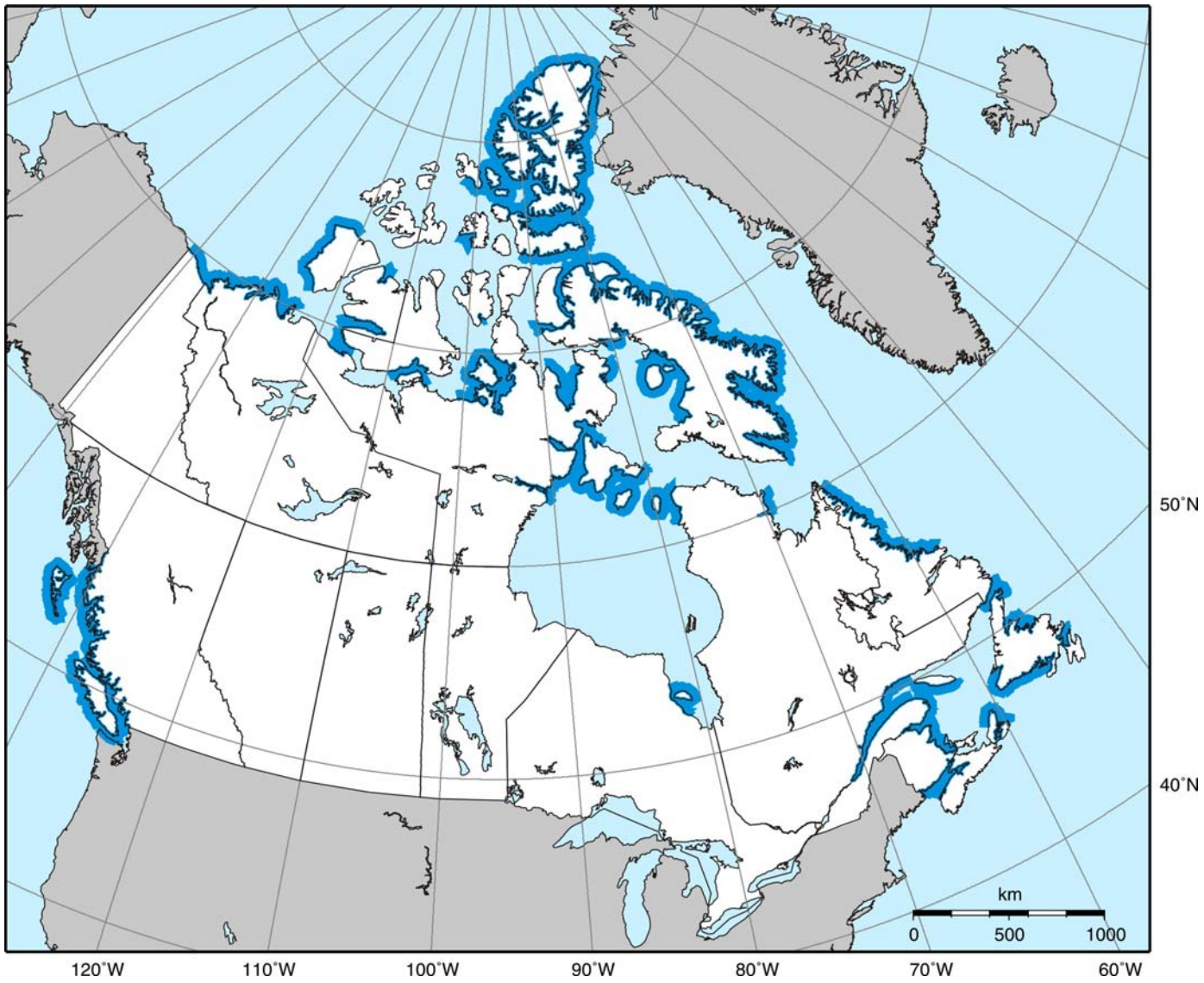

Figure 19. Canadian coastlines (blue) susceptible to local waves triggered by subaerial or submarine landslides or glacial calving. Hazard is based on the landslide susceptibility map of Bobrowsky and Dominguez (2010) and on the presence of glacial fjords.

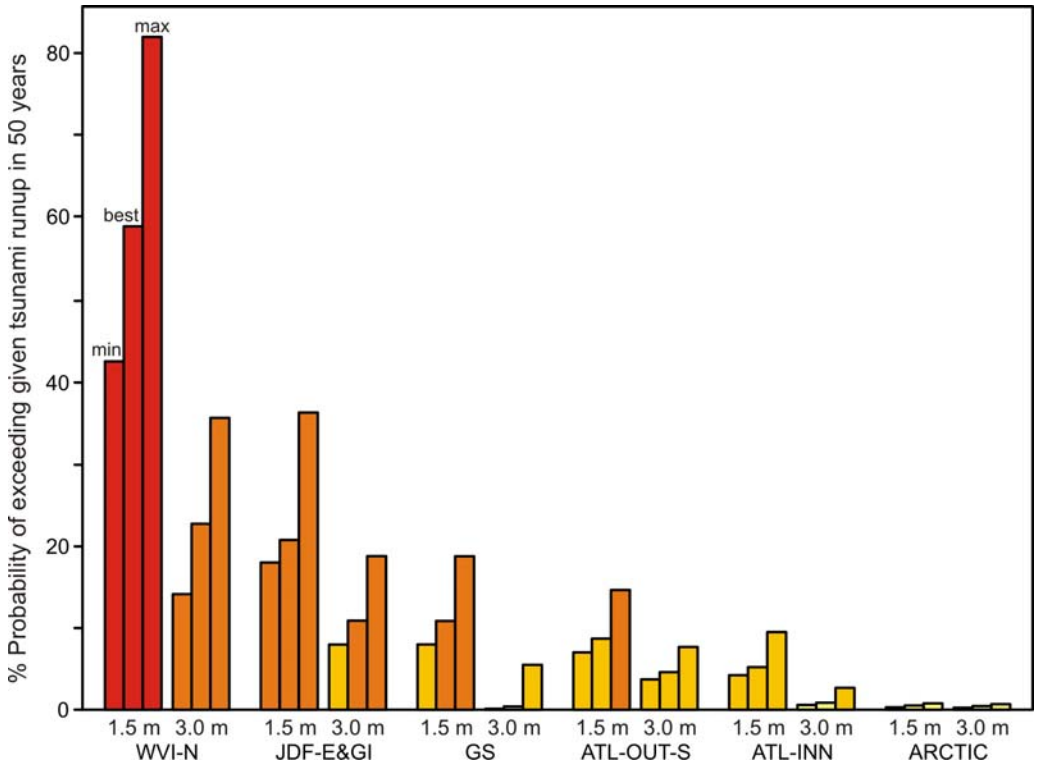

Figure 20. Tsunami hazard comparison between representative regions on the Pacific, Atlantic and Arctic coasts of Canada. Zones defined in Appendix C. Minimum, best, and maximum cumulative probability of exceedance (in 50 y) of tsunami runup of 1.5 m (left) and 3 m (right) is given for each region (from all relevant sources), as in Tables 22-24. Colour scheme represents the relative hazard as in Figures 17 and 18.

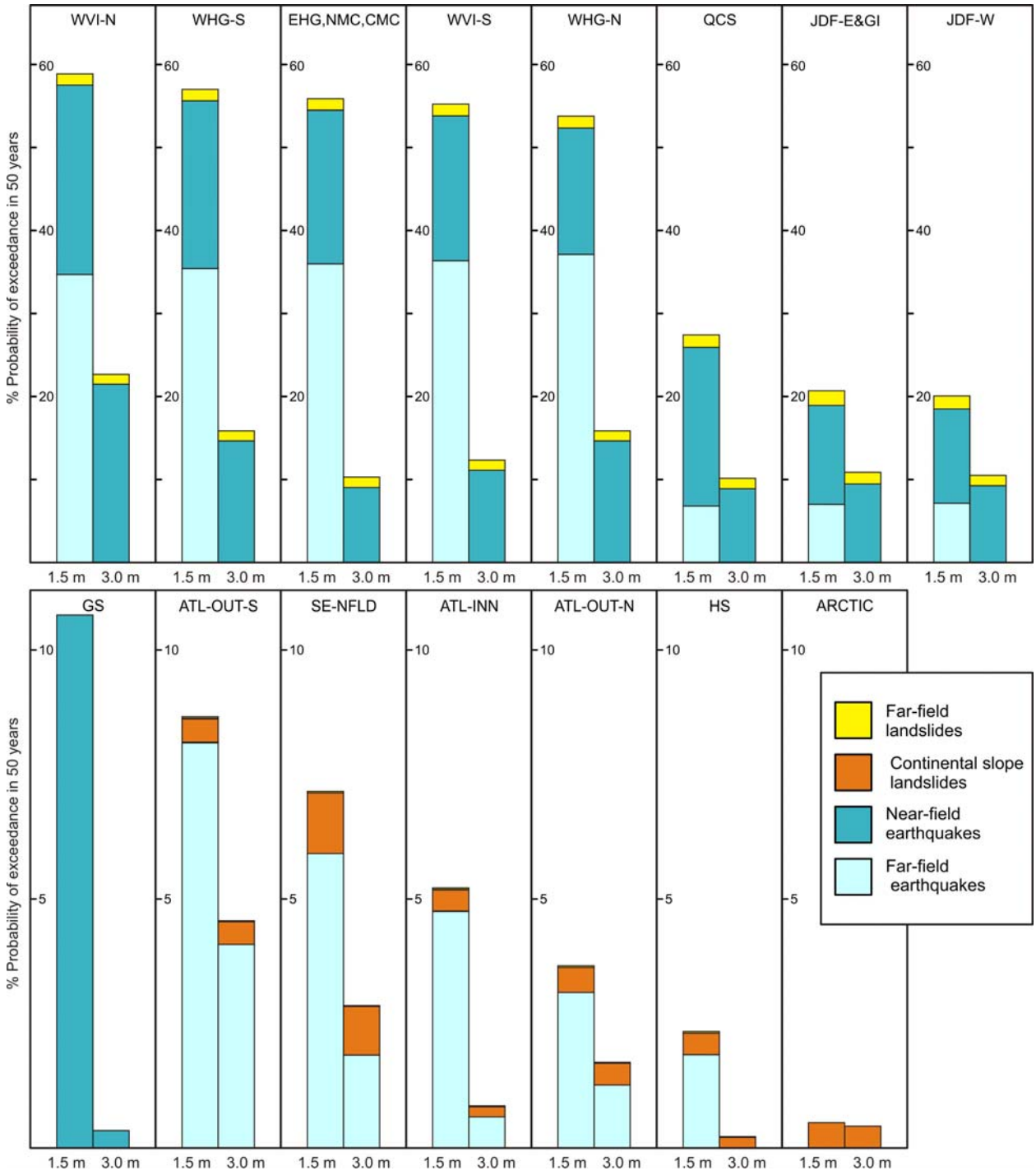

Figure 21. Relative contribution of all considered source types to the cumulative probabilistic tsunami hazard (1.5 and 3 m runup: best estimate) of each hazard zone (zones Appendix B), shown in order of decreasing 1.5 m hazard. Note: different scale for upper versus lower panels. Data details in Tables 22-24; a more complete version of this figure, with individual sources, in Appendix E. Continental slope landslide sources are not included for Pacific zones; compared to most other sources they are expected to contribute a negligible hazard, and triggering is most likely from large near-field megathrust tsunamigenic earthquakes (i.e., not an independent source).

APPENDIX A: GLOSSARY OF RELEVANT TECHNICAL TERMS

This glossary provides definitions of technical terms used in or relevant to the text of this open file report. *Italicized words* in definitions are also defined in the glossary.

Accretionary wedge (= accretionary prism)
A pile of deformed sediments accumulated on the oceanward side of a *subduction zone* by offscraping of sediment from the top of the downgoing plate by the leading edge of the upper plate.

Amplification
Increase in *wave amplitude* during *propagation*. The opposite of *attenuation*.

Aseismic slip
Slip (or creep) on a fault that occurs too slowly to generate an earthquake.

Asperity
An area on a fault plane that is stuck or locked during the *interseismic* period, relative to other areas where the friction is lower and some *aseismic slip* may occur. During an earthquake, *fault slip* on asperities accounts for most of the energy release.

Asteroid impact tsunami
A *tsunami* generated by the impact of an asteroid into the ocean. There are no global historical examples, but an asteroid impact at around 65 Ma that left a major crater on the Yucatán peninsula (Mexico) has also been linked to *tsunami deposits* in the region.

Attenuation
Reduction in *wave amplitude* during *propagation*. The opposite of *amplification*.

Bathymetry
Measurement of the depth of the ocean floor below sea level. Underwater equivalent of *topography*.

Characteristic earthquakes
Large earthquakes that occur periodically on a fault that experiences few or no smaller earthquakes. E.g., Cascadia *megathrust* earthquakes.

Coseismic
Occurring at the time of an earthquake, e.g., coseismic subsidence.

Décollement (= basal detachment fault)
A near-horizontal gliding plane between two rock masses in a *thrust fault* relationship. Detachment of the upper cover from its substratum.

Deformation front
A line defined by the most frontal (oceanward in an ocean-continent subduction zone) compressional (thrust and fold) structure in an *accretionary wedge*. Approximately represents the intersection of the *megathrust* with the seafloor in a *subduction zone*.

Dip-slip fault
A fault across which relative motion is dominantly vertical.

Dispersion
The separation (during *propagation*) of an initial *tsunami* wave into a wave train of smaller-amplitude waves. Important in long-distance *propagation*.

Earthquake tsunami (= seismic sea wave)
A *tsunami* generated by vertical displacement of the ocean floor due to faulting during an earthquake. The largest earthquake tsunamis are generated at *subduction zones*, e.g., 1960 Chile, 1964 Alaska, 2004 Sumatra, 2011 Japan.

Edge waves (= trapped waves)
Tsunami waves that travel along the coastline, "trapped" on the continental shelf due to the superposition of coastally-reflected and incoming waves.

Eocene
The geological time between 55.8 and 33.9 million years ago.

Epicentre
The point on the Earth's surface directly above the *hypocentre* of an earthquake.

Far-field tsunami (= teletsunami)
A *tsunami* generated by a distant *source* that is located generally more than 1000 km or more than 3 hours tsunami *travel time* from the area of interest.

Fault slip
Relative motion across a fault.

Hypocentre
The location below the Earth's surface at which an earthquake occurs.

Geodetic data
Positional data (e.g., *GPS* data) used in earthquake studies to measure relative motions of plates and across faults.

GPS
Satellite-based Global Positioning System. High-precision GPS data are used in earthquake studies to measure relative motions between plates and across faults.

Great earthquake
An earthquake with a magnitude (e.g., *moment magnitude*) greater than or equal to 8.

Historical earthquake
An earthquake documented in the written historical record that was observed by one or more eyewitness(es) or instrument(s).

Historical tsunami
A tsunami documented in the written historical record that was observed by one or more eyewitness(es) or instrument(s).

Holocene
The geological time that started at the end of the last major glaciation about 10,000 years ago and continues to the present day.

Interseismic
Occurring during the time between earthquakes.

Inundation
The inland penetration of a *tsunami*.

Inundation distance
The horizontal distance travelled inland by a *tsunami*, measured perpendicular to the shoreline.

ka
Kiloannum. Abbreviation for thousand years ago, e.g., 10 ka is 10 thousand years ago.

ky
Kiloyears. Abbreviation for thousand years, e.g., 10 ky is 10 thousand years.

Landslide tsunami
A *tsunami* generated by rapid displacement of the water column by either an underwater landslide or a coastal landslide that enters the water. Landslide tsunamis tend to have a shorter *wavelength* than *earthquake tsunamis* and to impact a more localized area.

Left-lateral (= sinistral) fault
A *strike-slip fault* where, when viewed from one side of the fault, the motion of the other side is to the left.

Local tsunami
A *tsunami* from a nearby *source*, with significant waves confined to coastlines within ~100 km or ~1 hour tsunami *travel time*. May also refer to a *tsunami* from a nearby *source* that also has far-reaching impacts.

Ma
Megaannum. Abbreviation for million years ago, e.g., 10 Ma is 10 million years ago.

Mass movement
The downslope movement of material (rock/soil/sediment). Types of mass movement include landslides, slumps, rock falls, debris flows, and creep.

Mass-transport deposits
Sedimentary units that were remobilized after initial deposition, transported downslope and re-deposited. Include deposits from creep, slides, slumps, mass flows, and other slope failures, but not turbidites.

Megathrust
The plate-boundary *thrust fault* in a *subduction zone*. E.g., the Cascadia megathrust.

Meteorological tsunami (= meteotsunami)
Atmosphere-induced *tsunami*-like destructive ocean waves. May be triggered by a variety of air pressure disturbances including atmospheric gravity waves, pressure jumps, frontal passages, hurricanes and squalls.

Miocene
The geological time between 23 and 5.3 million years ago.

Moment magnitude (M_w)
A measure of the relative size of an earthquake based on the *seismic moment*. The moment magnitude scale is the preferred magnitude scale, and the most accurate for large earthquakes.

Near-field tsunami
A *tsunami* that is generated from a *source* located close to the area of interest (typically less than 30 minutes tsunami *travel time*).

Normal fault
An extensional *dip-slip fault* where the overlying side of the fault (hanging wall) moves downwards relative to the underlying block (footwall).

Oligocene
The geological time between 33.9 and 23 million years ago.

Paleocene
The geological time between 65.5 and 55.8 million years ago.

Paleoearthquake
An earthquake that occurred prior to the historical time period, or for which there is no written documentation. Paleoearthquakes are identified using *paleoseismic data*.

Paleoseismic data
Geological evidence for prehistoric earthquakes (*paleoearthquakes*). May include evidence for sudden displacements across a fault and/or earthquake shaking (liquefaction, landslides, *turbidites*).

Paleotsunami
A *tsunami* that occurred prior to the historical time period, or for which there is no written documentation. Paleotsunamis are primarily identified on the basis of coastal *tsunami deposits*.

Peak-to-trough wave amplitude (= double amplitude)
The vertical distance between an adjacent wave crest and trough, corrected for tidal changes over the time between the two. Often referred to as wave height in the tsunami literature, whereas in the tsunami hazard literature wave height generally refers to the zero-to-peak *wave amplitude*. See Figure A1.

Period (= wave period)
The amount of time between the passage of two successive wave crests in a wave train. Tsunamis typically have a wave period ranging from 5 minutes to 2 hours. See Figure A1.

Pleistocene
The geological time between 2.6 million years ago to 10,000 years ago.

Pliocene
The geological time between 5.3 and 2.6 million years ago.

Postseismic
Occurring in the time period following an earthquake. Postseismic deformation typically occurs within a few years to decades after a large earthquake.

Propagation
The travel stage of a *tsunami* (between *tsunami generation* and coastal *inundation*). *Tsunami speed* is proportional to the water depth. The main *propagation* direction depends on the orientation of the *source*, e.g., a north-south linear earthquake source will propagate energy mainly to the west and east. *Tsunami* waves are also affected by wave *reflection* and *refraction* during *propagation* due to interactions with ocean floor and coastline features (*bathymetry* and *topography*).

Quaternary
The geological time period from 2.6 million years ago to the present.

Radial spreading
A phenomenon by which *wave amplitude* is reduced as a *tsunami* wave propagates away from its *source* due to the distribution of energy over an increasingly large area. *Tsunamis* from long linear sources such as *subduction zones* are less affected by radial spreading than are point sources such as landslides. The sphericity of the Earth also leads to spreading and reductions in

wave energy up to a distance of 90° from the *source*; beyond this, wave energy will increase again.

Recurrence interval
The amount of time between events (e.g., earthquakes, *tsunamis*) on a specific fault or in a specific region.

Reflection
A change in direction experienced by a wave as it rebounds from a barrier.

Refraction
A change in direction experienced by a wave as it enters shallower water, due to slowing of those parts of the wave that enter shallower water first; the *propagation* direction bends to a direction more parallel to the seafloor contours.

Regional tsunami
A *tsunami* that affects a particular geographic region, generally within 1000 km or 1-3 hours tsunami *travel time* from its *source*.

Resonance amplification
Increase in tsunami *wave amplitudes* due to the extended reflection and interference of *tsunami* waves within a harbour, narrow bay or inlet. Occurs when the tsunami *period* matches the natural resonant *period* of the harbour/bay/inlet (which depends on their dimensions). E.g., in a harbour with a natural resonant *period* of 30 minutes, resonance *amplification* will occur for tsunamis with 15, 30 and 60-minute *periods*).

Reverse fault
A compressional *dip-slip fault* where the overlying side of the fault (hanging wall) moves upwards relative to the underlying block (footwall)

Right-lateral (= dextral) fault
A *strike-slip fault* where, when viewed from one side of the fault, the motion of the other side is to the right. E.g., Queen Charlotte fault.

Runup (= runup height)
Elevation reached by a *tsunami* at maximum *inundation*, measured relative to a datum such as mean sea level or the sea level at the time of the *tsunami* (state of tide).

Rupture zone
Area of a fault that undergoes *fault slip* during an earthquake.

Seiche
A wave that oscillates on the surface of an enclosed or partially enclosed body of water. It may be initiated by long-*period* seismic waves (an earthquake), winds, tides, or a *tsunami*.

Seismic data
Subsurface data obtained by analysis of the recording of seismic waves that pass through the Earth. Seismic waves travel at different speeds depending on the density of the material they travel through, and reflect or refract when they reach a density contrast, thus revealing the structure of the subsurface – layers, faults, mass-transport deposits etc. Source of seismic waves may be passive (earthquakes, background noise) or controlled (explosives/air gun/vibrations).

Seismic moment (M_o)
A measure of the size of an earthquake that represents the energy released. It is the product of (1) the area that ruptured in the earthquake (*rupture zone*), (2) the average amount of *fault slip*, and (3) the rigidity (*shear modulus*) of the rocks on either side of the fault. (See also Equation 8 in the text).

Seismicity
The distribution of earthquakes in space, time, and magnitude.

Seismogenic zone
The part of a fault on which earthquakes may be generated. Typically occurs at depths below the surface where the temperature ranges from ~150 to 350 °C.

Shear modulus (= rigidity) (μ)
The ratio of shear stress to shear strain. The greater the shear modulus of a material, the greater the stress needed to produce the same amount of deformation.

Slab rollback
A process involving subduction of old (cold and dense) oceanic crust, whereby gravity acts to steepen the subducted slab, causing it to "roll back" through the mantle. The overlying plate may also be pulled with the slab, leading to extension.

Source (= tsunami source)
Location of *tsunami* origin; site of earthquake/landslide/volcanic eruption/asteroid impact that causes sudden displacement of the water to generate a *tsunami*.

Splay fault
A minor fault that branches at an acute angle off a major fault, with the same sense of slip.

Strike-slip fault
A fault across which the relative motion is primarily horizontal. E.g., Queen Charlotte fault.

Subduction zone
A convergent plate boundary where one plate moves underneath another along a *megathrust* fault. E.g., the Cascadia subduction zone.

Thrust fault
A *reverse fault* with a low angle of dip (< 45°).

Tide gauge
An instrument that measures the height (rise and fall) of sea level over time. *Tsunami* waves detected by tide gauges may be quantified relative to the predicted state of tide.

Topography
Measurement of the elevation of land above sea level.

Transpression
Deformation that contains components of both compression and strike-slip, e.g., relative motion on an oblique *reverse fault*.

Transtension
Deformation that contains components of both extension and strike-slip, e.g., relative motion on an oblique *normal fault*.

Travel time
The time taken for the first *tsunami* wave to propagate from its *source* to the point of interest.

Trench
Long linear depression of the seafloor, marking where an oceanic plate begins to descend beneath the overriding plate at a *subduction zone*.

Triple junction
The point where three plate boundaries meet. E.g., the Queen Charlotte triple junction occurs at the intersection of the Pacific-North America, Explorer-North America, and Pacific-Explorer plate boundaries.

Tsunami
A series of long-*wavelength*, long-*period* travelling water waves generated by displacement of a large volume of water. May be generated by earthquakes, landslides, volcanic eruptions, asteroid impacts or meteorological phenomena. A tsunami extends through the whole water column, accounting for the great amount of energy propagated. Tsunamis are not related to the tides; the term tidal wave is a misnomer.

Tsunami deposit (= tsunamiite)
Sediment (usually sandy) deposited by a *tsunami* in coastal areas. A sand sheet deposited by a *tsunami* may consist of several layers representing successive waves, and it will thin and fine inland. Tsunami deposits in the coastal sedimentary record provide evidence of *historical tsunamis* and *paleotsunamis*.

Tsunami generation (= tsunami generation)
Mechanism by which a *tsunami* is initiated, by displacement of a large volume of water. Tsunami *sources* may include earthquakes, landslides, volcanic eruptions and asteroid impacts. The potential energy imparted into the water column results in tsunami generation, i.e. energy in the form of long-*period* waves radiating away from the *source*.

Tsunamigenic
Capable of generating a *tsunami*, e.g., tsunamigenic fault.

Tsunami hazard
The probability that a *tsunami* of given size will impact a coastal point of interest within a given time period.

Tsunami hazard assessment
An analysis to estimate the probability of a damaging *tsunami* occurring at coastal areas of interest. *Tsunami hazard* assessment requires knowledge of probable tsunami *sources* (including earthquakes and landslides), their likelihood of occurrence, and their expected tsunami *runup*/*inundation* at the site of interest.

Tsunami risk
Tsunami hazard multiplied by the exposure of a coastal point of interest. The probability that a *tsunami* of given size will impact a site within a given time period, multiplied by the expected tsunami damage and number of potential victims.

Tsunami simulation
Numerical modelling of *tsunami generation*, *propagation* and *inundation*.

Tsunami speed
The velocity of a *tsunami* is proportional to the depth of the water through which it propagates. It can be approximated as the square root of the product of water depth and gravity. In the deep open ocean, tsunamis have low *wave amplitudes* (< 1 m) and travel at speeds of 500-1000 km/hr. When the *tsunami* reaches shallow water near a coastline, velocities drop to tens of km/hr and *wave amplitudes* increase (sometimes up to tens of metres).

Turbidite
A sedimentary deposit resulting from a *turbidity current* in an ocean or lake. Turbidites may be used to infer the occurrence of earthquake shaking, in concert with other *paleoseismic data*, although *turbidity currents* may be triggered by other phenomena such as storms.

Turbidity current
An underwater avalanche. A turbulent subaqueous density-driven flow of suspended sediment, triggered by sediment loading or disturbances such as storms or earthquake shaking.

Wadati-Benioff zone
A dipping planar zone of earthquakes in a *subduction zone* that may extend as deep as 700 km.

Wave amplitude (= zero-to-peak amplitude = wave height above the state of tide)
The vertical distance between a wave crest (or trough) and the undisturbed sea level at the time. Alternatively, half the vertical distance between an adjacent wave crest and trough, corrected for tidal changes over the time between the two. Often referred to as wave height in the tsunami hazard literature (including this open file). See Figure A1.

Wave height
May refer to either the *wave amplitude* (zero-to-peak; as in tsunami hazard literature) or the *peak-to-trough wave amplitude* (as in the general tsunami literature). For the purposes of this open file report, wave height is equivalent to the zero-to-peak amplitude, unless otherwise specified.

Wavelength
The horizontal distance between two successive wave crests (or troughs), measured in the direction of wave *propagation*. Wavelengths of *earthquake tsunamis* range from 20 to 300 km, whereas those of *landslide tsunamis* are typically in the range of a few hundred metres to tens of kilometres. See Figure A1.

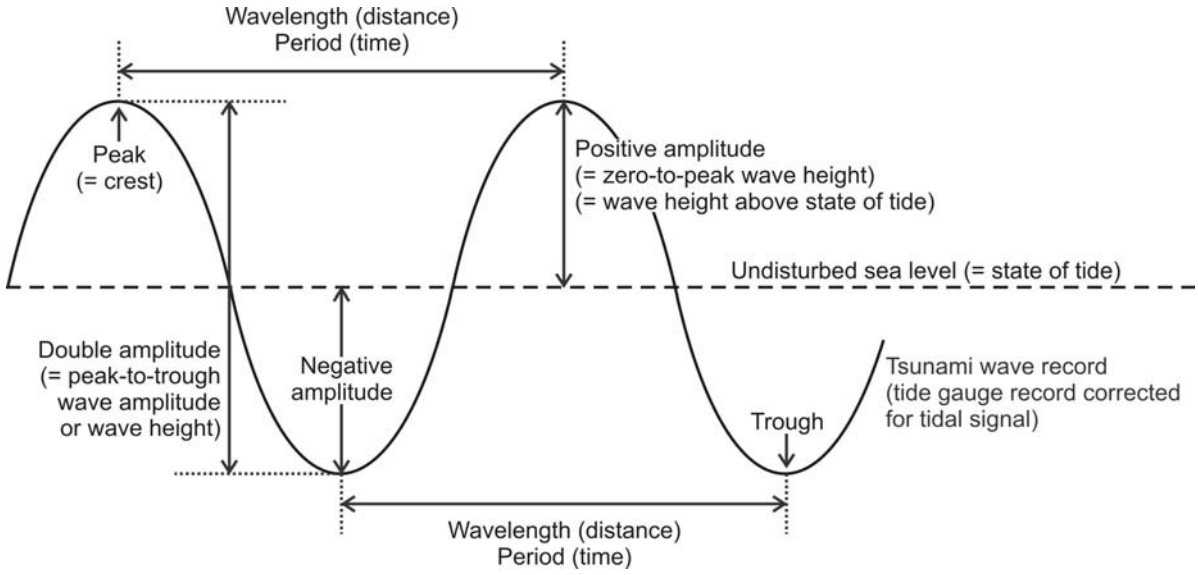

Figure A1. Labelled diagram of a wave.

APPENDIX B: DEFINITION OF FAULT PARAMETERS FOR EARTHQUAKE MAGNITUDE ESTIMATION

Fault rupture area

The fault rupture area is approximated from the fault length multiplied by the downdip seismogenic width, which is thought to be controlled by temperature, with full coseismic rupture occurring between ~150 and 350 °C, rupture decreasing downdip through a transition zone to zero at ~450 °C (Hyndman and Wang, 1995). For example, a full-rupture area of ~99,000 km^2 for the Cascadia subduction fault results from multiplying the fault length (~1100 km) by the average width (60 km average seismogenic zone width plus half the 60 km average transition zone width, assuming a linear downdip decrease in coseismic slip through the transition zone, e.g., Satake et al., 2003; Wang et al., 2003). The coseismic transition zone described here is approximately half the width of the interseismic time-dependent effective transition zone defined by Wang et al. (2003).

We note that in some cases the rupture areas in the database of Strasser et al. (2010) used to calibrate their area-magnitude relation (Equation 6) may be larger than the coseismic rupture area defined here and used in Equation 8; where defined by aftershock distribution, the rupture area may include the full area of the coseismic transition zone and/or other areas adjacent to the coseismic rupture. For the Cascadia subduction zone, the full-rupture area of 99,000 km^2 provides an estimated maximum magnitude of M_w 8.7 (8.4-9.0), whereas a larger rupture area of 132,000 km^2 (including the full area of the transition zone) suggests a maximum M_w of 8.8 (8.5-9.1) (Equation 6). Thus, it is possible that our use of the full-rupture area in Step 1 may slightly underestimate maximum magnitude; however, for fault areas smaller than the Cascadia megathrust, the effect is likely negligible.

Slip rate

The long-term fault slip or convergence rate is generally estimated from geodetic and/or geologic plate motion data. At Cascadia, convergence across the subduction zone varies along the margin according to the plate rotation vector and changes in strike; the average convergence rate is ~36 mm/y (e.g., Wang et al., 2003).

Shear modulus

Estimation of the shear modulus (μ; the ratio of shear stress to shear strain; rigidity) is critical to the calculation of slip magnitude occurring during an earthquake (Equation 8), and therefore also the estimated recurrence of potentially tsunamigenic events (Equation 9). Overestimating the shear modulus will lead to an underestimation of the slip and of the event recurrence interval, and thus an overestimation of the event probability; conversely, underestimation of μ will lead to an underestimation of the probability. However, the shear modulus of fault zones is generally poorly constrained.

For subduction megathrust studies, the shear modulus is often assumed to be ~3-4 x 10^{10} N/m^2 (e.g., McCaffrey et al., 2000; Satake et al., 2003; Liu and Rice, 2007; Becker and Meier,

2010), based on an average value for sedimentary rocks (0.4-5 x 10^{10} N/m^2; Turcotte and Schubert, 2002) or the Preliminary Reference Earth Model (PREM: 4.4 x 10^{10} N/m^2 at ~20 km depth; Dziewonzki and Anderson, 1981).

For the Cascadia subduction zone, using M_w = 8.8, A = 99,000 km^2, and μ = 3 x 10^{10} N/m^2 in Step 3 (Equation 8) provides a coseismic slip estimate of 6 m (4 m at μ = 4 x 10^{10} N/m^2), leading to an average recurrence interval (Step 4) of 166 years (125 years for the larger shear modulus). These values are significantly lower than the slip in the 1700 CE Cascadia megathrust earthquake estimated from paleotsunami data (best-fit 19 m slip approximated from modelling of far-field tsunami heights; Satake et al., 2003) and the average Holocene recurrence interval constrained by paleoseismic data (~530 ± 260 years; Goldfinger et al., 2012). One way to resolve this inconsistency is by using a lower value of shear modulus; it follows that a lower value should also be used in Step 3 of our calculations on potentially tsunamigenic thrust faults in similar shallow subduction environments.

We calculate an "effective" shear modulus based on the Cascadia example. Constraining the recurrence interval to 530 years provides a slip estimate of 19 m (at 36 mm/y); with the rupture area and moment magnitude as defined above, we calculate an effective shear modulus of ~1 x 10^{10} N/m^2. This lower value of rigidity is consistent with more recent studies of shallow subduction zones; Bilek and Lay (1999) find a stronger depth dependence of the shear modulus in subduction zones than the PREM model (which represents the interplate environment). Lower rigidity at shallower depths may reflect the greater prevalence of water-saturated sedimentary rocks (e.g., Geist and Bilek, 2001). The upper 20 km is typically characterized by a shear modulus less than 3 x 10^{10} N/m^2, with 1 x 10^{10} N/m^2 an average value at ~10-15 km depth (Bilek and Lay, 1999); the Cascadia locked zone, where the majority of coseismic slip is expected to occur, lies within the upper 10-15 km.

APPENDIX C: HAZARD ZONES

Tsunami hazard zones considered are shown in Figure C1 and defined in the sections below. The locations of zone boundaries are also discussed. Zone boundaries do not necessarily reflect a sharp contrast in hazard. Within each zone, hazard from each source is likely to vary considerably (depending on factors that include bathymetry, coastline shape, wave directivity, and resonance amplification), but without detailed modelling such variations cannot be estimated. In particular, some inlets, bays, and harbours may have amplitude maxima significantly higher than the zone average, and that may exceed our estimates of the zone maxima, e.g., tsunami amplitudes at Port Alberni are significantly higher for certain events than at Tofino due to resonance amplification (both in zone WVI-S, defined below; Fine et al., 2009). The zones are chosen such that within each zone similar runup is expected from each source, i.e. values exceeding 1.5 m and 3 m are likely to occur within the zone (at given probabilities), but these values may not occur over the entire zone.

Pacific

The large number of zones considered for the Pacific coastline (10) reflects the greater number and diversity of sources than the Atlantic and Arctic coastlines, particularly those that are local/regional. The final hazard maps appear to show a smaller number of zones, because many of the zones have similar cumulative levels of hazard. WHG-N: northern west coast of Haida Gwaii; WHG-S: southern west coast of Haida Gwaii. The boundary between WHG-N and WHG-S is chosen arbitrarily as the midpoint of the straight-line length of the west coast of the islands. NMC&EHG-N: northernmost mainland coast and north and northeastern coasts of Haida Gwaii; CMC&EHG-S: central mainland coast and southeastern coast of Haida Gwaii. The boundary between NMC&EHG-N and CMC&EHG-S lines up with the boundary between WHG-N and WHG-S in a margin-perpendicular direction, to reflect approximately equal tsunami travel distance from regional sources to the south. WVI-N: northern west coast of Vancouver Island; WVI-S southern west coast of Vancouver Island. The boundary between WVI-N and WVI-S is chosen arbitrarily as the midpoint of the straight-line distance between NW Vancouver Island and the western edge of Juan de Fuca Strait. JDF-W: western Juan de Fuca Strait; JDF-E&GI: eastern Juan de Fuca Strait, Haro Strait and the Gulf Islands. The boundary between JDF-W and JDF-E&GI is arbitrarily chosen as the midpoint of the length of Juan de Fuca Strait from the Pacific open ocean opening to Victoria, BC. GS: Georgia Strait and Discovery Passage, Johnstone Strait and adjoining inlets. QCS: Queen Charlotte Strait (boundaries are the geographically-defined borders of the Strait from the western entrance of Johnstone Strait in the south to Cape Sutil and Cape Caution in the north).

WHG-N and WHG-S are equally affected by all sources except the Explorer subduction fault, which presents a greater hazard to WHG-S. NMC&EHG-N is assigned the same hazard as WHG-N and WHG-S for all far-field sources and for Cascadia subduction zone sources; relative to WHG-N, it has lower hazard from the Queen Charlotte subduction fault, but the same level of hazard from the Explorer subduction fault. CMC&EHG-S is assigned the same hazard as NMC&EHG-N, except that hazard from the Explorer fault is higher (the same as WHG-S). WVI-N and WVI-S are assumed to have equal hazard from far-field sources and from full ruptures of the Cascadia subduction zone. Relative to the south (WVI-S), the north coast (WVI-N) has greater hazard from Explorer and Queen Charlotte sources and lower hazard from

southern ruptures of the CSZ. JDF-W and JDF-E&GI are assumed to have equal hazard from all sources, except that JDF-E&GI is assumed to have greater hazard from local crustal fault sources. Compared with WVI-S, both JDF-W and JDF-E&GI have similar hazard (at 1.5 and 3 m level) from full ruptures of the Cascadia subduction zone and from far-field landslide tsunami sources, lower hazard from southern Cascadia subduction zone ruptures and from far-field subduction zone sources; the Juan de Fuca Strait is assumed to be not at risk from Queen Charlotte and Explorer sources. Haro Strait and the Gulf Islands are included in JDF-E&GI; these areas are assumed to have hazard that is more similar to eastern Juan de Fuca Strait than to Georgia Strait, which is more sheltered. GS is assumed to be sheltered from all far-field sources and all other sources, except for Cascadia subduction zone ruptures, local crustal fault sources and local landslide-generated waves. QCS is assumed to have the same hazard from most sources as zone CMC&EHG-S, the central mainland coast. Exceptions are lower hazard from far-field subduction zone sources, and no known hazard from crustal fault sources. CMC&EHG-S is assumed to have a similar far-field subduction zone hazard to the west coast of Vancouver Island (i.e., Tofino tide gauge data), whereas QCS is assumed to be similar to JDF-E&GI (i.e., Victoria tide gauge), based on similar tsunami heights at Port Hardy (e.g., Stephenson and Rabinovich, 2009).

Atlantic

The Atlantic margin is divided into six zones, defined below. However, in the final hazard maps, five of them fall into the same hazard categories for runup exceeding 1.5 m (2-10% probability in 50 years). ATL-OUT-S: the outer coasts of southern Newfoundland, Nova Scotia, and New Brunswick (including the Bay of Fundy); SE-NFLD: southeastern Newfoundland; ATL-INN: the southeastern coast of Quebec, the coast of Prince Edward Island, and the inner coasts of New Brunswick, Nova Scotia and Newfoundland; ATL-OUT-N: the outer coast of northeastern Newfoundland and Labrador, and the southeastern coast of Baffin Island south of the Arctic circle; HS: Hudson Strait; HB: Hudson Bay.

SE-NFLD is considered separately from ATL-OUT-S; due to the shape of the continental shelf edge, southeastern Newfoundland is likely exposed to continental slope landslide tsunamis from three source areas (Orphan Basin, Flemish Pass, and the Salar Basin; Fig. 12), whereas other parts of the outer Atlantic coast are exposed only to one landslide source area offshore. However, in regard to most other tsunami sources, SE-NFLD and ATL-OUT-S are considered to have equal hazard. ATL-INN and HS are expected to be relatively sheltered from most sources compared to the outer coasts, and therefore have lower hazard. ATL-OUT-N is a northeast-facing coastline, and is expected to be relatively sheltered from subduction zone sources located to the south (Puerto Rico and Lesser Antilles), but to have equal hazard from local and other far-field sources to ATL-OUT-S. HB is assumed to be sheltered from potentially damaging tsunami waves from all sources considered, except for local landslide-generated waves.

Arctic

The zone ARCTIC comprises all coastlines north of the Arctic circle (66° 33’ N), as well as those parts of Foxe Basin (Fig. 1) that lie south of this latitude. The potential Mackenzie thrust fault source considered would only pose a hazard to the westernmost Canadian Arctic coasts, but

this source is not included in the final hazard maps due to poor constraints. All but the innermost (more sheltered) coasts are assumed to be vulnerable to potentially damaging tsunami runup from continental slope landslide sources. Due to the absence of knowledge (complete lack of modelling) about which particular Arctic coastlines are susceptible and those that may be considered protected, equal hazard is applied across the entire zone. Additional uncertainty arises from the fact that tsunami hazard will vary seasonally with changes in ice cover, with greatest hazard at times of lowest ice cover (i.e., July-September). The final estimated hazard at both 1.5 and 3 m levels falls into the lowest hazard category for the 50 and 100 year time periods (< 2% probability of tsunami runup exceeding either 3 m or 1.5 m).

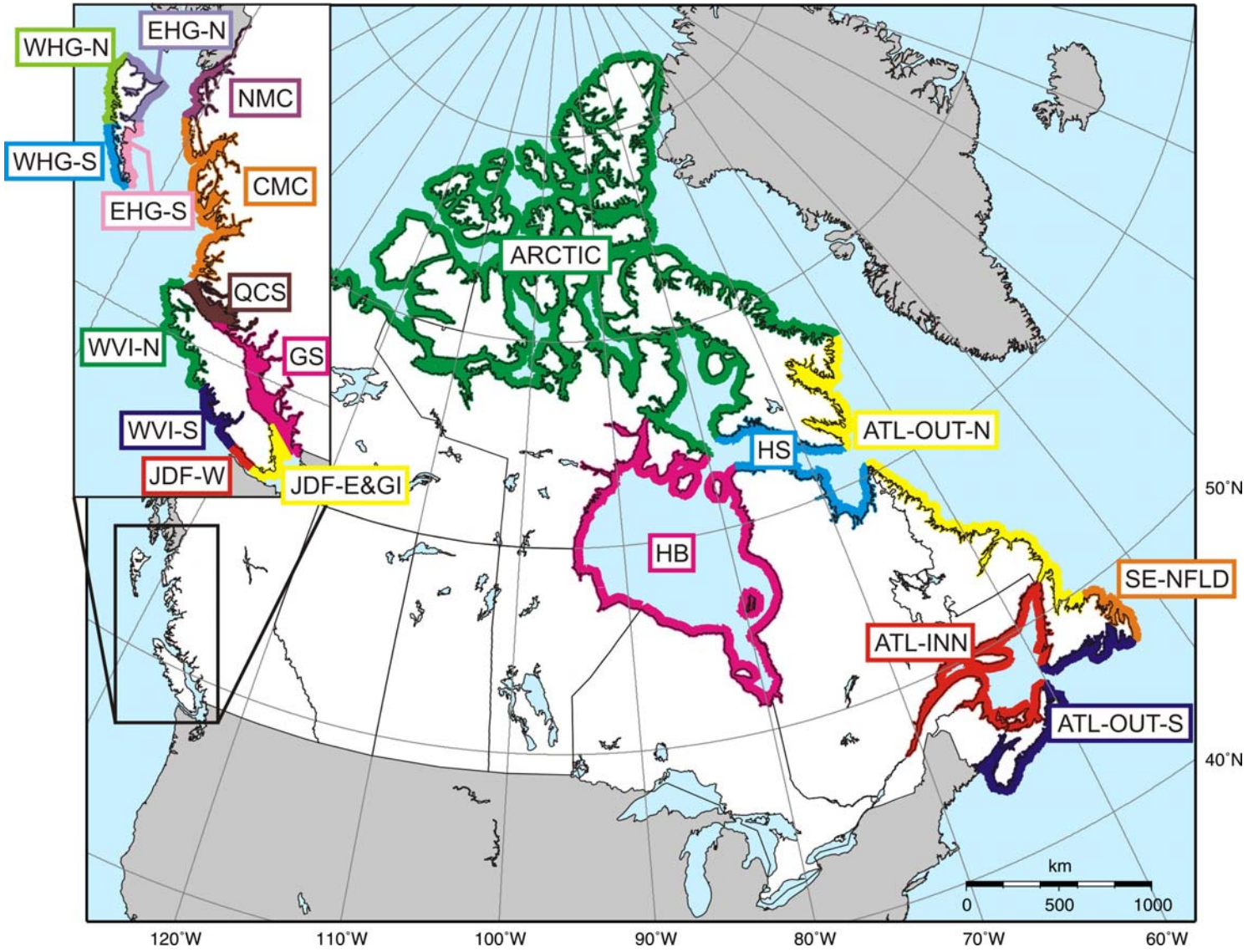

Figure C1. Tsunami hazard zones considered for the tsunami hazard map of Canada. Colour is used to distinguish between labelled zones and does not indicate relative hazard. See text for definition and justification of zones.

APPENDIX D: PROBABILISTIC TSUNAMI HAZARD MAPS FOR CANADA FOR VARIOUS TIME PERIODS

Throughout the main text, we have considered probabilities of exceeding 1.5 and 3 m tsunami runup within a 50-year time period at Canadian coastlines. Here, we use these probabilities to assess the highest runup level at each site that may occur within different timeframes, i.e., the 100-year tsunami runup, (Fig. D1) and the 500-, 1000-, and 2500-year tsunami runup (Figs. D2-4). For each time period, the runup level is shown as a best estimate (main map) with minimum and maximum estimates given on inset maps. The information is also given in Tables 25-27.

The highest runup level shown is that exceeding 3 m; ideally the maximum values would be provided for each time period. For some events, expected runup may exceed 3 m by a significant amount, e.g., on western Vancouver Island, runup is expected to exceed 5-10 m or more during *M*~9 Cascadia subduction zone tsunamis (representing the 500-year (and greater) tsunami runup). Many more detailed studies are required in order to discern the maximum runup expected from the various sources, and to adequately distinguish locations of higher hazard within the broad zones considered here. This is particularly important for populated areas.

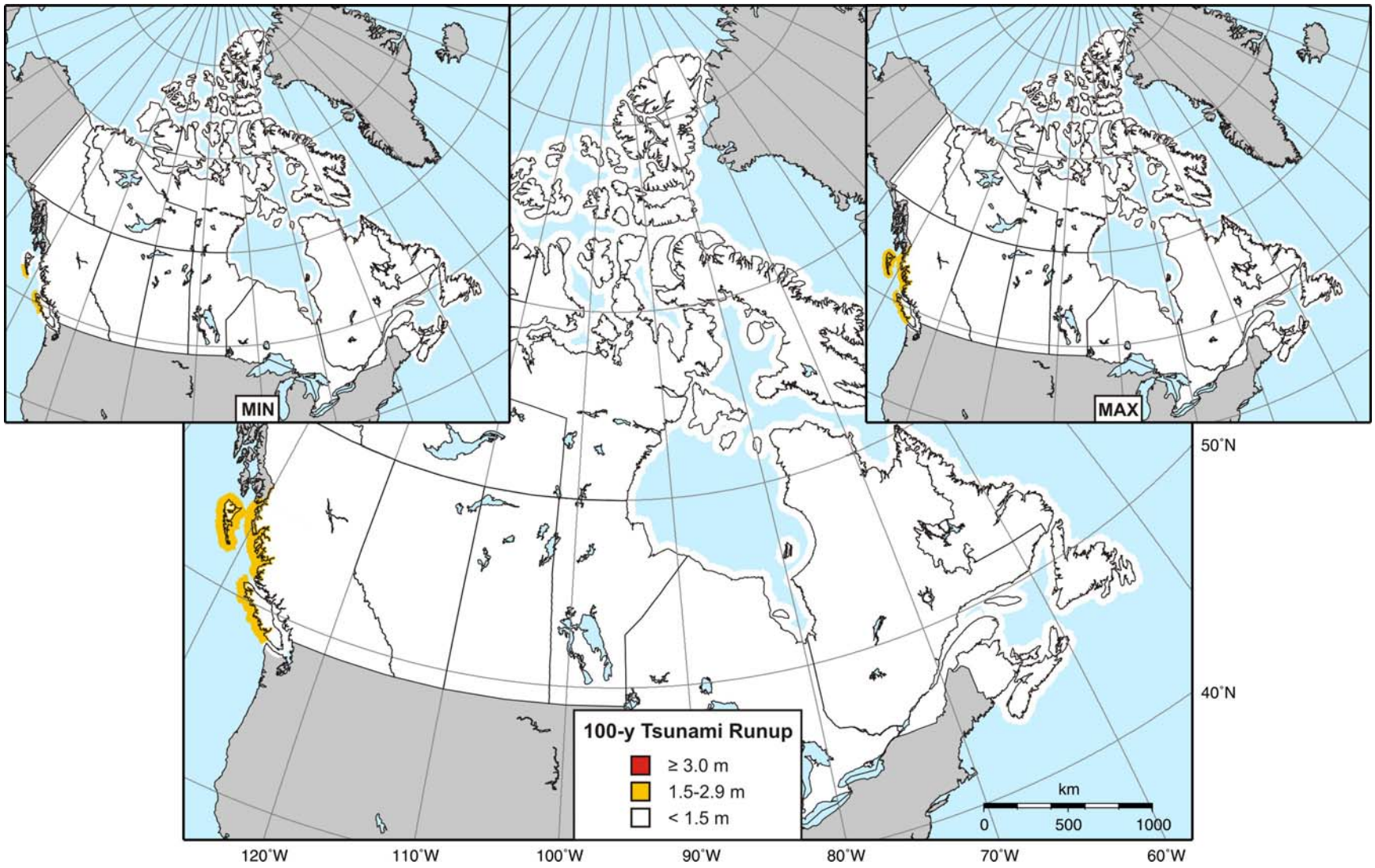

Figure D1. Probabilistic tsunami hazard map of Canada: runup levels for the 100-y tsunami, i.e., an event with probability ≥ 39.35% in 50 years. Best estimate values are shown on main map, with min and max values on inset maps.

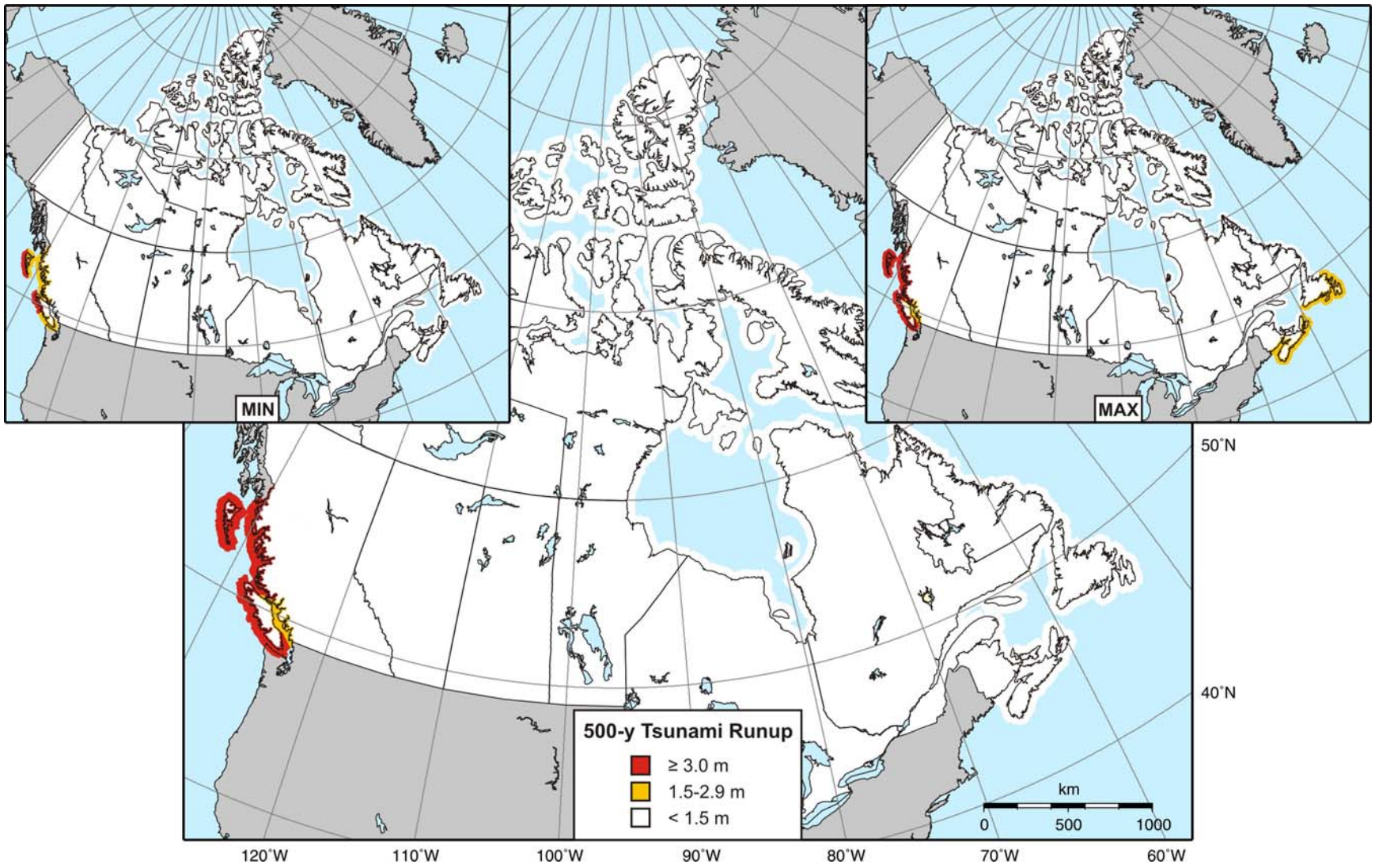

Figure D2. Probabilistic tsunami hazard map of Canada: runup levels for the 500-y tsunami, i.e., an event with probability ≥ 9.52% in 50 years. Best estimate values are shown on main map, with min and max values on inset maps.

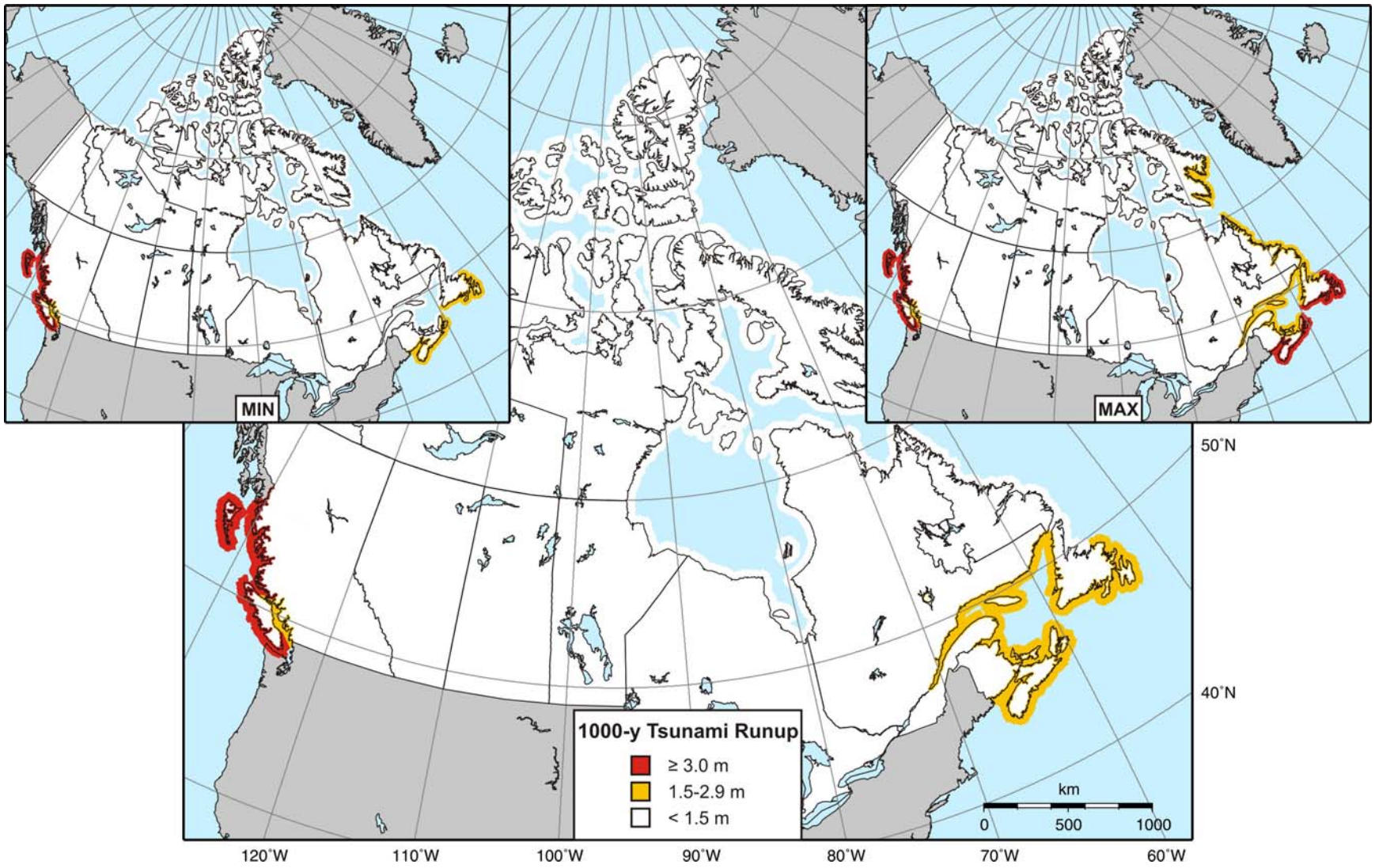

Figure D3. Probabilistic tsunami hazard map of Canada: runup levels for the 1000-y tsunami, i.e., an event with probability ≥ 4.88% in 50 years. Best estimate values are shown on main map, with min and max values on inset maps.

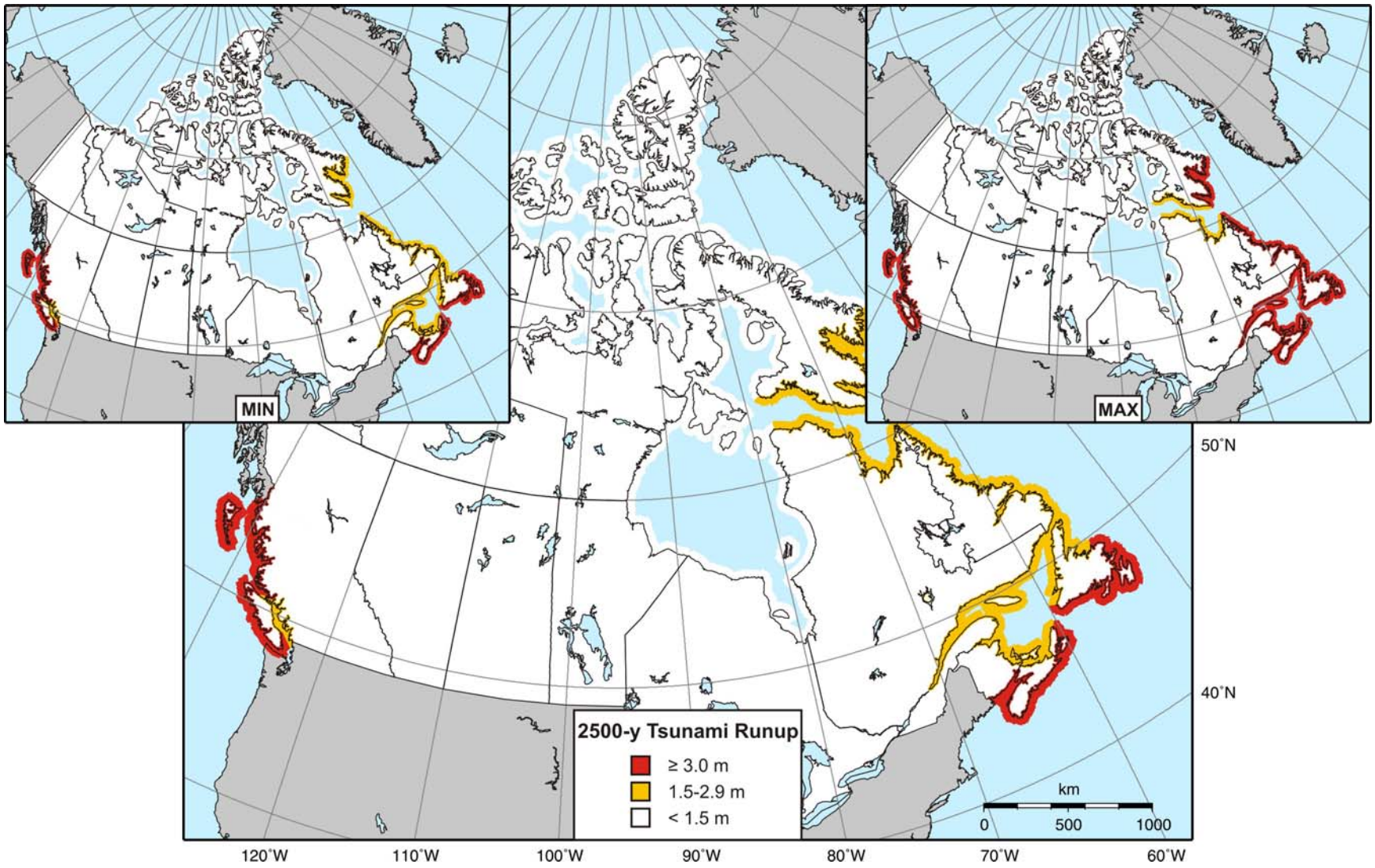

Figure D4. Probabilistic tsunami hazard map of Canada: runup levels for the 2500-y tsunami, i.e., an event with probability ≥ 1.98% in 50 years. Best estimate values are shown on main map, with min and max values on inset maps.

APPENDIX E: SOURCE CONTRIBUTIONS TO THE TSUNAMI HAZARD OF EACH ZONE

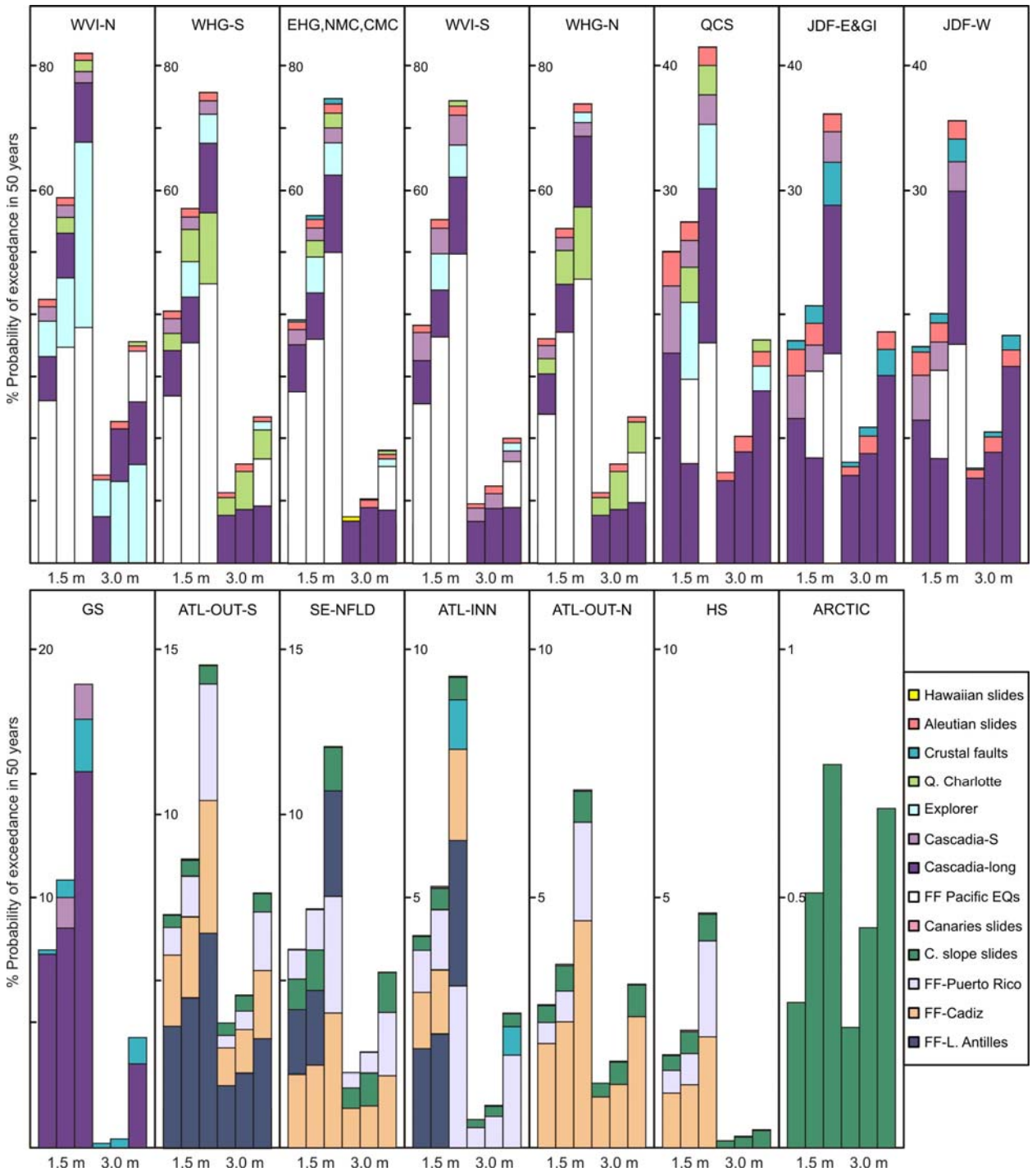

Figure E1. Relative contribution of all considered sources to the cumulative probabilistic tsunami hazard of each hazard zone (1.5 and 3 m runup: min, best, and max; zones in Appendix C), shown in decreasing order of 1.5 m hazard (data in Tables 22-24). Note: scale varies between zones. Sources as described in the text. FF: far-field; C. slope: continental slope.